Chemical segregation in hot cores with disk candidates

Allen, Veronica Amber; van der Tak, Floris; Sánchez-Monge, Á.; Cesaroni, R.; Beltrán, M. T.

Published in:
Astronomy & Astrophysics

DOI:
10.1051/0004-6361/201629118

Publication date:
2017

A&A 603, A133 (2017)
DOI: 10.1051/0004-6361/201629118

Astronomy & Astrophysics

Chemical segregation in hot cores with disk candidates

An investigation with ALMA

V. Allen[1,2], F. F. S. van der Tak[1,2], Á. Sánchez-Monge[3], R. Cesaroni[4], and M. T. Beltrán[4]

[1] Kapteyn Astronomical Institute, University of Groningen, 9712 Groningen, The Netherlands
e-mail: allen@astro.rug.nl; vdtak@sron.nl
[2] SRON, 9747 Groningen, The Netherlands
[3] I. Physikalisches Institut, 50937 Köln, Germany
[4] INAF, Osservatorio Astrofisico di Arcetri, 50125 Firenze, Italy

Received 15 June 2016 / Accepted 17 May 2017

ABSTRACT

Context. In the study of high-mass star formation, hot cores are empirically defined stages where chemically rich emission is detected toward a massive YSO. It is unknown whether the physical origin of this emission is a disk, inner envelope, or outflow cavity wall and whether the hot core stage is common to all massive stars.
Aims. We investigate the chemical makeup of several hot molecular cores to determine physical and chemical structure. We use high spectral and spatial resolution submillimeter observations to determine how this stage fits into the formation sequence of a high-mass star.
Methods. The submillimeter interferometer ALMA (Atacama Large Millimeter Array) was used to observe the G35.20-0.74N and G35.03+0.35 hot cores at 350 GHz in Cycle 0. We analyzed spectra and maps from four continuum peaks (A, B1, B2 and B3) in G35.20-0.74N, separated by 1000–2000 AU, and one continuum peak in G35.03+0.35. We made all possible line identifications across 8 GHz of spectral windows of molecular emission lines down to a 3σ line flux of 0.5 K and determined column densities and temperatures for as many as 35 species assuming local thermodynamic equilibrium (LTE).
Results. In comparing the spectra of the four continuum peaks, we find each has a distinct chemical composition expressed in over 400 different transitions. In G35.20, B1 and B2 contain oxygen- and sulfur-bearing organic and inorganic species but few nitrogen-bearing species whereas A and B3 are strong sources of O-, S-, and N-bearing organic and inorganic species (especially those with the CN bond). Column densities of vibrationally excited states are observed to be equal to or greater than the ground state for a number of species. Deuterated methyl cyanide is clearly detected in A and B3 with D/H ratios of 8 and 13%, respectively, but is much weaker at B1 and undetected at B2. No deuterated species are detected in G35.03, but similar molecular abundances to G35.20 were found in other species. We also find co-spatial emission of isocyanic acid (HNCO) and formamide (NH_2CHO) in both sources indicating a strong chemical link between the two species.
Conclusions. The chemical segregation between N-bearing organic species and others in G35.20 suggests the presence of multiple protostars surrounded by a disk or torus.

Key words. astrochemistry – stars: formation – stars: massive – ISM: individual objects: G35.20-0.74N – submillimeter: stars – ISM: individual objects: G35.03+0.35

1. Introduction

Studying the formation of high-mass stars (>8 $M_\odot$) is important because they drive the chemical evolution of their host galaxies by injecting energy, through UV radiation, strong stellar winds, and supernovae, and heavy elements into their surroundings (Zinnecker & Yorke 2007). In the study of high-mass star formation, several models have been proposed to explain the earliest processes involved. In particular, the work of McKee & Tan (2003) describes a process similar to that of low-mass stars including a turbulent accretion disk and bipolar outflows (see also Tan et al. 2014), the model by Bonnell & Smith (2011) proposes that matter is gathered competitively from low-turbulence surroundings between many low-mass protostars funneling more material to the most massive core, and the model by Keto (2007) uses gravitationally trapped hypercompact HII regions to help a massive protostar to acquire more mass. All of these models predict the existence of disks as a mechanism to allow matter to accrete onto the protostar despite high radiation pressure (Krumholz et al. 2009). However, until recently only a few candidate disks around B-type protostars were known. Several disks have been detected through the study of complex organic molecules (COMs), molecular species bearing carbon and at least six atoms, allowing for the detection of more disks (Cesaroni et al. 2006; Kraus et al. 2010; Beltrán & de Wit 2016).

While the earliest stages of high-mass star formation have not yet been clearly determined, it is well known that a chemically rich stage exists, known as a hot molecular core (HMC; see Tan et al. 2014 for a review of high-mass star formation). In this stage COMs are released from the icy surfaces of dust grains or formed in the hot circumstellar gas (Herbst & van Dishoeck 2009). These hot cores are dense ($n_H > 10^7$ cm^{-3}), warm (100–500 K), and compact (<0.05 pc) and are expected to last up to 10^5 yr. The signpost of the hot core stage is a rich molecular emission spectrum including many COMs like methanol (CH_3OH) and methyl cyanide (CH_3CN). These species may be

formed on dust grain surfaces in a cooler place (or time) and released from grain surfaces as the forming star heats the grains. Alternatively, they may form in the hot gas surrounding these massive young objects as the higher temperature allows for endothermic reactions to take place more readily. In reality, it is likely that both formation paths are necessary to achieve the molecular abundances seen around hot cores. High spatial and spectral resolution observations can help us to disentangle the different COMs and their spatial distribution during this phase. Disks candidates have been discovered in a few HMC sources, suggesting a link between disks and HMC chemistry. Studying the chemistry of such regions can help us to understand the process of high-mass star formation as chemical differences across small physical scales provide clues to the different evolutionary stages involved.

With the advent of the Atacama Large Millimeter Array (ALMA), it is now possible to make highly sensitive, high spectral, and spatial resolution observations of less abundant molecular species. The search continues for the precursors of life, such as the simplest amino acid, glycine (H_2NCH_2COOH), but complex organic species with up to 12 atoms have already been detected[1]. These include important precursors to amino acids, such as aminoacetonitrile (H_2NCH_2CN), detected by Belloche et al. (2008); the simplest monosaccharide sugar glycolaldehyde (CH_2OHCHO), first observed in a hot molecular core outside the Galactic center by Beltrán et al. (2009); and formamide (NH_2CHO) extensively studied by López-Sepulcre et al. (2015). With ALMA we have the ability to detect hot cores and study their properties in detail to determine how the spatial distribution of COMs influences the formation of massive stars. Despite advances in technology, astronomers have yet to determine whether the emission from the hot core arises from the inner envelope (spherical geometry) or from a circumstellar disk (flat geometry). It is also possible that these hot cores could be outflow cavity walls as has been recently modeled for low-mass stars by Drozdovskaya et al. (2015).

In this paper we study the chemical composition and spatial distribution of species in two high-mass star-forming regions, G35.20-0.74N and G35.03+0.35 (hereafter G35.20 and G35.03 respectively), which have been shown to be strong disk-bearing candidates. We present a line survey of the hot core in G35.03 and in four continuum peaks in the G35.20 hot core containing ~18 different molecular species (plus 12 vibrationally excited states and 22 isotopologues) of up to 10 atoms and >400 emission lines per source. We also present our analysis of the chemical segregation within core B of G35.20 depicting a small-scale (<1000 AU) separation of nitrogen chemistry and temperature difference. A chemical separation on the scale of a few 1000s of AU within a star-forming region has been seen before in Orion KL (Caselli et al. 1993), W3(OH) and W3(H_2O) (Wyrowski et al. 1999b), and AFGL2591 (Jiménez-Serra et al. 2012).

The distance to both sources has been estimated from parallax measurements to be 2.2 kpc for G35.20 (Zhang et al. 2009) and 2.32 kpc for G35.03 (Wu et al. 2014). G35.20 has a bolometric luminosity of 3.0×10^4 $L_\odot$ (Sánchez-Monge et al. 2014) and has been previously studied in Sánchez-Monge et al. (2013) and Sánchez-Monge et al. (2014) in which they report the detection of a large ($r \sim 2500$ AU) Keplerian disk around core B and a tentative Keplerian disk in core A. The bolometric luminosity of G35.03 is 1.2×10^4 $L_\odot$ and was reported to have a Keplerian disk ($r \sim 1400$–2000 AU) around the hot core A in Beltrán et al. (2014).

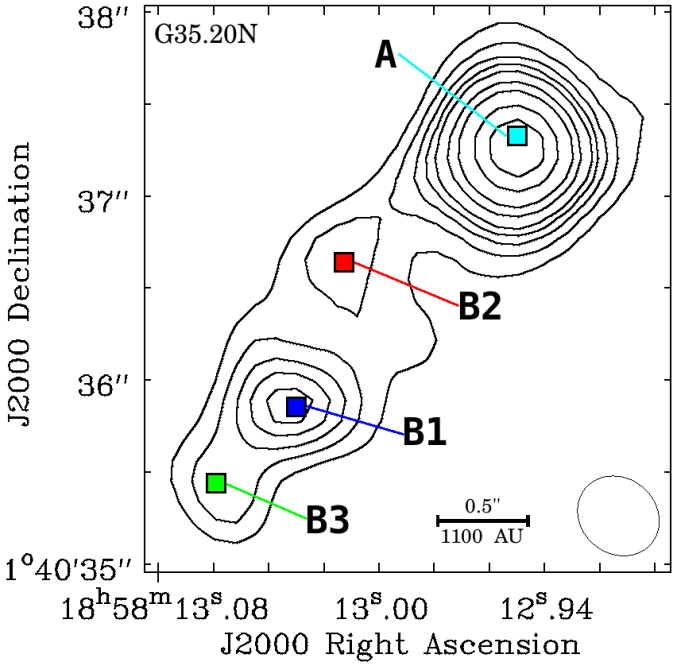

Fig. 1. Image of the 870 μm continuum emission from Cycle 0 ALMA observations of G35.20. Contour levels are 0.03, 0.042, 0.055, 0.067, 0.08, 0.10, 0.13, 0.18, and 0.23 Jy/beam (σ = 1.8 mJy/beam). The pixel-sized colored squares indicate each of the spectral extraction points.

2. Observations and method

2.1. Observations

G35.20 and G35.03 were observed with ALMA in Cycle 0 between May and June 2012 (2011.0.00275.S). The sources were observed in Band 7 (350 GHz) with the 16 antennas of the array in the extended configuration (baselines in the range 36–400 m) providing sensitivity to structures 0.4″–2″. The digital correlator was configured in four spectral windows (with dual polarization) of 1875 MHz and 3840 channels each, providing a resolution of ~0.4 km s^{-1}. The four spectral windows covered the frequency ranges [336 849.57–338 723.83] MHz, [334 965.73– 336 839.99] MHz, [348 843.78–350 718.05] MHz, and [346 891.29–348 765.56] MHz. The rms noise of the continuum maps are 1.8 mJy/beam for G35.20 and 3 mJy/beam for G35.03. For full details, see Sánchez-Monge et al. (2014) and Beltrán et al. (2014).

2.2. Line identification process

Spectra were extracted from the central pixel of the continuum peak in core A and the three continuum peaks in core B (B1, B2, B3) in G35.20 and the continuum peak in core A in G35.03 using CASA[2] (see Figs. 1 and 2 for spectra extraction positions and continuum levels and Table 1 for the J2000 coordinates and a summary of statistics). The other peaks (B-F in G35.03 and C-G in G35.20) were not analyzed because they do not show hot core chemistry, i.e., little or no emission from COMs. The three continuum peaks in G35.20 B

[1] https://www.astro.uni-koeln.de/cdms/molecules

[2] Common Astronomy Software Applications is available from http://casa.nrao.edu/

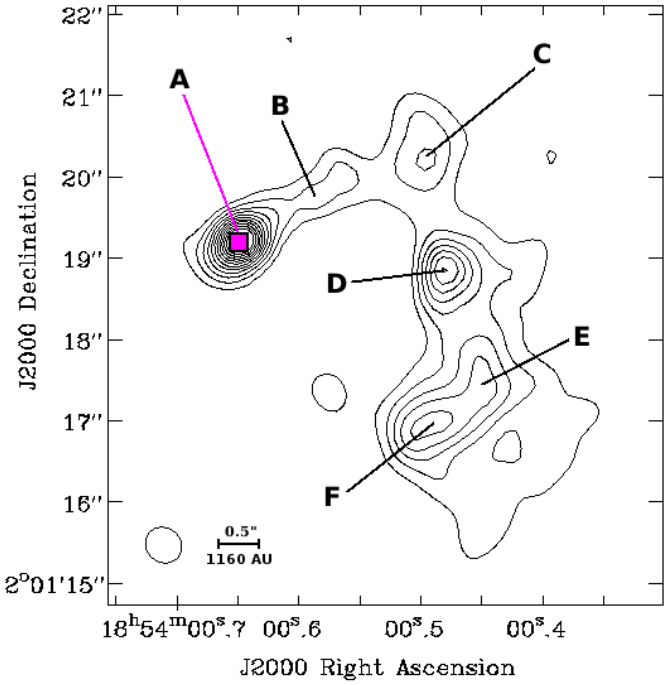

Fig. 2. Image of the 870 μm continuum emission from Cycle 0 ALMA observations of G35.03. Contour levels are 8.6, 16.8, 24.9, 33, 41.2, 49.3, 57.4, 65.5, 73.6, 81.8, and 89.9 mJy/beam (σ = 3.0 mJy/beam). The pixel-sized colored square indicates the spectral extraction point. The cores identified in Beltrán et al. (2014) are labeled A–F.

were chosen to investigate the chemical structure across the disk shown in Sánchez-Monge et al. (2014; who analyzed B as a single core); however, the disk in G35.03 A only has a single continuum point associated with the hot core, so analysis for this source was from this peak. G35.20 A was analyzed as the strongest continuum source in the region with hot core chemistry and was also analyzed at the single continuum peak. Line parameters (listed in Appendix B) were determined using Gaussian profile fits to spectral lines from each continuum peak via Cassis[3], primarily using the Cologne Database for Molecular Spectroscopy (CDMS; Müller et al. 2005) database and Jet Propulsion Laboratory (JPL; Pickett et al. 1998) database for deuterated methanol (CH_2DOH), ethanol (C_2H_5OH), NH_2CHO, acetaldehyde (CH_3CHO), and CH_3OH (ν = 2) transitions.

The process of identifying all species present in these spectra consisted of several parts. Bright lines (T_B > 5 K) from known species were identified first (i.e., those from Sánchez-Monge et al. (2014): CH_3OH, methyl formate (CH_3OCHO), CH_3CN, simple molecules) numbering about 100 lines per source. The remaining bright lines (>5 K) were identified by choosing the most likely molecular candidate, namely the transition with the higher Einstein coefficient that is limited to a minimum of about 10^{-7} s^{-1}, or with a upper level energy (E_{up}) within the expected range, generally less than 500 K, composed of C, H, O and/or N and within 2 km s^{-1} (~2 MHz) of the rest frequency of the transition. This brings the total to about 200 per source. Finally, for any remaining unidentified lines >3σ (~0.5 K) a potential species was selected, then the entire spectrum was checked for nondetections of expected transitions of this species. The total number of identified lines was over 400 for each source, including partially blended and blended transitions for which it was evident or implied by the line shape that another transition was present. It is noted in Appendix B if the line identity is uncertain in case of strong blending or multiple probable candidates.

The remaining total of unidentified and unclear identity (where there is more than one potential species) lines is about 80 for the peaks in B and G35.03 with an additional 30 in G35.20 A. These unknown transitions could be either species whose transitions for this frequency regime have not yet been measured/calculated or species whose likely identity was not clear. The peak intensities of the unknown lines were all less than 5 K. Line parameters were measured by fitting a Gaussian profile to the emission line with the Cassis line spectrum tool. In some cases, partially blended lines were fit together with one or more extra Gaussians for a more accurate measurement, although in those cases the errors were larger. The full line survey can be found in Appendices A and B, but an example is given in Table 2, where the parameters obtained for thioformaldehyde (H_2CS) are listed. The line identities are first presented ordered by frequency, and then, to emphasize the chemistry of these objects, the tables of measured line parameters are sorted by molecular species.

To validate the line identifications, fits were made simultaneously to all identified species via the XCLASS software Möller et al. (2017)[4]. This program models the data by solving the radiative transfer equation for an isothermal object in one dimension, taking into account source size and dust attenuation. The residuals between the fitted lines and observed spectra are between 5 and 25%, validating the XCLASS fits and our line identifications. The observed spectra and the XCLASS fits can be found in Appendix E and further information about the XCLASS analysis is detailed in Sect. 3.4.

2.3. Image analysis

To confirm our identifications of several complex organic species, maps were made of unblended transitions. Similar spatial distributions and velocity profiles of transitions with similar upper energy levels are consistent with these being the same species. Figure 3 shows integrated intensity (moment zero) maps of CH_3OCHO ν = 0 and ν = 1 transitions, H_2CS, $(CH_2OH)_2$, CH_3CHO ν = 0, and ν = 2 transitions in G35.20 and Fig. 4 shows the same transitions in G35.03. During this process, we discovered a difference in spatial extent between N-bearing species and O-bearing species in G35.20 core B. The N-bearing species peak at the location of continuum peak B3 and are generally not found at the other side of the disk near continuum peak B2. We comment on this difference in detail in Sect. 4.2. Channel maps were made in CASA for 20 different species for interesting isolated lines with a range of upper energy levels (see Table 3) to determine the spatial distribution of various species. Zeroth (integrated intensity), first (velocity), and second (dispersion) moment maps were also made for these species. A selection of integrated intensity maps can be found in Figs. 3 and 4.

3. Results and analysis

3.1. Line detections

A total of 431 different transitions were identified in 52 different catalog entries (18 "regular" ν = 0 main isotopes species plus

[3] CASSIS has been developed by IRAP-UPS/CNRS (http://cassis.irap.omp.eu).

[4] The software can be downloaded from here: https://xclass.astro.uni-koeln.de/

Table 1. Source continuum characteristics.

Continuum peak	Right ascension	Declination	Size ($''$)[a]	S_ν (Jy)[b]	$T_{\rm kin}$ (K)[c]	$N(H_2)$ (cm^{-2})[d]	Mass ($M_\odot$)[e]
G35.20 A	18:58:12.948	+01:40:37.419	0.58	0.65	285	2.4×10^{25}	13.0
G35.20 B1	18:58:13.030	+01:40:35.886	0.61	0.19	160	6.4×10^{24}	3.8
G35.20 B2	18:58:13.013	+01:40:36.649	0.65	0.12	120	3.3×10^{24}	2.2
G35.20 B3	18:58:13.057	+01:40:35.442	0.58	0.08	300	2.5×10^{24}	1.4
G35.03 A	18:54:00.645	+02:01:19.235	0.49	0.21	275	1.1×10^{25}	4.4

Notes. [a] Deconvolved average diameter of the 50% contour of the 870 μm continuum. [b] Integrated flux density within the 10σ contour of the 870 μm continuum. [c] Average kinetic temperature based on CH_3CN line ratios as calculated using RADEX. For details, see Sect. 3.3. [d] Calculated from source size, continuum flux density, and kinetic temperature (Sect. 3.3). [e] Sources mass calculated as in Sánchez-Monge et al. (2014) using the average kinetic temperatures.

Table 2. Line detections and measurements for H_2CS.

Transition	Frequency	G35.20 A		G35.20 B1		G35.20 B2		G35.20 B3		G35.03 A	
	(MHz)	*FWHM* (km s^{-1})	$T_{\rm peak}$ (K)	*FWHM* (km s^{-1})	$T_{\rm peak}$ (K)	*FWHM* (km s^{-1})	$T_{\rm peak}$ (K)	*FWHM* (km s^{-1})	$T_{\rm peak}$ (K)	*FWHM* (km s^{-1})	$T_{\rm peak}$ (K)
H_2CS $\nu = 0$											
$10_{1,10}$–$9_{1,9}$	338 083	5.9 ± 0.1	51.7 ± 0.9	2.7 ± 0.1	27.3 ± 1.0	2.4 ± 0.1	28 ± 1	2.54 ± 0.06	44.3 ± 0.9	6.6 ± 0.1	21.0 ± 0.3
$10_{1,9}$–$9_{1,8}$	348 532	5.8 ± 0.1	59.2 ± 1.3	2.6 ± 0.1	31 ± 1	2.3 ± 0.1	31 ± 1	2.58 ± 0.04	52.1 ± 0.7	6.33 ± 0.09	21.3 ± 0.3
$H_2C^{33}S$											
$10_{1,10}$–$9_{1,9}$	335 160	7.5 ± 0.2	3.91 ± 0.09	1.6 ± 0.5	0.4 ± 0.1	1.5 ± 0.6	0.4 ± 0.2	2.5 ±0.2	1.47 ± 0.08	<3σ	
$H_2C^{34}S$											
$10_{0,10}$–$9_{0,9}$	337 125	blended		1.2 ± 0.7	0.7 ± 0.4	1.5 ± 0.2	1.0 ± 0.1	1.9 ± 0.1	2.5 ± 0.1	<3σ	
$10_{4,6}$–$9_{4,5}$	337 460	blended with CH_3OH $\nu = 1$		in abs. feature		1.5 ± 0.4	0.55 ± 0.09	blended with CH_3OH $\nu = 1$		blended with CH_3OH $\nu = 1$	
$10_{2,9}$–$9_{2,8}$	337 475	6.3 ± 0.3	16.0 ± 0.3	1.66 ± 0.08	3.8 ± 0.2	1.7 ± 0.1	3.8 ± 0.2	3.1 ± 0.2	4.9 ± 0.2	blended with CH_3OH $\nu = 1$	
$10_{3,8}$–$9_{3,7}$	337 555	blended		2.0 ± 0.2	0.78 ± 0.05	1.7 ± 0.5	0.6 ± 0.2	2.03 ± 0.04	2.35 ± 0.03	<3σ	
$10_{3,7}$–$9_{3,6}$	337 559	blended		2.16 ± 0.09	1.55 ± 0.04	1.3 ± 0.1	0.54 ± 0.04	2.37 ± 0.06	2.26 ± 0.03	<3σ	
$10_{2,8}$–$9_{2,7}$	337 933	blended		1.2 ± 0.5	0.8 ± 0.2	1.8 ± 0.5	0.7 ± 0.1	2.3 ± 0.1	2.4 ± 0.1	<3σ	

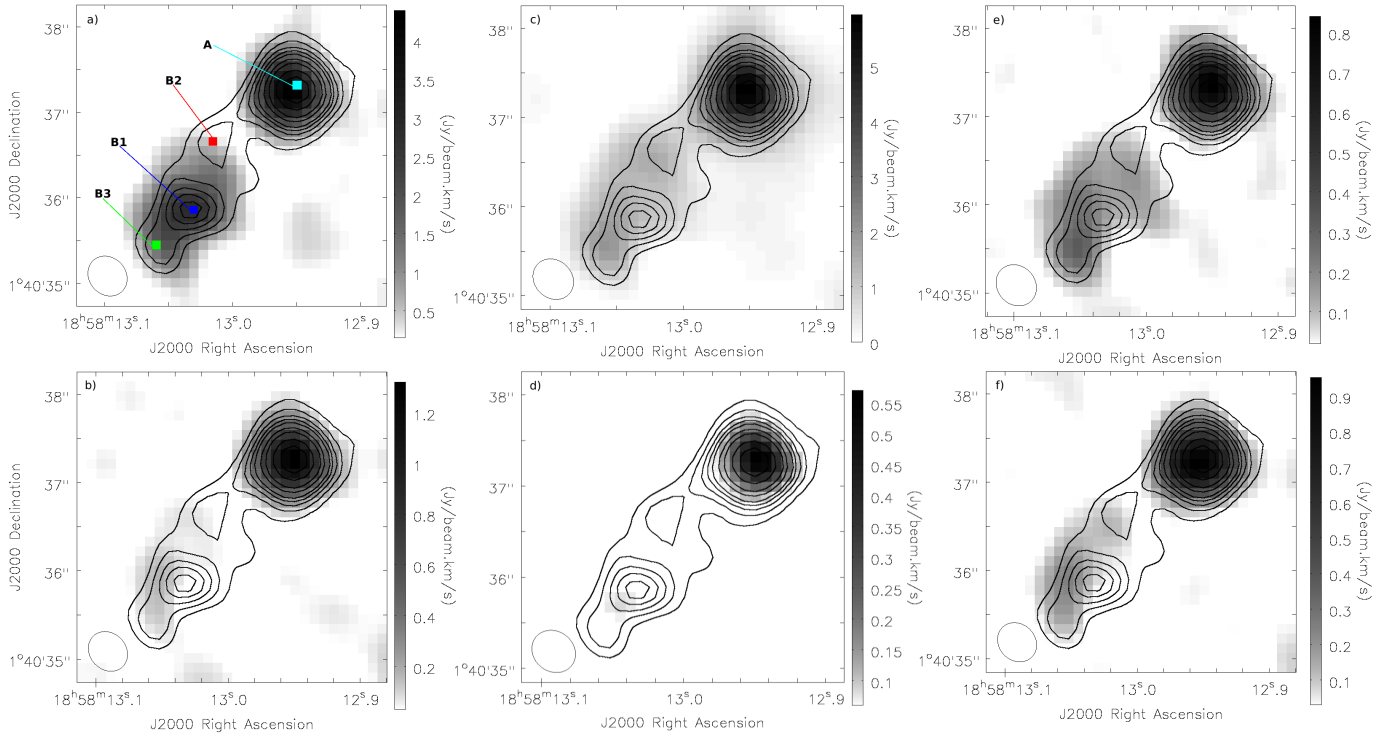

Fig. 3. Integrated intensity maps of six species across G35.20, where the contours are the 870 μm continuum with the same levels as Fig. 1. Panel **a)** shows the CH_3OCHO $\nu = 0$ emission at 336.086 GHz integrated from 18.5 to 38 km s^{-1}. Panel **b)** shows the CH_3OCHO $\nu = 1$ emission at 348.084 GHz integrated from 26 to 38.5 km s^{-1}. Panel **c)** shows the H_2CS emission at 338.083 GHz integrated from 24.5 to 38.5 km s^{-1}. Panel **d)** shows ethylene glycol ($(CH_2OH)_2$) emission at 335.030 GHz integrated from 25–36.5 km s^{-1}. Panel **e)** shows CH_3CHO $\nu = 0$ emission at 335.318 GHz integrated from 22.5 to 37 km s^{-1}. Panel **f)** shows CH_3CHO $\nu = 2$ emission at 349.752 GHz integrated from 24 to 29 km s^{-1}. It can clearly be seen between panels **a)** and **b)** and between **e)** and **f)** that vibrationally excited states have a much smaller emitting region. It is also clear in panel **d)** that $(CH_2OH)_2$ is only seen in core A.

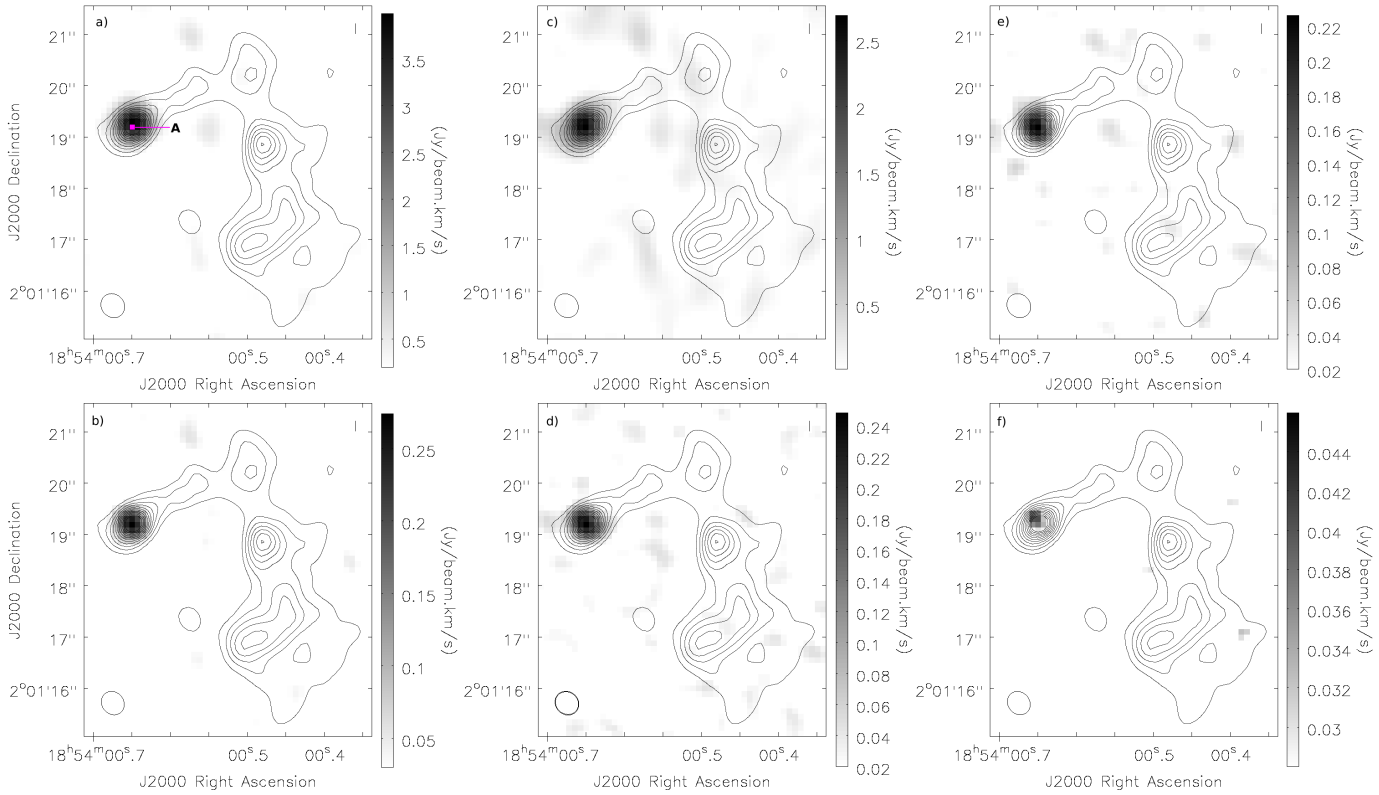

Fig. 4. Integrated intensity maps of six species across G35.03, for which the contours are the 870 μm continuum with the same levels as Fig. 2. Panel **a)** shows the CH_3OCHO $\nu = 0$ emission at 336.086 GHz integrated from 37 to 57 km s^{-1}. Panel **b)** shows the CH_3OCHO $\nu = 1$ emission at 348.084 GHz integrated from 42 to 50 km s^{-1}. Panel **c)** shows the H_2CS emission at 338.083 GHz integrated from 37 to 52 km s^{-1}. Panel **d)** shows $(CH_2OH)_2$ emission at 335.030 GHz integrated from 38.5 to 48.5 km s^{-1}. Panel **e)** shows CH_3CHO $\nu = 0$ emission at 335.318 GHz integrated from 39.5 to 48.5 km s^{-1}. Panel **f)** shows CH_3CHO $\nu = 2$ emission at 349.752 GHz integrated from 42 to 47 km s^{-1}. It is clear between panels **a)** and **b)** and between **e)** and **f)** that vibrationally excited states have a much smaller emitting region. It is also clear in panel **d)** that $(CH_2OH)_2$ is observed in this source.

Table 3. Table of source line characteristics.

Continuum peak	Species (total)	E_{up} (K)	$\langle FWHM \rangle$ (km s^{-1})	$\langle v_{LSR} \rangle$ (km s^{-1})
G35.20 A	23 (52)	17–1143	5.2	32.2
G35.20 B1	21 (42)	17–1074	2.1	29.2
G35.20 B2	21 (41)	17–973	1.9	32.3
G35.20 B3	22 (50)	17–1143	2.4	28.5
G35.03 A	22 (46)	17–1143	4.7	45.3

Notes. Column 1 lists the name of the peak. Column 2 shows the number of molecular species with one or more transition detected. The total in parentheses indicates the number of XCLASS catalog entries including isotopologues and vibrationally excited transitions separately. Column 3 gives the range of upper level energies observed. Column 4 is the average line width for each peak. Column 5 is the average velocity of the lines at each peak. Averages are calculated from all Gaussian line measurements as listed in Appendix B.

34 vibrationally excited states and isotopologues). Table 3 shows the number of species detected per source and Table 4 shows the number of unblended and partially blended transitions detected per species in each source. In addition, a few species were identified from a single transition and are listed in Table 6.

The peak with the most transitions is the weakest continuum source, B3. The strongest continuum source, G35.20 A, suffers greatly from blending and therefore has fewer unblended transitions, but is also chemically diverse (containing 23 identified species versus 22 in B3). G35.03 A, the second strongest continuum source, contains the third most molecular species, mainly because deuterated species are not present. Regarding line flux, B3 generally has the brightest emission of core B except in a few cases where B1 has slightly brighter lines. Overall B2 has the weakest emission, but still has a diverse range of species. The lines in G35.03 A are less bright than G35.20 A and are generally brighter than B3. The line fluxes from continuum peak G35.20 A are higher than any of the peaks in B except in a few cases in which B3 has higher line fluxes.

3.2. Line profiles

Most lines are fit by single Gaussians, but some profiles are more complex. Table 3 shows a summary of line properties at each peak. The average measured line width for G35.20 A was 5.2 km s^{-1} with an average v_{LSR} of 32.2 km s^{-1}. In G35.20 A, 23% of identified unblended lines are double peaked and nearly all of the rest are broad (FWHM in A is 5–8 km s^{-1} compared to 1–3 km s^{-1} at the B peaks; see below) suggesting that rotation of an unresolved structure is present (see Fig. 5). As the double peaked transitions tend to have higher upper energies (typically ~300 K), we propose that these originate in a warmer region closer to the central source, therefore indicating Keplerian-type rotation. This effect is especially prominent in the CH_3OCHO, C_2H_5OH, and CH_2DOH lines. Fits were made to each of the two components for CH_3OCHO using Cassis and the peaks were

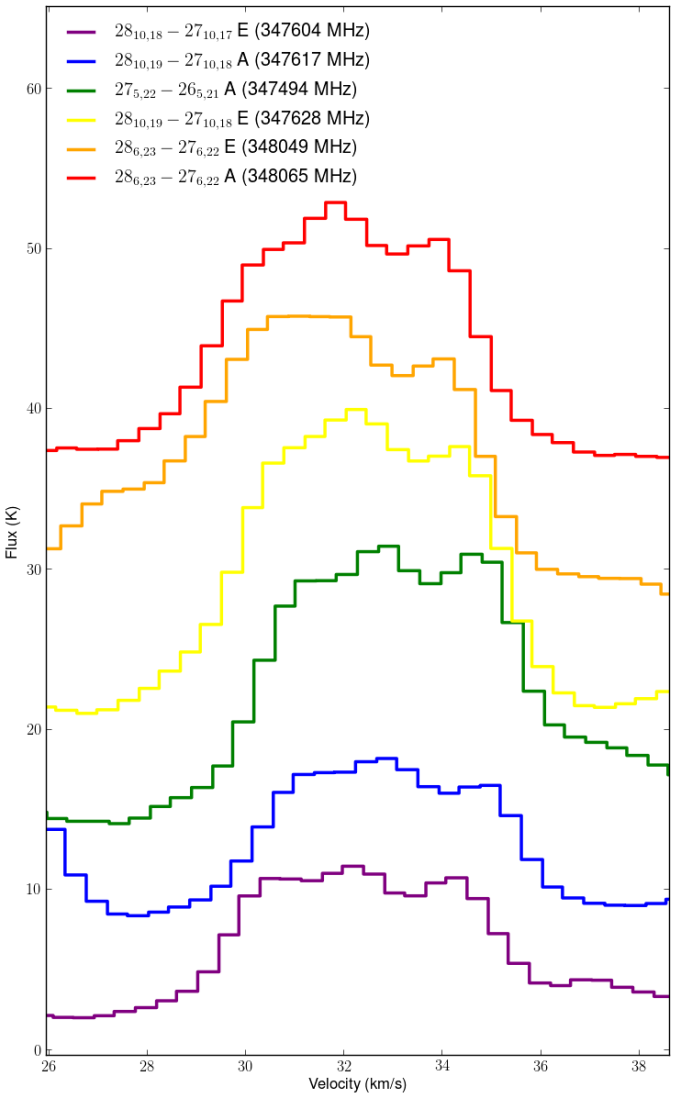

Fig. 5. Profiles of CH_3OCHO transitions toward source G35.20 A showing double peaked emission lines. Features at the edge of the frame are separate lines. If the source is more compact than the beam, this could indicate rotation.

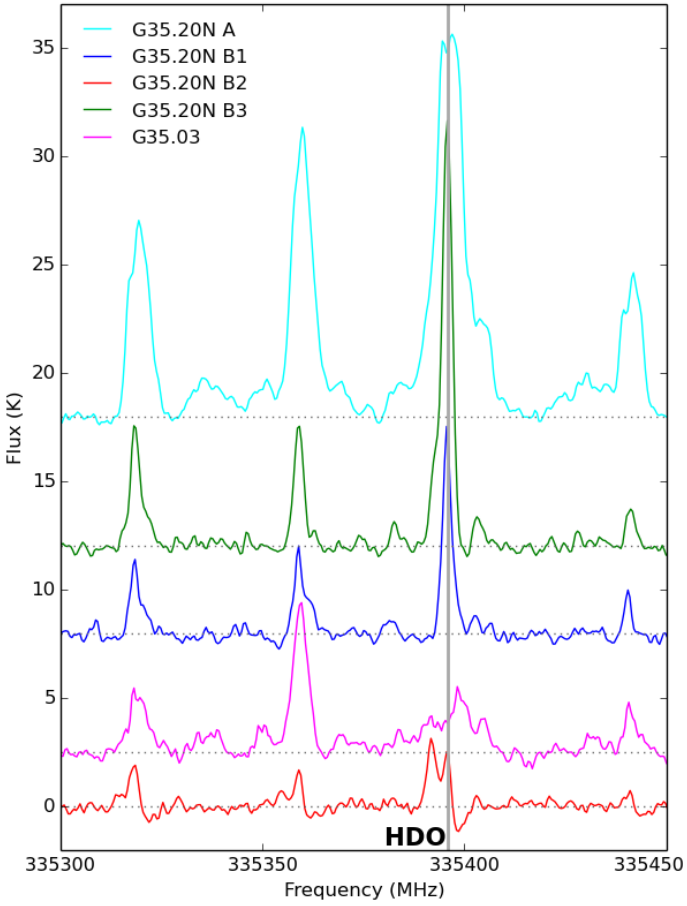

Fig. 6. Sample spectrum for the frequency range 335.3–335.45 GHz in the rest frame of each peak to indicate the diversity of these sources. G35.03 and G35.20 A do not appear to have any absorption features (in this range), but it is notable that the lines for these two sources are broader. The deuterated water (HDO) emission line at 335.396 is especially strong in B3, double peaked in G35.20 A, possibly has two velocity components in B2, and is either very weak or offset by several km s^{-1} in G35.03.

found to be separated by about 2.5 km s^{-1}. Double peaked lines are indicated in the line property tables in Appendix B. Line blending is prominent for G35.20 A, possibly because the object is more compact and therefore less resolved than core B. This could also be a consequence of G35.20 A being more chemically rich or having intrinsically broader line widths. There are a number of emission lines that are weakly detected in A and undetected at any other continuum peak. This is possibly because A is the brightest source in both line and continuum emission, so these species may also be present at the continuum peaks in B, but are lost in the noise. The emission lines from G35.20 A were fit with a single Gaussian for consistency, even where double peaked lines appeared, as the goal was chemical not kinematic analysis.

The average line widths for the emission lines from continuum peaks B1, B2, and B3 were 2.1, 1.9, and 2.4 km s^{-1}, respectively. The v_{LSR} of each of the continuum peaks in core B corresponds well with the velocity gradient of the disk observed in Sánchez-Monge et al. (2014). At B3 in the southeast of the core, the average measured v_{LSR} is 28.5 km s^{-1}, at B1, the brightest in continuum in the center of the core, the average v_{LSR} is 29.2 km s^{-1}, and at B2 in the northernmost part of core B the average v_{LSR} is 32.3 km s^{-1}. For the continuum peaks B1, B2, and B3, only the emission component was measured and taken into account for LTE modeling.

The spectra of sources B1, B2, and B3 show apparent absorption features, which originate in gaps in the observations due to emission larger than about 2″ being resolved out. In the spectra from B1, apparent redshifted absorption features are seen in every bright line except SO_2 and SO. In CH_3CN, the absorption is less pronounced, but the emission lines are asymmetrically blue. In the spectra of B2, the apparent absorption features are blueshifted and are obvious in all lines and are especially deep (~2.5 K) for CH_3CN. In B3, the apparent absorption features can be seen weakly in all species but are strong (~5 K) for CH_3OH $\nu = 0$ transitions.

G35.03 A generally has weaker lines than the brightest sources in G35.20 (A and B3) and broader lines than those in B1, B2, and B3 with an average FWHM of 4.7 km s^{-1}. The measured average v_{LSR} of the emission lines from this continuum peak was 45.3 km s^{-1}. There are no strong absorption features or double peaked emission lines. Figure 6 shows the different properties of each source in example spectra.

Table 4. Results of XCLASS LTE modeling for each of our sources.

	G35.20 A				G35.20 B1				G35.20 B2				G35.20 B3				G35.03 A			
Species	Lines	Size	T_{ex}	N_{col}	Lines	Size	T_{ex}	N_{col}	Lines	Size	T_{ex}	N_{col}	Lines	Size	T_{ex}	N_{col}	Lines	Size	T_{ex}	N_{col}
CH_3OH ($v = 0$)	29	0.6	164	3.5×10^{18}	28	0.3	234	6.9×10^{17}	24	0.36	136	5.3×10^{17}	33	0.35	155	6.2×10^{17}	29	0.40	142	1.8×10^{18}
CH_3OH ($v_{12} = 1$)	21	0.5	218	4.8×10^{18}	24	0.36	153	1.2×10^{18}	23	0.32	145	6.2×10^{17}	24	0.36	189	9.8×10^{17}	21	0.30	239	2.6×10^{18}
CH_3OH ($v_{12} = 2$)	14	0.4	227	3.8×10^{18}	18	0.18	154	2.2×10^{18}	18	0.15	152	1.0×10^{18}	19	0.20	172	1.8×10^{18}	14	0.20	192	5.1×10^{18}
$^{13}CH_3OH$	5	1.0	121	1.6×10^{17}	6	0.3	113	3.9×10^{16}	6	1.1	97	8.0×10^{15}	7	1.20	89	1.6×10^{16}	5	0.6	120	5.0×10^{16}
$CH_3\ ^{18}OH$	4	1.1	121	4.4×10^{16}	6	0.3	82	1.4×10^{16}	4	0.9	75	1.4×10^{15}	5	1.20	111	5.8×10^{15}	4	1.2	130	1.0×10^{16}
$H_2C^{18}O$	3	0.6	188	8.5×10^{14}	4	0.3	41	5.7×10^{14}	4	0.32	29	1.5×10^{15}	4	1.09	125	4.2×10^{14}	1	0.50	62	2.1×10^{14}
CH_3OCHO ($v = 0$)	28	0.98	103	8.1×10^{16}	38	0.5	285	4.5×10^{16}	33	0.5	64	2.0×10^{16}	31	0.59	67	2.7×10^{16}	28	0.2	100	2.3×10^{15}
CH_3OCH_3	10	0.34	229	3.7×10^{17}	11	0.22	156	3.8×10^{17}	8	0.4	67	1.3×10^{16}	19	0.49	97	1.7×10^{17}	10	0.7	150	8.3×10^{16}
CH_3CHO ($v = 0$)	14	0.4	234	1.7×10^{16}	19	0.33	206	7.0×10^{16}	18	0.26	88	2.3×10^{15}	20	1.16	170	2.1×10^{15}	14	0.5	120	1.3×10^{15}
CH_3CHO ($v_{15} = 1$)	7	1.1	278	5.5×10^{15}	7	0.2	300.0	2.3×10^{14}	4	⋆			13	0.56	224	1.4×10^{15}	7	0.5	220	1.3×10^{15}
CH_3CHO ($v_{15} = 2$)	4	0.7	295	4.3×10^{15}	1	⋆			0	⋆			3	0.12	102	8.1×10^{14}	0	⋆		
HCOOH	5	0.6	103	1.4×10^{16}	4	0.3	156	1.1×10^{15}	2	⋆			7	0.4	173	3.8×10^{15}	5	0.7	100	5.0×10^{15}
C_2H_5OH	30	0.8	281	7.1×10^{16}	33	0.7	78	6.0×10^{15}	33	0.12	297	1.0×10^{15}	32	0.43	178	1.3×10^{16}	30	0.4	150	4.9×10^{16}
$(CH_2OH)_2$	23	0.6	172	3.5×10^{16}	0	⋆			0	⋆			0	⋆			34	0.70	100	2.8×10^{16}
NH_2CHO	3	0.7	98	7.6×10^{15}	3	0.3	50	5.7×10^{15}	2	0.6	45	2.3×10^{14}	4	0.3	53	1.6×10^{15}	3	0.8	43	4.7×10^{15}
$NH_2{}^{13}CHO$	2	†		1.4×10^{14}	2	†		1.0×10^{14}	2	†		5.1×10^{12}	2	†		5.1×10^{13}	2	†		8.5×10^{13}
CH_3CN ($v = 0$)	10	0.45	208	3.9×10^{16}	9	0.32	129	7.2×10^{15}	9	0.62	132	1.3×10^{15}	10	0.35	208	6.5×10^{15}	10	0.30	186	3.0×10^{16}
CH_3CN ($v_8 = 1$)	11	0.6	359	3.2×10^{16}	5	0.29	283	3.5×10^{15}	4	⋆			13	0.8	213	1.3×10^{15}	11	0.30	216	3.6×10^{16}
$CH_3\ ^{13}CN$	2	1.0	263	5.0×10^{14}	4	0.7	262	2.0×10^{14}	3	0.44	55	1.4×10^{14}	9	0.7	118	5.4×10^{14}	2	0.35	70	1.4×10^{15}
CH_2DCN	4	0.5	82.3	4.1×10^{15}	7	0.1	180	3.0×10^{13}	1	⋆			6	0.8	90	1.1×10^{15}	1	⋆		
C_2H_5CN	13	0.9	125	1.5×10^{16}	8	⋆			3	⋆			18	0.8	160	4.5×10^{14}	13	0.5	78	5.0×10^{15}
$CH_3{}^{13}CH_2CN$	2	†		6.9×10^{14}	0	⋆			0	⋆			0	⋆			0	⋆		
$^{13}CH_3CH_2CN$	1	†		6.9×10^{14}	0	⋆			0	⋆			0	⋆			0	⋆		
CH_3CHDCN	13	0.6	97	2.9×10^{15}	0	⋆			0	⋆			0	⋆			0	⋆		
C_2H_3CN	6	0.6	77	1.3×10^{16}	0	⋆			0	⋆			11	0.8	207	7.3×10^{14}	0	⋆		
HCCCN ($v = 0$)	1	1.2	176	1.7×10^{15}	1	0.9	119	9.2×10^{14}	1	0.8	122	2.0×10^{14}	1	1.2	251	1.8×10^{15}	1	0.6	140	2.3×10^{15}
$HC^{13}CCN$ ($v = 0$)	1	†		3.4×10^{13}	0	⋆			1	⋆			1	†		3.8×10^{13}	1	⋆		
$HCC^{13}CN$ ($v = 0$)	0	†		3.4×10^{13}	0	⋆			0	⋆			1	†		3.8×10^{13}	0	⋆		
HCCCN ($v_6 = 1$)	1	0.6	200	3.1×10^{15}	0	⋆			0	⋆			2	0.4	256	2.4×10^{15}	0	⋆		
$HCC^{13}CN$ ($v_6 = 1$)	1	†		6.2×10^{13}	0	⋆			0	⋆			1	†		5.4×10^{13}	0	⋆		
HCCCN ($v_7 = 1$)	2	0.37	251	5.3×10^{15}	3	0.8	219	5.8×10^{14}	2	⋆			3	0.98	288	2.1×10^{15}	2	0.8	194	5.9×10^{15}
$H^{13}CCCN$ ($v_7 = 1$)	2	†		1.0×10^{15}	0	⋆			0	⋆			2	†		4.6×10^{13}	0	⋆		
$HC^{13}CCN$ ($v_7 = 1$)	1	†		1.0×10^{15}	0	⋆			0	⋆			1	†		4.6×10^{13}	0	⋆		
$HCC^{13}CN$ ($v_7 = 1$)	1	†		1.0×10^{15}	1	⋆			0	⋆			2	†		4.6×10^{13}	0	⋆		
HCCCN ($v_7 = 2$)	1	0.20	350	2.2×10^{15}	0	⋆			0	⋆			4	0.35	473	1.3×10^{15}	0	⋆		
H_2CS	2	1.3	165	1.4×10^{16}	2	2.0	230	3.3×10^{15}	2	1.0	50	1.2×10^{15}	2	0.9	87	6.1×10^{15}	2	1.7	96	3.7×10^{15}
$H_2C^{34}S$	1	†		5.3×10^{14}	5	†		1.9×10^{14}	6	†		8.9×10^{13}	5	†		6.1×10^{14}	0	⋆		
SO_2	5	1.4	260	1.7×10^{16}	5	1.44	279	3.3×10^{16}	5	2.42	114	6.6×10^{15}	5	1.3	288	3.9×10^{16}	5	1.2	281	7.5×10^{16}
$^{33}SO_2$	1	†		1.7×10^{14}	1	†		2.5×10^{14}	1	†		1.4×10^{14}	2	†		1.9×10^{15}	1	†		3.4×10^{15}
$^{34}SO_2$	1	†		1.2×10^{14}	1	†		1.2×10^{14}	1	†		1.6×10^{14}	1	†		1.3×10^{15}	1	⋆		
CH_2DOH ‡	18		150	5.0×10^{16}	35		140.0	9.0×10^{15}	31		240.0	6.0×10^{15}	32		160.0	1.5×10^{16}	1			
CH_3OCHO ($v = 1$) ‡	8		120	1.9×10^{17}	6		140.0	9.0×10^{15}	4				8				4			

Notes. Four columns are shown under each source name: 1) number of unblended or partially blended transitions per species detected; 2) modeled source size (″); 3) excitation temperature (K); and 4) column density (cm^{-2}). The errors on each value are shown in Appendix C. Star (⋆) symbols indicate that a species was not modeled in XCLASS for this peak. † indicates that this species was coupled to the main isotopologue for fitting and the isotope ratio was calculated keeping the source size and excitation temperature the same as the main isotope. The column density indicated in these cases reflects the best-fit isotope ratio. To improve the fits for various HC_3N states, the $^{12}C/^{13}C$ isotope ratio was fixed at 50. ‡ these species were analyzed using Cassis because they were not yet incorporated in the XCLASS database.

3.3. Kinetic gas temperatures

To estimate the kinetic temperature ($T_{\rm kin}$) for each region without assuming local thermodynamic equilibrium (LTE), we use RADEX (van der Tak et al. 2007), which is a radiative transfer code that assumes an isothermal and homogeneous medium, treats optical depth with a local escape probability, and uses collisional rate coefficients from the LAMDA database (Schöier et al. 2005; Green 1986). We use this software to calculate line intensity ratios across a range of kinetic temperatures and densities and determine whether it is reasonable to assume LTE.

We used the CH_3CN line ratios for these sources as this species is a known tracer (Wang et al. 2013) of kinetic temperature as a near-symmetric top molecule where transitions with different energy levels have similar critical densities. We consider as input parameters the ratios of the peaks of unblended CH_3CN lines. The transitions used were 19_8–18_8, 19_6–18_6, 19_5–18_5, 19_4–18_4, 19_3–18_3, and 19_2–18_2 with a column density of 5×10^{15} cm^{-2}. The line ratios were modeled for kinetic temperatures between 100 and 500 K and for H_2 densities between 10^6 and 10^9 cm^{-3}. Errors were calculated from the measured error on the Gaussian fit of each spectral line.

We find that B2 is the coolest region with an average $T_{\rm kin}$ of 120 K and a range from 90–170 K. Next hottest is B1 with an average $T_{\rm kin}$ of 160 K and a range from 120–220 K. G35.20 A is significantly hotter than these with an average $T_{\rm kin}$ of 285 K and a range from 150–450 K. B3 is consistently the hottest, ranging from 175–490 K with an average $T_{\rm kin}$ of 300 K. The kinetic temperatures in G35.03 are also very high, ranging from 100–450 K with an average $T_{\rm kin}$ of 275 K.

The varying temperatures for different transition ratios may indicate a temperature gradient within the sampled gas, which requires advanced methods such as RATRAN (Hogerheijde & van der Tak 2000) or LIME (Brinch & Hogerheijde 2010) to model. The $K = 6/K = 4$ ratio consistently traces the lowest temperature. The $K = 8/K = 3$ ratio traces the highest temperature for A, B3, and G35.03, while the highest temperatures for B1 and B2 are traced by the $K = 6/K = 3$ and $K = 6/K = 5$ ratios, respectively.

These average kinetic temperatures were used in calculating the mass of the core and H_2 column density based on the 870 μm continuum flux as in Sánchez-Monge et al. (2014). Using a dust opacity of 1.75 cm^2 g^{-1} and a gas-to-dust ratio of 100, core A has a mass of 13.0 $M_\odot$, B1 has a mass of 3.8 $M_\odot$, B2 has a mass of 2.2 $M_\odot$, B3 has a mass of 1.4 $M_\odot$, and G35.03 has a mass of 4.4 $M_\odot$. G35.20 A generally has a lower kinetic temperature than B3, but higher energy transitions are observed and it is also much more massive with a continuum flux density that is 10 times higher.

3.4. Molecular column densities

To estimate the column densities of each detected species, we used the XCLASS software. For any given set of parameters (source size, temperature, column density, velocity, and line width) XCLASS determines the opacity for each spectral channel for each species, and these opacities are added to produce a spectrum of the opacity changing with frequency. In a last step, the opacity is converted into brightness temperature units to be directly compared with the observed spectrum. The fitting process compares the synthetic spectrum to the observed spectrum, and minimizes the χ^2 by changing the five parameters indicated above. As input parameters, we limited the line width and $v_{\rm LSR}$ to ± 1 km s^{-1} from the measured values so the transitions could easily be identified by the fitting algorithm. Source size, excitation temperature ($T_{\rm ex}$), and column density ($N_{\rm col}$) were allowed to vary widely to begin with and then were better constrained around the lowest χ^2 fits per parameter per species. For species that were observed to be located only in the regions of the hot cores (mostly complex organic molecules), the source size was varied from 0.1–1.5″ to be comparable with the observed emission extent and the $T_{\rm ex}$ was allowed to vary from 50–500 K. The column density was allowed to vary from 10^{13}–10^{19} cm^{-2}. For species that were observed to emit over a more extended region (H_2CS and SO_2), the source size input range was varied between 1.0–3.5″, the $T_{\rm ex}$ input range was 20–200 K, and the column density input range was 10^{12}–10^{16} cm^{-2}.

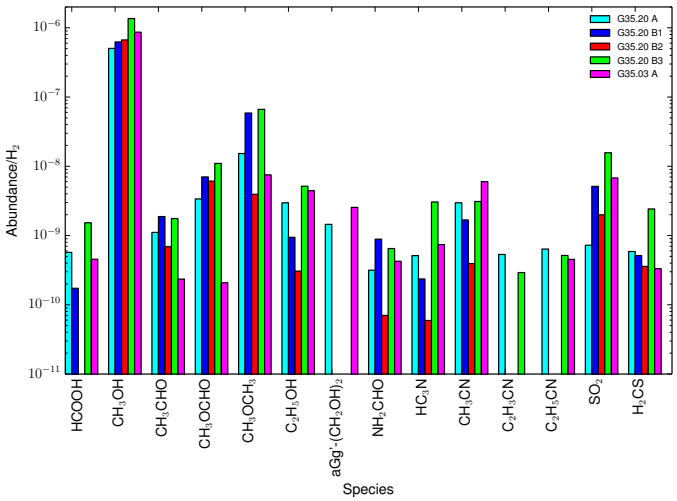

Fig. 7. Abundances vs. H_2 as determined using the XCLASS software package for each of the sources modeled. All main isotope species modeled from more than one transition are shown. The column densities for vibrationally excited states were added to the $v = 0$ state for CH_3OH, CH_3CHO, CH_3CN, and cyanoacetylene (HC_3N) to determine abundances. The CN-bearing species in both plots clearly indicate the missing emission in B1 and B2 for vinyl cyanide (C_2H_3CN) and ethyl cyanide (C_2H_5CN) and reduced abundances in B2 for CH_3CN and HC_3N. We stress that as these species do not always trace the same gas, these abundances are lower limits.

For a few species (SiO, $H^{13}CO^+$, $C^{17}O$, $H^{13}CN$, and $C^{34}S$) only one transition was observed, so we kept the source size fixed at the measured extent of the emission at 3σ and the excitation temperature fixed at 50 K and 100 K to determine the column densities at these two possible temperatures. The results for the single line transitions are given in Table 6.

Figure 7 presents a summary of the abundances observed per core as modeled via XCLASS. The excitation temperatures ranged from about 100–300 K generally with a few species outside this range. The H_2 column densities used were based on the 870 μm continuum emission (values shown in Table 1) as determined in Sect. 4.1 of Sánchez-Monge et al. (2014). These mass and column density estimates are lower limits as Sánchez-Monge et al. (2014) determined that in our observations we recover 30% of the flux compared to SCUBA 850 μm observations. The modeled values for column density and excitation temperature were checked against rotational diagrams from Cassis and found to be in agreement. The column densities determined using Cassis are lower than those from XCLASS, but this is an effect of a less robust optical depth analysis and assuming the source size fills the beam.

Uncertainties on excitation temperatures tend to be 10–20%, but for some species the fit results are upper or lower limits. For entries that are not upper or lower limits, the range of errors is 1–160 K with an average temperature error of 40 K (or 37%). Source size uncertainties are generally 0.1–0.3″ with an average error of 0.2″, but range from 0.01–1.0″. Error ranges for column densities were typically less than 1 order of magnitude (with an average error of 0.7 orders of magnitude) with a range between 0.2 and 2.8 orders of magnitude. For species where only one transition is modeled uncertainties for the column densities of these species are up to two orders of magnitude. Table 4 shows the full list of detected species and isotopologues with the number of transitions detected in each core and indicates whether the listed species or isotopologue was modeled in XCLASS. The resulting synthetic spectra are shown together with the observed spectra in Appendix E and can be seen to be very good fits of the data. The results of the XCLASS analysis are summarized in Appendix D.

In the following subsections, we outline any special considerations used in modeling specific molecules. Section 3.4.1 outlines the treatment of most complex organic molecules and their isotopologues and excited states. Section 3.4.2 details the special treatment of the observed HC_3N emission. Section 3.4.3 explains the fitting methods for SO_2 and H_2CS. Section 3.4.4 shows how simple molecules with only one transition are modeled. Section 3.4.5 summarizes how the few species not included in the XCLASS database are handled.

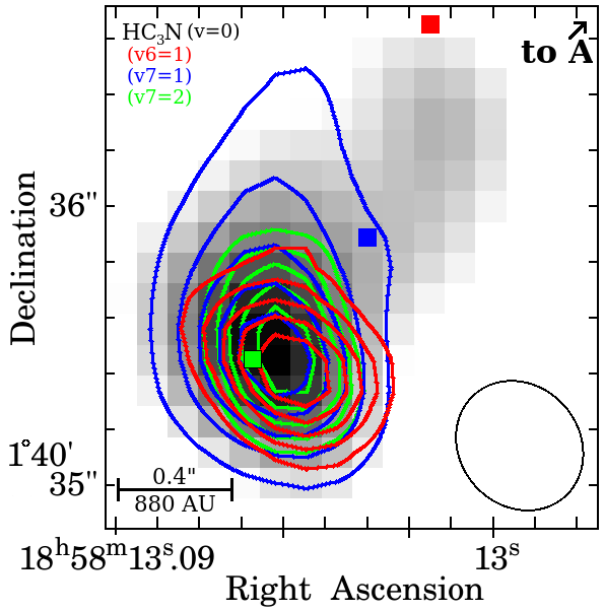

Fig. 8. Integrated intensity of HC_3N J = 37–36 emission is shown: (v = 0) (grayscale), v_7 = 1 (blue contours), v_6 = 1 (red contours), and v_7 = 2 (green contours). The green contours are 0.05, 0.069, 0.088, 0.106, and 0.125 Jy/beam km s^{-1}. Blue contours are 0.2, 0.422, 0.644, 0.866, and 1.088 Jy/beam km s^{-1}. Red contours are 0.043, 0.067, 0.092, 0.117, and 0.141 Jy/beam km s^{-1}. Sources B1, B2, and B3 are indicated with colored boxes as in Fig. 1.

3.4.1. Complex organic molecules

We modeled 10 different species containing 6 or more atoms: methanol (CH_3OH), ethanol (C_2H_5OH), methyl formate (CH_3OCHO), acetaldehyde (CH_3CHO), dimethyl ether (CH_3OCH_3), formamide (NH_2CHO), ethylene glycol ($(CH_2OH)_2$), methyl cyanide (CH_3CN), vinyl cyanide (C_2H_3CN), and ethyl cyanide (C_2H_5CN).

Several species with ^{13}C isotopologues were detected, along with many cases of deuteration. The ^{18}O isotopologue for methanol and formaldehyde were detected in all cores, but in no other species. This is due, in part, to limited laboratory data where the properties of these transitions have not yet been measured or calculated.

High energy transitions in our sources are observed to emit from a much smaller area than lower energy transitions (see Figs. 3 and 4) and many are not observed in B1 or B2. Because these vibrationally excited states emit from a smaller region, we assume that this emission originates from a denser and possibly hotter region and therefore, the continuum derived H_2 column density is a lower limit. For this reason the column densities for these species cannot be easily converted to abundances, and cannot be precisely compared to their v = 0 states. Nevertheless, noting their derived excitation temperatures and densities is useful in comparing the properties of the different regions of gas.

3.4.2. Cyanoacetylene (HC_3N) and vibrational temperature

Between 2 and 10 different states were detected in each source for this species, but with only a few transitions, so the isotopologues were coupled to the main isotopologue for each vibrational state and fixed at a $^{12}C/^{13}C$ isotope ratio of 50. The v = 0 state was modeled for all regions and the isotopologue $HC^{13}CCN$ v = 0 was coupled with HC_3N v = 0 to improve the uncertainty (from fitting one transition to fitting two). The fit for $HCC^{13}CN$ v = 0 was also coupled with HC_3N v = 0 for B3, as this is the only location where this species was detected.

Each of the vibrational states (v_6 = 1, v_7 = 1, v_7 = 2) were modeled separately due to their differing spatial extent (Fig. 8) and the source size was observed to be more compact with higher excitation. No vibrationally excited states were modeled for B2, as they were not detected in the observations and only the v_7 = 1 state was modeled for B1 and G35.03. HC_3N v_6 = 1 was modeled for A and B3 and was coupled with $HCC^{13}CN$ v_6 = 1 with the $^{12}C/^{13}C$ isotope ratio fixed at 50. HC_3N v_7 = 1 was also modeled coupled with the three different ^{13}C isotopologues of HC_3N v_7 = 1 for A and B3 with the isotope ratio fixed at 50. HC_3N v_7 = 2 was only modeled for A and B3 where the emission becomes very compact.

We determined vibrational temperatures from all of the observed HC_3N lines for each peak and found them to be in agreement with our RADEX and XCLASS results (see Table 5 and Fig. 9). The temperatures ranged from 120–210 K, which indicates that our assumption of LTE is reasonable, even where species are vibrationally excited. The vibrational temperature for peak B3 is smaller than the kinetic temperature, but is consistent within errors (see Table 5).

The ratio of intensities of HC_3N v_7 and v_0 transitions indicates the proportion of vibrationally excited to ground-state molecules in the region (Wyrowski et al. 1999a). For G35.20 B1 and B2 this ratio is ~0.15 and for A and B3 it is ~0.3. Our sources are all similar to the other hot cores studied in Wyrowski et al. (1999a), where G35.20 A is similar to SgrB2N, B1 and B2 similar to Orion KL and W3(H_2O), and B3 similar to G29.96-0.02. Vibrational temperature analysis for G35.03 A could not be completed as the only unblended HC_3N lines detected were from the vibrational state v_7 = 1.

Table 5. Temperatures (vibrational, kinetic, and excitation) and column densities determined using different methods.

Source	T_{vib} (K)	N_{col} (vib) (cm^{-2})	T_{kin} (K)	T_{ex} (K)	N_{col} (XCLASS) (cm^{-2})
G35.20 A	210 ± 80	$4^{+11}_{-3} \times 10^{15}$	285^{+165}_{-135}	280	1.2×10^{16}
G35.20 B1	160 ± 20	$6.2^{+340}_{-6.0} \times 10^{14}$	160^{+60}_{-40}	210	1.6×10^{15}
G35.20 B2	120 ± 60	$5^{+27}_{-4} \times 10^{14}$	120^{+50}_{-30}	130	2×10^{14}
G35.20 B3	160 ± 20	$2.4^{+1.4}_{-0.9} \times 10^{15}$	300^{+190}_{-125}	310	8.4×10^{15}
G35.03 A	n/a	n/a	275 ± 175	170	8.1×10^{15}

Notes. Columns 2 and 3 list vibrational temperatures for HC_3N with corresponding column densities. Fluxes for ^{13}C isotopologues were multiplied by 50 to be comparable to Galactic isotope ratios. Columns 4 and 5 correspond to the kinetic temperatures (from RADEX) and the average excitation temperatures (from all XCLASS modeled HC_3N vibrational states) and Col. 6 is the total column density from the XCLASS fits.

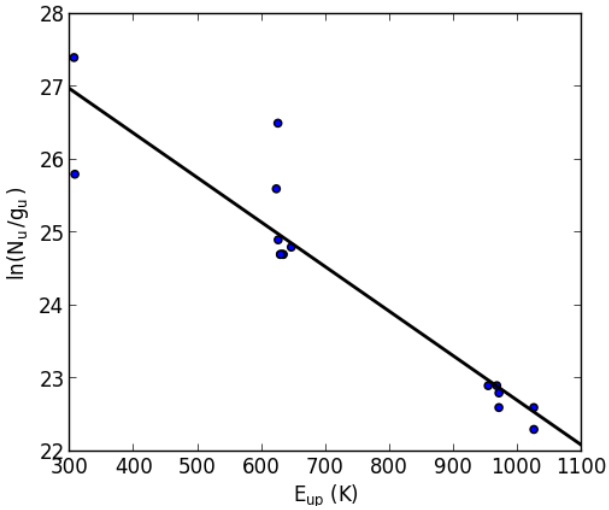

Fig. 9. Vibrational diagram for all of the HC_3N transitions from G35.20 B3 including ground and vibrationally excited states with J = 37–36 and J = 38–37. Fluxes for ^{13}C isotopologues were multiplied by 50 to be comparable to Galactic isotope ratios. The vibrational temperature calculated for peak B3 is 160 ± 20 K

3.4.3. Sulfur bearing molecules

Sulfur bearing molecules SO_2 and H_2CS were modeled with their detected isotopologues coupled to the main isotopologue varying the isotope ratio. Sulfur isotope ratios in the ISM have been shown to be 15–35 for $^{32}S/^{34}S$ and 4–9 for $^{34}S/^{33}S$ (Chin et al. 1996). Solar isotope ratios are 22.6 for $^{32}S/^{34}S$ and 5.5 for $^{34}S/^{33}S$ (Anders & Grevesse 1989). Our best-fit isotope ratio for $^{32}SO_2/^{33}SO_2$ was between 16 and 100. The ratio of $^{32}SO_2/^{33}SO_2$ in space has been reported for Orion KL in Esplugues et al. (2013), with varying ratios for different parts of the region ranging from 5.8–125 reporting a ratio of 25 in the Orion hot core. The best-fit isotope ratio for our observations of $^{32}SO_2/^{34}SO_2$ was around 33. The main isotopologue fit of H_2CS was made based on three transitions and was modeled with $H_2C^{34}S$ coupled (only the abundance ratio was varied). The best-fit isotopic ratio for $H_2C^{32}S/H_2C^{34}S$ was 11, where the ratio reported for SgrB2 by Belloche et al. (2013) was 22.

3.4.4. Simple molecules

For the following simple species (those with less than six atoms), only a single transition was observed, so to estimate their column densities, the source size and excitation temperatures were fixed. The temperatures were modeled at 50 K and 100 K for all but $C^{17}O$, which was modeled at 20 K and the source size was fixed at the measured extent of the 3σ emission. Several species were previously demonstrated to have quite extended emission ($H^{13}CO^+$, $C^{17}O$, SiO) in Sánchez-Monge et al. (2014), Beltrán et al. (2014). A summary of the results for these species is given in Table 6.

- Formyl cation ($H^{13}CO^+$ 4–3) – only the emission component of this species was modeled. Extended emission shown in Sánchez-Monge et al. (2014), Beltrán et al. (2014).
- Carbon monoxide ($C^{17}O$ 3–2) – at the location of our pixel sources there was a lot of uncertainty in identifying of this line owing to severe line blending at this frequency. For G35.20 A this could not be modeled owing to line confusion. Extended emission indicates that this species is seen in the surrounding cloud, so a larger source size and a lower temperature were used.
- Heavy (Deuterated) water (HDO $3_{3,1}$–$4_{2,2}$) – this transition, along with all other deuterated species, was not clearly detected in G35.03, so HDO $3_{3,1}$–$4_{2,2}$ was not modeled there. For the other peaks, the emission was fairly extended and the best-fit source sizes were between 0.6″ (at B2) and 1.5″ (at B3).

3.4.5. Species analyzed with Cassis

Some species could not be modeled with XCLASS as they were not yet included in its database. These species were measured and analyzed with Cassis.

- Deuterated methanol (CH_2DOH) – rotational diagrams were created using Cassis for all peaks in G35.20. The rotational temperatures ranged from 140–240 K and column densities were 0.6–5.0 × 10^{16} cm^{-2}. The CH_3OH $\nu = 0$ rotational diagrams were made using Cassis to compare to these values to determine deuteration fraction.
- Vibrationally excited methyl formate (CH_3OCHO $\nu = 1$) – rotational diagrams were made from all CH_3OCHO transitions and the high energy $\nu = 1$ transitions continued the trend of the rotational diagrams well. Therefore the reported rotational temperatures and column densities are those of all transitions for that peak.
- Doubly deuterated formaldehyde (D_2CO) – this species was not modeled because only a single partially blended transition was detected.

4. Discussion

4.1. Overall chemical composition

Despite originating from different clouds, G35.03 and G35.20 have similar (within an order of magnitude) abundances of all modeled species except deuterated isotopologues (see Sect. 4.4). We find peak B3 shows the highest abundances within G35.20 B versus H_2 of all species except for NH_2CHO and CH_3CHO, for which peak B1 has the highest abundance and H_2CO, for which peak B2 has the highest abundance.

It is possible that comparing the column densities of various complex organic molecules to that of H_2 is a less effective

Table 6. Column densities (cm^{-2}) determined via XCLASS for species with single transition detections.

	G35.20 A			G35.20 B1			G35.20 B2			G35.20 B3			G35.03 A		
Species	Size	50 K	100 K	Size	50 K	100 K	Size	50 K	100 K	Size	50 K	100 K	Size	50 K	100 K
$HN^{13}C$	1.5	3.1×10^{13}	4.1×10^{13}	0.8	1.7×10^{13}	1.6×10^{13}	1.0	1.6×10^{13}	1.6×10^{13}	1.5	1.1×10^{14}	1.2×10^{14}	1.2	2.5×10^{12}	5.8×10^{12}
SO	1.5	3.6×10^{13}	3.6×10^{13}	1.4	3.7×10^{17}	3.6×10^{17}	1.2	3.7×10^{16}	1.7×10^{16}	1.2	3.7×10^{16}	1.1×10^{17}	1.3	2.4×10^{17}	1.1×10^{17}
$H^{13}CO+$	1.5	1.6×10^{13}	5.3×10^{12}	0.8	8.3×10^{12}	8.2×10^{12}	1.0	3.1×10^{13}	3.1×10^{13}	1.5	6.5×10^{12}	2.8×10^{13}	1.5	1.7×10^{13}	2.1×10^{13}
SiO	1.4	7.1×10^{13}	7.2×10^{13}	1.1	9.0×10^{13}	8.7×10^{13}	1.1	6.2×10^{12}	6.2×10^{12}	0.8	1.2×10^{11}	2.8×10^{11}	1.1	5.7×10^{13}	1.1×10^{14}
$C^{34}S$	1.7	2.8×10^{15}	1.2×10^{15}	1.2	3.4×10^{14}	2.9×10^{14}	1.0	4.6×10^{14}	3.5×10^{14}	1.1	5.3×10^{14}	6.8×10^{14}	1.5	8.1×10^{14}	7.1×10^{14}
HNCO	1.3	2.3×10^{16}	7.5×10^{16}	1.0	1.2×10^{16}	6.9×10^{15}	1.0	2.2×10^{15}	9.4×10^{14}	1.1	2.3×10^{16}	8.4×10^{15}	1.1	1.8×10^{16}	7.7×10^{15}
HDCO	1.5	1.6×10^{15}	2.6×10^{13}	1.2	4.5×10^{14}	1.0×10^{15}	1.0	1.7×10^{14}	2.6×10^{14}	1.5	1.6×10^{15}	1.5×10^{15}		N/A	
HDO	1.3	1.8×10^{18}	4.8×10^{17}	0.9	5.6×10^{17}	3.3×10^{16}	0.7	1.8×10^{17}	7.8×10^{15}	1.0	9.2×10^{17}	7.6×10^{16}		N/A	

Notes. Each peak was modeled with the excitation temperatures fixed at 50 K and 100 K. The source sizes are the measured diameter of the 3σ emission in arcseconds (″).

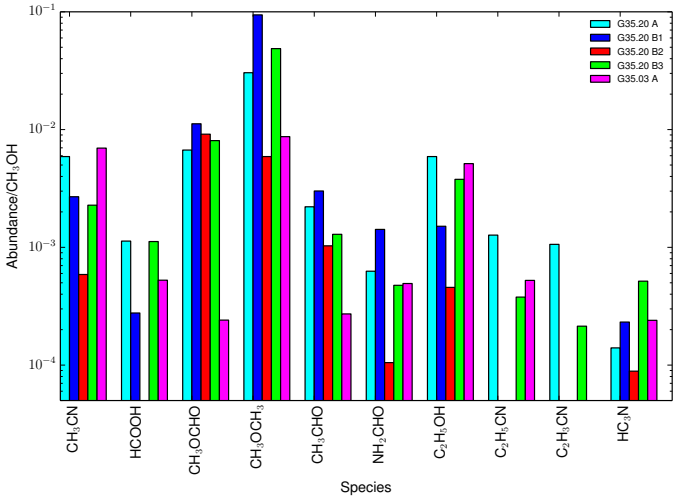

Fig. 10. Molecular abundances vs. CH_3OH as determined using the XCLASS software package for each of the sources modeled. The column densities for vibrationally excited states were added to the ν = 0 state for CH_3OH, CH_3CHO, CH_3CN, and HC_3N to determine abundances.

method of comparing abundances between these sources. The value for H_2 column density derived from the continuum (and therefore the dust) does not necessarily reflect the density of the warm dense gas where COMs are formed. Given the uncertainty of the H_2 column densities, we also estimated the abundances of some molecules relative to CH_3OH, whose emission is less resolved than the continuum emission. Figure 10 shows the relative abundance for several species. This figure confirms the main result of Fig. 7 namely that abundances in B3 are higher than the other continuum peaks in G35.20 B except in NH_2CHO and CH_3CHO. We thus conclude that B3 appears to be the most chemically rich of the three sources in G35.20 B. The ratio versus methanol for our sources are less than any of the different types of objects reviewed in Herbst & van Dishoeck (2009). Comparing the ratio of CH_3CN to CH_3OH in our sources to those in Öberg et al. (2013), we see that to reach a similar ratio in NGC 7538 IRS9, the gas would be over 7000 AU from the center.

In Öberg et al. (2014), it is suggested that the ratio of abundances of CH_3CHO + CH_3OCHO (X-CHO) and CH_3OCH_3 + C_2H_5OH (X-CH_3) is related to the temperature and type of source. Laboratory experiments have shown that higher abundance of CHO-bearing molecules indicates the importance of cold ice COM chemistry. If X-CHO/X-CH_3 is near 1, then the source is a cooler, lower mass source and a ratio much less than 1 corresponds to a hotter and more massive source. In line with their observation, we also see a higher ratio of X-CHO/X-CH_3 at the coolest peak, G35.20 B2, where the ratio is 1.6, and low ratios at the hottest peaks, G35.20 A, B1, B3, and G35.03 A (0.25, 0.15, 0.18, and 0.04, respectively). From Fig. 1 in Öberg et al. (2014), peak G35.20 B2 could be a massive hot core, but it could also be low mass, whereas peaks G35.20 A, B1, B3, and G35.03 A definitely fall into the massive hot core regime, where warm ice chemistry becomes more important.

Our XCLASS model fits show higher or nearly equal column densities for several vibrationally excited states versus their ground states. The XCLASS analysis is satisfactory as long as the energy of the lines span a relatively small range, but a single temperature model is inadequate to fit lines with very different excitation energy. Because of the presence of temperature gradients in these sources, the ground state lines and vibrationally excited lines can be fitted with significantly different temperatures since they trace gas originating from smaller areas with equal or higher column densities.

4.2. Chemical segregation in G35.20

Sánchez-Monge et al. (2013) show evidence for a Keplerian disk in core B of G35.20. When analyzing the chemical structure of this core at continuum peaks B1, B2, and B3, we see a striking chemical difference within this disk, which argues against a simple axisymmetric disk scenario. Our data show clear evidence for chemical segregation of the G35.20 core on a scale of 100s of AU. Nitrogen-bearing species, especially those containing the cyanide (CN) group (HC_3N, C_2H_5CN, etc.), are only observed in A and the southern part of B (peak B3) except for CH_3CN ν = 0, which appears in all four locations, although the abundance compared to CH_3OH at B3 is four times that at B2; $HN^{13}C$, where the abundance versus CH_3OH at B3 is six times more than at B2; and HC_3N ν = 0, where the abundance compared to CH_3OH at B3 is 7.5 times that at B2 (see Fig. 10). The linear scale for this separation of chemistry is less than 1000 AU, which is the smallest observed chemical separation in a star-forming region to date. Figures 8 and 11 show that cyanides (HC_3N, C_2H_5CN, etc.) are only observed toward A and the southern part of B with higher abundances at peak B3 and low abundances or missing emission toward B1 and B2.

There are three plausible scenarios to explain this chemical differentiation. First, core B could be a disk in the process of fragmenting on scales that are not well resolved in this dataset, where each of the fragments are developing their own chemistry. Second, there could also be two or three distinct sources within

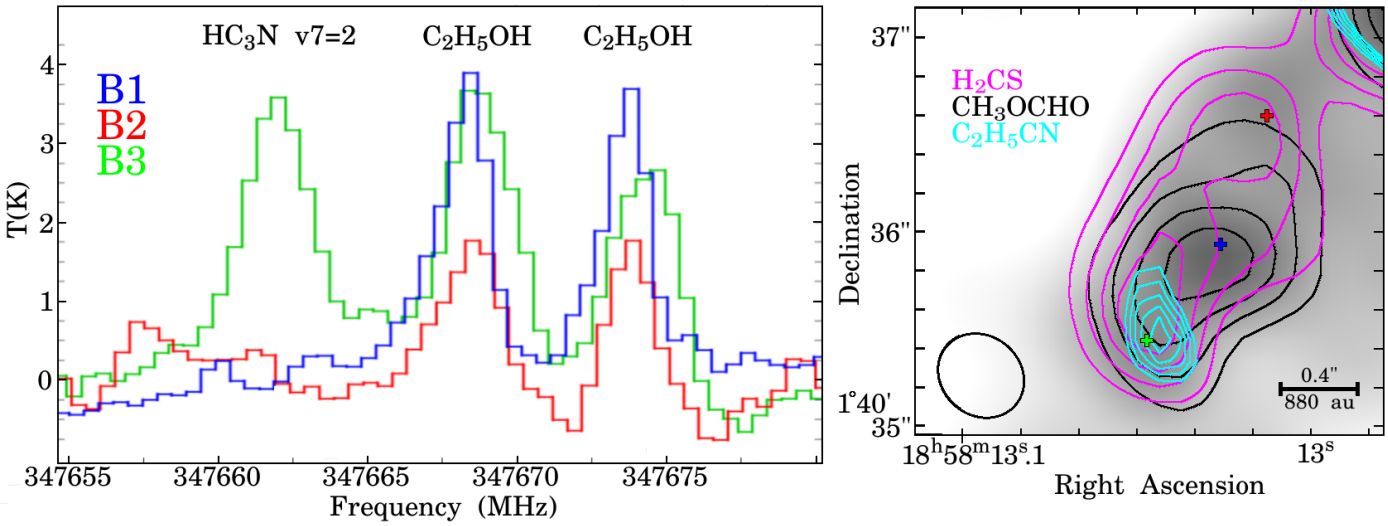

Fig. 11. G35.20 core B shows clear evidence for small-scale chemical segregation. On the *left* are spectra extracted from each continuum peak in core B (corresponding to the red, blue, and green crosses in the map to the *right*). It can clearly be seen in the spectra that the N-bearing species (HC_3N) is only strong in B3, where the O-bearing species (C_2H_5OH) is strong in all 3 regions. On the *right*, the integrated intensity contours of H_2CS $10_{1,9}$–$9_{1,8}$ (0.55, 0.94, 1.34, and 1.73 Jy/beam km s^{-1}), CH_3OCHO $27_{9,18}$–$26_{9,17}$ (0.70, 1.28, 1.85, and 2.43 Jy/beam km s^{-1}), and C_2H_5CN $40_{1,39}$–$39_{1,38}$ (0.085, 0.100, 0.115, 0.130, and 0.145 Jy/beam km s^{-1}) are shown overlaid on the continuum (grayscale) for core B of G35.20. While the O- and S-bearing organics are distributed across core B, the N-bearing species is only found toward the southwestern part.

core B, each uniquely influencing the chemistry of their surroundings, which could be due to evolutionary age and/or physical conditions. If the higher kinetic temperature of this region is driving the nitrogen enrichment, Crockett et al. (2015) showed that cyanides can also be made more easily in the hot gas phase than other COMs. If the age is a factor, then an age difference between sources would affect the chemistry of the surroundings. With enhanced abundances of almost all species, it is possible that B3 contains the hottest source in a multicore system sharing a circumcluster disk with sources at B1 and B2.

Third, G35.20B could be a disrupted disk, where it is possible that there are chemical changes within the rotation period of the disk, which is 9700–11 100 yr (based on the observed radial velocity 3.5–4 km s^{-1} and minimum linear diameter of 2500 AU and assuming an edge-on circular orbit). This is quite a short period of time chemically, although warm-up chemical models like those seen in Crockett et al. (2015) show a sharp increase in abundance from 10^{-10} to 10^{-8} over about 5000 yr for CH_3CN. Although N-bearing species are limited to the east side of the disk, N- and O-bearing species formamide (NH_2CHO) and isocyanic acid (HNCO) have a more extended range but show significantly reduced emission at B2 as seen in Fig. 12. These chemical relationships will be further investigated in a following paper using chemical models.

4.3. HNCO and formamide co-spatial emission

It has previously been proposed (Bisschop et al. 2007; Mendoza et al. (2014; López-Sepulcre et al. 2015) based on single dish observations that formamide (NH_2CHO) forms through the hydrogenation of HNCO because there appears to be a constant abundance ratio across a large range of source luminosities and masses. Figure 12 shows that these two species have almost the same spatial extent in G35.20 B and their emission peaks are only 0.15″ (or ∼300 AU) apart in G35.20 B. The separation is less than 0.11″ (240 AU) in G35.20 A. The velocity intervals spanned by the line peak velocities in each pixel differ by only 0.5–1 km s^{-1}. Our modeled abundance values show N(HNCO)/N(NH_2CHO) is between 2 and 8 for HNCO at 50 K and between 1 and 10 for HNCO modeled at 100 K.

In G35.03, the HNCO and formamide emissions have a separation of less than 0.11″ (255 AU), with the velocity peak differences between 0.5 and 1.0 km s^{-1}. The striking physical connection between these two species makes a strong case for the formation of formamide predominantly through the hydrogenation of HNCO. Coutens et al. (2016) has also recently observed co-spatial emission in HNCO and formamide in the low-mass protobinary system IRAS 16293.

4.4. Deuteration

We detect seven deuterated species in G35.20, four of which we detect with only one or two observed transitions. We determined the deuterium fractionation of the other three, i.e., CH_2DCN, CH_2DOH, and CH_3CHDCN, using rotation diagrams in Cassis for consistency because CH_2DOH was not in the XCLASS database. From these rotation diagrams, we calculated the D/H values based on the best-fit column densities obtained using the opacity function in Cassis. Relatively little has previously been written about the D/H ratio in methyl cyanide (CH_3CN). In its place of first discovery, Orion KL, the D/H ratio is 0.4–0.9% (Gerin et al. 1992). In a recent paper by Belloche et al. (2016), CH_2DCN was detected in Sgr B2 with a D/H of 0.4%. A D/H for methyl cyanide of 1.3% was also reported in Taquet et al. (2014) in low-mass protostar IRAS 16293-2422. Our values for G35.20 are significantly higher and the varying deuterium fractionation across core B is quite pronounced for this species. The D/H range in methyl cyanide for each continuum peak is 1–11% at A, 0.3–6% at B1, and 7–21% at B3. Only one unblended transition of CH_2DCN was detected at continuum peak B2, so the D/H could not be determined. The D/H percentages for methyl cyanide determined using the XCLASS fits were 10% at A, 0.4% at B1, and 15% at B3, which fall within the ranges determined using Cassis. We are therefore justified in using Cassis to determine D/H for methanol.

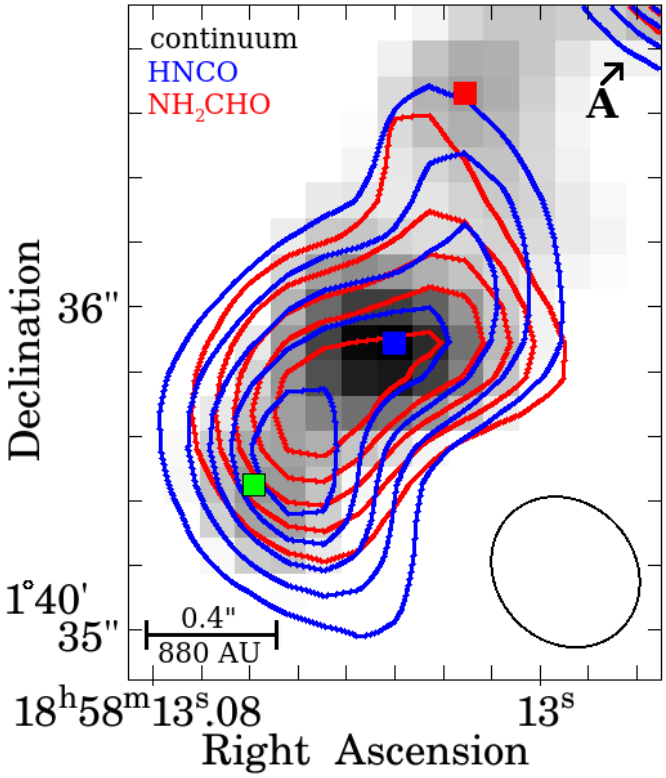

Fig. 12. Formamide $16_{2,15}$–$15_{2,14}$ (red contours) and HNCO $16_{1,16}$–$15_{1,15}$ (blue contours) emissions are shown overlaid on the dust continuum (grayscale) for core B. These N- and O-bearing species are present in B3 and B1, but B2 is just outside the outermost contour (indicating 1σ). The red contours are 0.20, 0.33, 0.47, 0.61, and 0.74 Jy/beam km s^{-1} and the blue contours are 0.40, 0.75, 1.10, 1.45, and 1.80 Jy/beam km s^{-1}. B1, B2, and B3 are denoted with colored boxes as in Fig. 1.

Table 7. Deuterium fractionation percentages (%) at continuum peaks in G35.20 as calculated using Cassis.

Source	$\frac{\text{CH2DCN}}{\text{CH3CN}}$	$\frac{\text{CH2DOH}}{\text{CH3OH}}$	$\frac{\text{CH3CHDCN}}{\text{CH3CH2CN}}$
A	6 ± 5	4^{+4}_{-2}	13^{+13}_{-10}
B1	$3^{+3}_{-2.7}$	4^{+3}_{-2}	×
B2	×	5^{+3}_{-2}	×
B3	12^{+9}_{-5}	6^{+4}_{-3}	×

Notes. Deuterated ethyl cyanide is only detected at peak A and determining deuterium fractionation for methyl cyanide was not possible for B2.

Deuteration in methanol has been more widely studied. In low-mass star-forming regions the CH_2DOH/CH_3OH abundance fraction has been observed to be about 37% (Parise et al. 2002) in IRAS 16293, and in prestellar core L1544 it was close to 10% (Bizzocchi et al. 2014). For G35.20, the D/H ratio was 3–9% at peaks B1 and B2, 4–12% at B3, and 7–17% at A. These values are very similar across core B, although they are slightly enhanced at B3. It is possible that because the methanol emission is more extended, it is more homogeneous. The extra few percent at B3 could be linked to the high temperature and the possibility that this region has heated up recently allowing any deuterium enhancement on the grain surfaces to be released in the gas phase.

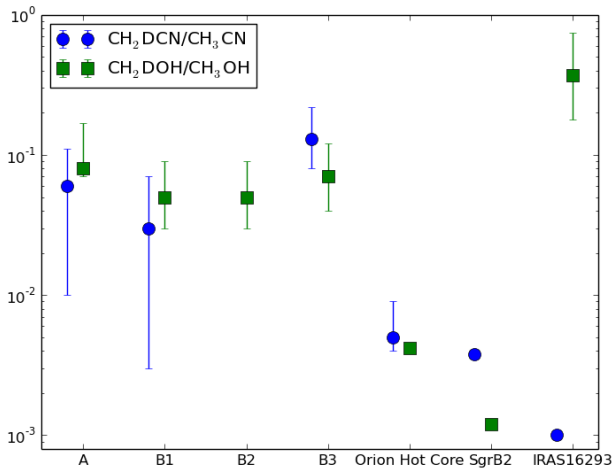

Fig. 13. D/H fractions for the four continuum peaks in G35.20 compared to the Orion hot core (HC), Sgr B2, and IRAS 16 293–2422. The deuterium fractionation in G35.20 is higher than that of other high-mass star-forming regions in Orion and the Galactic center, but lower (for methanol) than in the low-mass star-forming region IRAS 16293. The methyl cyanide D/H value for IRAS 16293 is from an unpublished analysis reported in Taquet et al. (2014).

Deuterated ethyl cyanide was detected at A with five unblended transitions, eight partially blended transitions, and two identifiable blended transitions. The errors are larger for this species owing to the line blending, but the D/H value for ethyl cyanide using Cassis was found to be between 3 and 26% with a best-fit value of 12% and the D/H from the XCLASS fit is 19%. A summary of these results is shown in Table 7 and Fig. 13.

In contrast, there is almost no sign of deuteration in G35.03. The presence of CH_2DOH is shown through a single line with a brightness temperature of less than 1 K, and HDO is not clearly present as it is either blended with other transitions or offset from v_{LSR} by more than 3 km s^{-1}. HDCO may be present, but is blended with other lines. Our RADEX analysis indicates that the kinetic temperature of the gas around peaks B3 and G35.03 is over 300 K, so the deuterium fraction is unlikely to be tied to the kinetic temperature in these hot cores. From our results there is no clear trend with either mass or temperature and deuterium fraction.

A high fraction of deuterium can indicate that an object is very young ($<10^5$ yr) as deuterated species are formed in cold environments where CO has been depleted onto dust grains (Millar et al. 1989). Once CO returns to the gas phase, deuterated species are destroyed, so a high deuterium fraction indicates that CO has only sublimated recently. We conclude that B3 is a much younger region than the hot core in G35.03, and in the case of multiple sources within the disk of core B, sublimation of CO from ice grains has happened at different times or rates across the core.

4.5. Comparison to other hot cores

The hot core and compact ridge in Orion KL (separation ~5000 AU) show a chemical difference between N-bearing and O-bearing species. In Caselli et al. (1993), the authors use a time-dependent model to explain the chemistry of both regions. In this model, shells at different distances were collapsing toward the nearby object IRc2, but when accretion stopped the regions heated up and the grain mantles sublimated showing different chemistry. The model does not perfectly replicate the Orion KL region, but is still a reasonable explanation. In G35.20,

there is no clear nearby accreting (or formerly accreting) object that could have caused this same scenario.

The chemical differentiation between W3(OH) and W3(H_2O) (Wyrowski et al. 1999b) shows that the latter is a strong N-bearing source with various complex organics, but the former only contains a handful of O-bearing species (both contain CH_3CN). In Qin et al. (2016), they conclude that this region is undergoing global collapse, but W3(OH) contains an expanding HII region, whereas W3(H_2O) contains a young stellar object that is accreting material but also has an outflow. This is similar to G35.20, but on a larger scale; the separation between these two sources is ~7000 AU.

Jiménez-Serra et al. (2012) observed that AFGL2591 has a hole in the methanol emission (diameter ~3000 AU), which is explained using concentric shells where methanol is mainly in a cooler outer shell and S- and N-bearing chemistry are driven by molecular UV photodissociation and high-temperature gas-phase chemistry within the inner shell where the extinction is lower. This differs from G35.20 because the hot N-bearing regions are toward the outer edges of the emission with O- and S-bearing species found between.

Of the three regions where chemical differentiation has been observed, G35.20 core B is most similar to W3(OH) and W3(H_2O). Chemical differences would reasonably be seen if core B contains multiple objects at different evolutionary stages.

5. Conclusions

This work describes the chemical composition of G35.20–0.74N and G35.03+0.35, while providing a template for future chemical study of hot cores in this wavelength regime. Chemical segregation in high-mass star-forming regions is observed on a small scale (<1000 AU) showing that the high spatial resolution capabilities of ALMA are needed to determine whether such segregation is common. Further observations are needed to determine whether core B in G35.20–0.74N contains a single or multiple sources. While the CH_3CN emission points to Keplerian rotation (Sánchez-Monge et al. 2013), the continuum implies several protostars and the chemical variation across the proposed disk indicates a complicated source unlike simpler low-mass disks. Both of the regions studied showed co-spatial emission from HNCO and NH_2CHO indicating a chemical link. Various deuterated species were detected at G35.20 peak B3 indicating a very young region. In contrast, G35.03 A shows no obvious deuteration.

Higher spatial resolution ALMA observations of this object are planned. This will allow us to better resolve the emission from core A and better determine the nature of the velocity gradient there. In addition it may allow us to better determine the origin of the chemical segregation in core B.

The XCLASS software package has a routine that carries out LTE analysis of each point in a map to demonstrate temperature and density differences pixel by pixel. Follow up work will be performed with this LTE analysis and non-LTE map analysis will be carried out with RADEX.

Time-dependent chemical modeling will help to determine if age is a significant factor in the presence of chemical segregation in star-forming regions. A physical chemical model can also help understand the nature of hot cores.

Acknowledgements. We would like to show our gratitude to the late Malcolm Walmsley, who acted as referee for this paper. His careful reading and numerous insightful comments have shaped this work into its complete form. This paper makes use of the following ALMA data: ADS/JAO.ALMA 2011.0.00275.S. ALMA is a partnership of ESO (representing its member states), NSF (USA) and NINS (Japan), together with NRC (Canada) and NSC and ASIAA (Taiwan), in cooperation with the Republic of Chile. The Joint ALMA Observatory is operated by ESO, AUI/NRAO, and NAOJ. This paper made use of information from the Red MSX Source survey database at `http://rms.leeds.ac.uk/cgi-bin/public/RMS_DATABASE.cgi`, which was constructed with support from the Science and Technology Facilities Council of the UK. Á.S.-M. is supported by Deutsche Forschungsgemeinschaft through grant SFB 956 (subproject A6).

References

Anders, E., & Grevesse, N. 1989, Geochim. Cosmochim. Acta, 53, 197
Belloche, A., Menten, K. M., Comito, C., et al. 2008, A&A, 482, 179
Belloche, A., Müller, H. S. P., Menten, K. M., Schilke, P., & Comito, C. 2013, A&A, 559, A47
Belloche, A., Müller, H. S. P., Garrod, R. T., & Menten, K. M. 2016, A&A, 587, A91
Beltrán, M. T., & de Wit, W. J. 2016, A&ARv, 24, 6
Beltrán, M. T., Codella, C., Viti, S., Neri, R., & Cesaroni, R. 2009, ApJ, 690, L93
Beltrán, M. T., Sánchez-Monge, Á., Cesaroni, R., et al. 2014, A&A, 571, A52
Bisschop, S. E., Jørgensen, J. K., van Dishoeck, E. F., & de Wachter, E. B. M. 2007, A&A, 465, 913
Bizzocchi, L., Caselli, P., Spezzano, S., & Leonardo, E. 2014, A&A, 569, A27
Bonnell, I. A., & Smith, R. J. 2011, Computational Star Formation, Proc. Int. Astron. Union, IAU Symp., 270, 57
Brinch, C., & Hogerheijde, M. R. 2010, A&A, 523, A25
Caselli, P., Hasegawa, T. I., & Herbst, E. 1993, ApJ, 408, 548
Cesaroni, R., Galli, D., Lodato, G., Walmsley, M., & Zhang, Q. 2006, Nature, 444, 703
Chin, Y.-N., Henkel, C., Whiteoak, J. B., Langer, N., & Churchwell, E. B. 1996, A&A, 305, 960
Coutens, A., Jørgensen, J. K., van der Wiel, M. H. D., et al. 2016, A&A, 590, L6
Crockett, N. R., Bergin, E. A., Neill, J. L., et al. 2015, ApJ, 806, 239
Drozdovskaya, M. N., Walsh, C., Visser, R., Harsono, D., & van Dishoeck, E. F. 2015, MNRAS, 451, 3836
Esplugues, G. B., Tercero, B., Cernicharo, J., et al. 2013, A&A, 556, A143
Gerin, M., Combes, F., Wlodarczak, G., et al. 1992, A&A, 259, L35
Green, S. 1986, ApJ, 309, 331
Herbst, E., & van Dishoeck, E. F. 2009, ARA&A, 47, 427
Hogerheijde, M. R., & van der Tak, F. F. S. 2000, A&A, 362, 697
Jiménez-Serra, I., Zhang, Q., Viti, S., Martín-Pintado, J., & de Wit, W.-J. 2012, ApJ, 753, 34
Keto, E. 2007, ApJ, 666, 976
Kraus, S., Hofmann, K.-H., Menten, K. M., et al. 2010, Nature, 466, 339
Krumholz, M. R., Klein, R. I., McKee, C. F., Offner, S. S. R., & Cunningham, A. J. 2009, Science, 323, 754
López-Sepulcre, A., Jaber, A. A., Mendoza, E., et al. 2015, MNRAS, 449, 2438
McKee, C. F., & Tan, J. C. 2003, ApJ, 585, 850
Mendoza, E., Lefloch, B., López-Sepulcre, A., et al. 2014, MNRAS, 445, 151
Millar, T. J., Bennett, A., & Herbst, E. 1989, ApJ, 340, 906
Möller, T., Endres, C., & Schilke, P. 2017, A&A, 598, A7
Müller, H. S. P., Schlöder, F., Stutzki, J., & Winnewisser, G. 2005, J. Mol. Struct., 742, 215
Öberg, K. I., Boamah, M. D., Fayolle, E. C., et al. 2013, ApJ, 771, 95
Öberg, K. I., Fayolle, E. C., Reiter, J. B., & Cyganowski, C. 2014, Faraday Discussions, 168, 81
Parise, B., Ceccarelli, C., Tielens, A. G. G. M., et al. 2002, A&A, 393, L49
Pickett, H. M., Poynter, R. L., Cohen, E. A., et al. 1998, J. Quant. Spectr. Rad. Transf., 60, 883
Qin, S.-L., Schilke, P., Wu, J., et al. 2016, MNRAS, 456, 2681
Sánchez-Monge, Á., Cesaroni, R., Beltrán, M. T., et al. 2013, A&A, 552, L10
Sánchez-Monge, Á., Beltrán, M. T., Cesaroni, R., et al. 2014, A&A, 569, A11
Schöier, F. L., van der Tak, F. F. S., van Dishoeck, E. F., & Black, J. H. 2005, A&A, 432, 369
Tan, J. C., Beltrán, M. T., Caselli, P., et al. 2014, Protostars and Planets VI, 149
Taquet, V., Charnley, S. B., & Sipilä, O. 2014, ApJ, 791, 1
van der Tak, F. F. S., Black, J. H., Schöier, F. L., Jansen, D. J., & van Dishoeck, E. F. 2007, A&A, 468, 627
Wang, K.-S., Bourke, T. L., Hogerheijde, M. R., et al. 2013, A&A, 558, A69
Wu, Y. W., Sato, M., Reid, M. J., et al. 2014, A&A, 566, A17
Wyrowski, F., Schilke, P., & Walmsley, C. M. 1999a, A&A, 341, 882
Wyrowski, F., Schilke, P., Walmsley, C. M., & Menten, K. M. 1999b, ApJ, 514, L43
Zhang, B., Zheng, X. W., Reid, M. J., et al. 2009, ApJ, 693, 419
Zinnecker, H., & Yorke, H. W. 2007, ARA&A, 45, 481

Appendix A: Properties of detected lines

Table A.1. Detected lines organized by frequency with species, upper energy level (K), and Einstein coefficients (s^{-1}) indicated.

Species	Frequency (MHz)	E_{up} (K)	A_{ij} (s^{-1})
CH_3OH $\nu = 0$	334 970	166.0	3.42E-8
CH_3CHO $\nu = 0$	334 980	359.9	1.28E-3
CH_3OCHO $\nu = 1$	335 016	443.5	5.33E-4
aGg'$(CH_2OH)_2$	335 030	279.4	9.34E-4
$HC^{13}CCN$ $\nu = 0$	335 092	305.6	3.01E-3
HDCO	335 097	56.2	1.04E-3
CCCS	335 109	474.6	2.98E-3
$HCC^{13}CN$ $\nu = 0$	335 124	305.6	3.01E-3
CH_3OH $\nu = 0$	335 134	44.7	2.69E-5
CH_3OCHO $\nu = 0$	335 145	94.9	1.39E-5
CH_3OCHO $\nu = 0$	335 158	257.1	3.58E-4
$H_2C^{33}S$	335 160	101.7	5.53E-4
aGg'$(CH_2OH)_2$	335 180	316.7	8.51E-4
CH_3OCHO $\nu = 0$	335 183	257.1	4.40E-5
t-C_2H_5OH	335 192	311.6	5.72E-5
CH_3OCHO $\nu = 0$	335 208	281.6	3.89E-5
CH_3OH $\nu = 0$	335 222	336.7	3.85E-8
CH_3CHO $\nu = 2$	335 224	469.0	8.96E-4
CH_3CHDCN	335 229	332.8	3.00E-4
NH_2CDO	335 234	170.5	2.61E-3
CH_3CHDCN	335 237	332.8	3.20E-3
CH_3CHDCN	335 239	332.8	3.20E-3
CH_3CHDCN	335 246	332.8	3.00E-4
C_2H_5CN	335 274	733.9	1.87E-4
CH_3CHO $\nu = 0$	335 318	154.9	1.30E-3
aGg'$(CH_2OH)_2$	335 357	319.7	8.15E-4
CH_3CHO $\nu = 0$	335 358	154.8	1.29E-3
CH_3OH $\nu = 0$	335 363	112.7	8.78E-8
$CH_3^{13}CH_2CN$	335 363	386.5	1.74E-4
$CH_3^{13}CH_2CN$	335 369	325.9	3.13E-3
CH_3CHO $\nu = 1$	335 382	361.5	1.31E-3
CH_3OCHO $\nu = 1$	335 392	453.0	5.66E-3
HDO	335 396	335.3	2.61E-5
aGg'$(CH_2OH)_2$	335 397	316.7	8.53E-4
CH_3OCHO $\nu = 0$	335 403	94.9	3.83E-5
$NH_2^{13}CHO$	335 403	149.1	2.74E-3
CH_3CHDCN	335 427	501.8	2.78E-3
CH_3CHDCN	335 430	476.0	2.84E-3
t-C_2H_5OH	335 441	293.6	2.17E-4
CH_3OCHO $\nu = 0$	335 454	94.9	2.44E-5
CH_3CHDCN	335 511	330.0	3.18E-3
CH_3CHDCN	335 513	430.1	2.95E-3
^{13}CH3OH	335 560	192.7	4.04E-4
CH_3OH $\nu = 0$	335 582	79.0	1.63E-4
t-C_2H_5OH	335 631	293.6	2.17E-4
aGg'$(CH_2OH)_2$	335 657	288.7	2.98E-4
CH_3OH $\nu = 0$	335 702	1074.0	5.64E-5
aGg'$(CH_2OH)_2$	335 739	304.8	9.77E-4
$H^{13}CCCN$ $\nu_7 = 1$	335 760	632.5	3.01E-3
$CH_3^{18}OH$	335 775	218.4	9.61E-4
CH_2DOH	335 796	381.1	3.98E-5
$H_2C^{18}O$	335 815	60.2	1.05E-3

Notes. Most species are detected in all sources. Ethylene glycol (aGg'$(CH_2OH)_2$) was only detected in G35.20 A and G35.03 A and deuterated ethyl cyanide (CH_3CHDCN) was only detected in G35.20 A. For specific transitions see Appendix B.

Table A.1. continued.

Species	Frequency (MHz)	E_{up} (K)	A_{ij} (s^{-1})
CH_3OCHO $\nu = 0$	335 828	225.2	3.95E-5
CH_3OCHO $\nu = 0$	335 839	225.2	6.97E-4
$HC^{13}CCN$ $\nu_7 = 1$	335 883	622.2	3.01E-3
C_2H_5CN	335 895	664.1	1.85E-4
CH_3OCHO $\nu = 0$	335 900	277.8	2.69E-4
aGg'$(CH_2OH)_2$	335 906	308.9	7.63E-4
HCC13CN ($v6 = 1$)	335 921	1009.6	3.02E-3
$HCC^{13}CN$ $\nu_7 = 1$	335 930	624.7	3.01E-3
t-C_2H_5OH	335 950	87.9	1.61E-4
CH_3OCHO $\nu = 1$	335 961	443.6	5.34E-4
CH_3CHDCN	335 989	478.7	1.75E-4
CH_2DOH	335 997	94.4	1.12E-4
aGg'$(CH_2OH)_2$	336 012	309.6	8.39E-4
CH_3CHO $\nu = 2$	336 025	535.3	1.31E-3
CH_3OCHO $\nu = 0$	336 028	277.8	5.14E-4
g-C_2H_5OH	336 030	227.3	3.35E-4
CH_3OCHO $\nu = 0$	336 032	277.8	5.39E-3
CH_3OCHO $\nu = 0$	336 086	277.9	5.39E-3
SO_2	336 089	276.0	2.67E-4
$CH_3^{18}OH$	336 100	35.1	1.83E-4
CH_3OCHO $\nu = 0$	336 111	277.9	5.15E-4
NH_2CHO $\nu = 0$	336 136	149.7	2.76E-3
t-C_2H_5OH	336 158	274.2	2.17E-4
NH_2CHO $\nu = 0$	336 161	135.5	1.20E-4
CH_3OCHO $\nu = 0$	336 219	277.9	2.70E-4
aGg'$(CH_2OH)_2$	336 223	304.7	7.84E-4
$H^{13}CCCN$ $\nu_7 = 1$	336 227	632.9	3.02E-3
t-C_2H_5OH	336 270	274.2	2.17E-4
aGg'$(CH_2OH)_2$	336 323	288.4	9.23E-4
CH_2DOH	336 325	442.1	1.35E-4
aGg'$(CH_2OH)_2$	336 334	301.9	8.63E-4
CH_3OCHO $\nu = 0$	336 351	249.4	5.49E-4
CH_3OCHO $\nu = 0$	336 355	230.6	9.84E-3
CH_3OCHO $\nu = 0$	336 368	249.4	5.49E-4
CH_3OCHO $\nu = 0$	336 374	230.6	5.57E-4
$HCC^{13}CN$ $\nu_7 = 1$	336 410	625.1	3.03E-3
CH_3CHO $\nu = 1$	336 416	359.6	1.30E-3
CH_3CHDCN	336 425	361.4	3.13E-3
CH_3OH $\nu = 0$	336 438	488.2	3.63E-5
CH_3CHDCN	336 453	361.4	3.13E-3
HC_3N ($\nu = 0$)	336 520	306.9	3.05E-3
SO	336 553	142.9	6.25E-6
g-C_2H_5OH	336 572	232.3	3.37E-4
CH_3OH $\nu = 2$	336 606	747.4	1.63E-4
C_2H_5CN	336 614	108.2	1.01E-4
t-C_2H_5OH	336 626	162.6	1.34E-4
SO_2	336 670	245.1	5.84E-5
$CH_3^{18}OH$	336 743	100.9	1.50E-4
aGg'$(CH_2OH)_2$	336 756	316.7	9.45E-4
t-C_2H_5OH	336 767	255.7	2.16E-4
g-C_2H_5OH	336 795	228.0	3.42E-4
aGg'$(CH_2OH)_2$	336 828	266.3	8.95E-4
t-C_2H_5OH	336 832	255.7	2.16E-4
CH_3OH $\nu = 0$	336 865	197.1	4.07E-4
CH_3OCHO $\nu = 0$	336 889	235.5	5.53E-4
CH_3OCHO $\nu = 0$	336 918	235.5	5.53E-4
aGg'$(CH_2OH)_2$	336 939	300.6	8.63E-4
CH_3OH $\nu = 2$	336 970	1022.7	4.56E-5

Table A.1. continued.

Species	Frequency (MHz)	E_{up} (K)	A_{ij} (s^{-1})
CH_3OH $\nu = 2$	337 022	971.8	1.36E-4
CH_3OH $\nu = 2$	337 030	941.4	1.55E-4
C_2H_3CN	337 040	309.7	3.19E-3
C_2H_3CN	337 051	308.4	3.14E-3
C17O	337 060	32.0	2.32E-6
CH_3OH $\nu = 2$	337 066	943.1	1.12E-4
HC_3N $\nu_6 = 1$	337 070	1025.1	3.05E-3
CH_3OH $\nu = 2$	337 079	901.5	8.38E-5
CH_3CHO $\nu = 2$	337 082	526.1	1.26E-3
aGg'$(CH_2OH)_2$	337 082	309.1	5.46E-4
CH_3OH $\nu = 2$	337 099	935.2	8.14E-5
CH_3OH $\nu = 2$	337 114	855.8	1.65E-4
CH_3OH $\nu = 2$	337 118	932.6	4.41E-5
$H_2C^{34}S$	337 125	89.1	5.77E-4
CH_3OH $\nu = 0$	337 136	61.6	1.58E-5
CH_3OH $\nu = 2$	337 159	755.0	4.54E-5
CH_3OH $\nu = 2$	337 175	801.4	1.15E-4
CH_3OH $\nu = 2$	337 186	791.1	1.68E-4
CH_3OH $\nu = 2$	337 198	690.2	8.26E-5
CH_3OH $\nu = 2$	337 252	722.8	1.39E-4
CH_3OH $\nu = 2$	337 274	679.3	1.13E-4
CH_3OH $\nu = 2$	337 279	701.8	1.54E-4
CH_3OH $\nu = 2$	337 284	573.0	2.16E-4
CH_3OH $\nu = 1$	337 297	390.0	1.65E-4
CH_3OH $\nu = 1$	337 303	651.0	1.55E-4
CH_3OH $\nu = 2$	337 312	588.9	1.65E-4
t-C_2H_5OH	337 323	238.0	2.15E-4
HC_3N $\nu_6 = 1$	337 335	1025.3	3.06E-3
HC_3N $\nu_7 = 1$	337 344	629.0	3.05E-3
C_2H_5CN	337 347	322.4	3.23E-3
CH_2DOH	337 349	96.3	1.46E-4
$C^{34}S$	337 400	64.8	8.04E-4
CH_3OCH_3	337 421	220.1	1.76E-4
t-HCOOH	337 429	386.6	2.80E-4
t-HCOOH	337 436	446.8	2.43E-4
t-HCOOH	337 444	332.8	3.13E-4
C_2H_5CN	337 445	322.4	3.23E-3
$H_2C^{34}S$	337 460	299.8	4.86E-4
CH_3OH $\nu = 1$	337 464	357.5	1.69E-4
CH_3OH $\nu = 1$	337 473	908.0	3.6E-4
$H_2C^{34}S$	337 475	141.8	5.56E-4
CH_3OCHO $\nu = 0$	337 490	267.1	5.34E-4
CH_3OH $\nu = 1$	337 491	558.2	4.34E-5
t-HCOOH	337 492	110.5	2.35E-3
CH_3OCHO $\nu = 0$	337 504	267.1	5.34E-4
CH_3OH $\nu = 1$	337 519	482.2	1.38E-4
CH_3OH $\nu = 1$	337 546	485.4	8.13E-5
$H_2C^{34}S$	337 555	207.7	5.27E-4
$H_2C^{34}S$	337 559	207.7	5.27E-4
CH_3OH $\nu = 1$	337 582	428.2	1.13E-4
t-HCOOH	337 590	243.9	3.68E-4
CH_3OH $\nu = 1$	337 605	429.4	1.56E-4
CH_3OH $\nu = 1$	337 611	387.4	1.37E-4
CH_3OH $\nu = 1$	337 626	363.5	1.55E-4
CH_3OH $\nu = 1$	337 636	363.5	1.55E-4
CH_3OH $\nu = 1$	337 642	356.3	1.65E-4
CH_3OH $\nu = 1$	337 644	365.4	1.69E-4
CH_3OH $\nu = 1$	337 646	470.2	1.14E-4
CH_3OH $\nu = 1$	337 648	611.0	8.23E-5
CH_3OH $\nu = 1$	337 655	460.9	1.38E-4

Table A.1. continued.

Species	Frequency (MHz)	E_{up} (K)	A_{ij} (s^{-1})
CH_3OH $\nu = 1$	337 671	464.7	1.56E-4
CH_3OH $\nu = 1$	337 685	545.9	1.14E-4
CH_3OH $\nu = 1$	337 708	478.2	1.65E-4
CH_3OCH_3	337 712	48.0	7.22E-5
CH_3OCH_3	337 722	48.0	9.63E-5
t-C_2H_5OH	337 727	221.2	2.13E-4
CH_3OCH_3	337 731	48.0	1.94E-4
CH_3OH $\nu = 1$	337 749	488.5	1.69E-4
CH_3OCH_3	337 770	48.0	1.22E-4
CH_3OCH_3	337 779	48.0	1.94E-4
CH_3OCH_3	337 787	48.0	1.94E-4
CH_3OCH_3	337 790	48.0	7.22E-5
g-C_2H_5OH	337 801	223.1	3.45E-4
aGg'$(CH_2OH)_2$	337 816	294.6	9.74E-4
HC_3N $\nu_7 = 1$	337 825	629.0	3.07E-3
CH_3OH $\nu = 0$	337 838	675.9	6.04E-5
CH_3OH $\nu = 2$	337 878	747.7	1.65E-4
$H_2C^{34}S$	337 933	141.9	5.58E-4
$CH_3^{13}CH_2CN$	337 951	332.2	3.21E-3
CH_3OH $\nu = 1$	337 969	390.1	1.66E-4
CH_2DOH	337 977	202.5	5.47E-5
D_2CO	338 016	342.8	1.04E-6
H_2CS	338 083	102.4	5.77E-4
t-C_2H_5OH	338 099	205.2	2.11E-4
t-C_2H_5OH	338 110	205.2	2.11E-4
CH_3OH $\nu = 0$	338 125	78.1	1.70E-4
C_2H_5CN	338 142	316.8	3.27E-3
t-HCOOH	338 144	180.5	4.09E-4
t-HCOOH	338 202	158.3	4.23E-4
C_2H_3CN	338 214	312.1	3.23E-3
aGg'$(CH_2OH)_2$	338 214	313.4	9.40E-4
aGg'$(CH_2OH)_2$	338 221	292.7	8.05E-4
aGg'$(CH_2OH)_2$	338 240	313.4	9.28E-4
t-HCOOH	338 249	180.5	4.09E-4
C_2H_3CN	338 278	300.1	3.22E-3
SO_2	338 306	196.8	3.27E-4
$^{34}SO_2$	338 320	92.5	2.27E-4
CH_3OCHO $\nu = 0$	338 338	267.2	5.92E-3
CH_3OH $\nu = 0$	338 345	70.5	1.67E-4
CH_3OCHO $\nu = 0$	338 356	267.2	5.39E-4
CH_3OCHO $\nu = 1$	338 393	443.1	4.61E-3
CH_3OCHO $\nu = 0$	338 396	257.7	5.50E-4
CH_3OH $\nu = 0$	338 405	243.8	4.48E-5
CH_3OH $\nu = 0$	338 409	65.0	1.70E-4
CH_3OCHO $\nu = 0$	338 414	257.7	5.50E-4
CH_3OH $\nu = 0$	338 431	253.9	4.51E-5
CH_3OH $\nu = 0$	338 442	258.7	4.50E-5
C_2H_3CN	338 448	312.0	3.24E-3
CH_3OH $\nu = 0$	338 456	189.0	8.31E-5
CH_2DOH	338 463	120.0	5.87E-5
CH_3OH $\nu = 0$	338 475	201.1	8.30E-5
CH_3OH $\nu = 0$	338 486	202.9	8.35E-5
CH_3OH $\nu = 0$	338 504	152.9	1.14E-4
CH_3OH $\nu = 0$	338 512	145.3	1.15E-4
CH_3OH $\nu = 0$	338 530	161.0	1.15E-4
CH_3OH $\nu = 0$	338 541	114.8	1.39E-4
CH_3OH $\nu = 0$	338 543	114.8	1.39E-4
CH_3OH $\nu = 0$	338 560	127.7	1.40E-4
CH_3OH $\nu = 0$	338 583	112.7	1.39E-4
SO_2	338 612	198.9	2.87E-4

Table A.1. continued.

Species	Frequency (MHz)	E_{up} (K)	A_{ij} (s^{-1})
CH_3OH $\nu = 0$	338 615	86.1	1.71E-4
CH_3OH $\nu = 0$	338 640	102.7	1.57E-4
HC_3N $\nu_7 = 2$	338 646	953.8	3.07E-3
t-C_2H_5OH	338 672	175.7	2.04E-4
t-C_2H_5OH	338 674	175.7	2.04E-4
CH_2DOH	346 924	521.6	1.30E-4
C_2H_5CN	346 925	161.4	1.64E-4
g-C_2H_5OH	346 929	280.5	3.45E-4
CH_3CHO $\nu = 0$	346 934	268.7	1.22E-3
g-C_2H_5OH	346 939	280.5	3.45E-4
C_2H_3CN	346 943	325.0	3.46E-3
HC_3N $\nu_7 = 1$	346 949	645.6	3.32E-3
CH_3CHO $\nu = 0$	346 957	268.6	1.22E-3
t-C_2H_5OH	346 963	185.8	2.42E-4
C_2H_5CN	346 970	104.6	1.20E-4
C_2H_5CN	346 976	129.6	1.49E-4
C_2H_5CN	346 979	122.7	1.44E-4
$H_2C^{18}O$	346 984	239.6	4.33E-4
$H^{13}CO^+$	346 998	41.6	3.29E-3
CH_2DCN	347 043	175.0	3.65E-3
CH_3CHO $\nu = 0$	347 071	239.4	1.28E-3
CH_3CHO $\nu = 0$	347 090	239.4	1.28E-3
CH_2DCN	347 110	309.7	3.42E-3
$H_2C^{18}O$	347 133	156.7	7.70E-4
CH_3CHO $\nu = 0$	347 133	239.3	1.28E-3
$H_2C^{18}O$	347 144	156.7	7.70E-4
g-C_2H_5OH	347 147	275.5	3.45E-4
g-C_2H_5OH	347 158	275.5	3.45E-4
CH_2DCN	347 166	261.2	3.52E-3
^{13}CH3OH	347 188	254.3	4.36E-4
CH_2DCN	347 216	223.5	3.50E-3
CH_3CHO $\nu = 1$	347 217	420.4	1.33E-3
CH_2DCN	347 219	223.5	3.57E-3
CH_2DOH	347 222	521.6	1.32E-4
C_2H_3CN	347 232	328.7	3.50E-3
CH_3CHO $\nu = 1$	347 252	419.7	1.33E-3
CH_3CHO $\nu = 0$	347 288	214.7	1.33E-3
CH_3CHO $\nu = 0$	347 295	214.7	1.33E-3
SiO	347 330	75.0	2.21E-3
CH_3CHO $\nu = 0$	347 345	214.6	1.33E-3
CH_3CHO $\nu = 0$	347 349	214.6	1.33E-3
t-C_2H_5OH	347 351	99.7	1.75E-4
aGg'$(CH_2OH)_2$	347 361	330.4	1.02E-3
CH_3OH $\nu = 0$	347 370	45.5	1.08E-8
CH_2DOH	347 371	478.8	1.30E-4
aGg'$(CH_2OH)_2$	347 378	330.4	1.01E-3
aGg'$(CH_2OH)_2$	347 387	282.6	9.81E-4
CH_2DCN	347 388	196.6	3.62E-3
C_2H_3CN	347 434	328.7	3.46E-3
t-C_2H_5OH	347 446	185.9	2.67E-4
CH_3OH $\nu = 1$	347 448	856.3	4.04E-5
CH_3CHO $\nu = 1$	347 459	473.2	1.22E-3
g-C_2H_5OH	347 474	267.1	3.57E-4
CH_3OCHO $\nu = 0$	347 478	247.3	6.14E-4
aGg'$(CH_2OH)_2$	347 487	317.0	9.51E-4
CH_3OCHO $\nu = 0$	347 494	247.3	6.14E-4
CH_3OH $\nu = 0$	347 507	57.1	1.78E-8
CH_3CHO $\nu = 0$	347 519	178.7	1.41E-3

Table A.1. continued.

Species	Frequency (MHz)	E_{up} (K)	A_{ij} (s^{-1})
CH_3CHO $\nu = 0$	347 563	178.1	1.41E-3
CH_3OCHO $\nu = 1$	347 568	460.2	4.88E-3
$NH_2CH^{18}O$	347 589	161.0	3.10E-3
CH_3OCHO $\nu = 0$	347 590	104.4	4.00E-5
CH_3OCHO $\nu = 0$	347 599	104.4	3.40E-5
CH_3OCHO $\nu = 0$	347 605	306.8	5.49E-4
CH_2DOH	347 610	478.8	1.31E-4
CH_3OCHO $\nu = 0$	347 617	306.8	5.59E-4
CH_3OCHO $\nu = 0$	347 628	306.8	5.49E-4
CH_3CHO $\nu = 1$	347 645	507.4	2.50E-5
CH_3CHO $\nu = 0$	347 650	194.5	1.38E-3
CH_3CHO $\nu = 2$	347 657	544.7	1.38E-3
HC_3N $\nu_7 = 2$	347 663	967.8	3.33E-3
g-C_2H_5OH	347 670	262.2	3.57E-4
g-C_2H_5OH	347 675	267.1	3.57E-4
C_2H_3CN	347 685	707.5	1.19E-4
g-C_2H_5OH	347 693	189.7	1.07E-4
CH_3OCHO $\nu = 1$	347 698	437.8	6.73E-3
NH_2CHO $\nu = 0$	347 729	435.3	1.06E-4
aGg'$(CH_2OH)_2$	347 732	302.2	9.92E-4
aGg'$(CH_2OH)_2$	347 738	317.0	9.52E-4
CH_3OH $\nu = 0$	347 745	71.0	2.64E-8
g-C_2H_5OH	347 755	256.2	3.66E-4
CH_3CHO $\nu = 0$	347 756	194.4	1.36E-3
C_2H_3CN	347 759	316.7	3.50E-3
CH_2DOH	347 767	438.2	1.29E-4
^{13}CH3OH	347 788	302.5	6.74E-5
HC_3N $\nu_7 = 2$	347 791	970.5	3.32E-3
aGg'$(CH_2OH)_2$	347 813	115.3	1.12E-4
CH_3CHDCN	347 816	354.3	3.56E-3
CH_3OCHO $\nu = 0$	347 818	274.0	3.40E-4
aGg'$(CH_2OH)_2$	347 821	115.0	1.22E-4
CH_3CHO $\nu = 0$	347 830	194.5	1.36E-3
CH_3CHO $\nu = 0$	347 838	194.5	1.38E-3
^{13}CH3OH	347 848	572.9	7.63E-5
$CH_3^{18}OH$	347 865	142.7	1.51E-4
g-C_2H_5OH	347 887	262.2	3.58E-4
g-C_2H_5OH	347 916	251.4	3.67E-4
HC_3N $\nu_7 = 2$	347 924	970.6	3.33E-3
CH_2DOH	347 953	438.2	1.30E-4
aGg'$(CH_2OH)_2$	347 963	108.4	1.39E-4
t-C_2H_5OH	347 975	222.1	1.01E-4
CH_3OCH_3	347 985	581.8	1.18E-4
CH_3OCH_3	347 989	581.8	1.87E-4
CH_3OCH_3	347 992	581.8	1.87E-4
$NH_2CH^{18}O$	348 029	154.7	3.10E-3
$H_2C^{18}O$	348 032	97.5	1.02E-3
CH_3OCHO $\nu = 0$	348 050	266.1	6.10E-4
CH_3OCHO $\nu = 1$	348 053	491.3	4.67E-5
$CH_3^{18}OH$	348 053	283.4	1.04E-3
CH_3OCHO $\nu = 0$	348 066	266.1	6.10E-4
CH_3OCHO $\nu = 1$	348 084	469.7	5.58E-4
CH_3CHO $\nu = 1$	348 088	443.3	1.28E-3
^{13}CH3OH	348 100	162.4	1.08E-4
CH_3OH $\nu = 0$	348 123	87.3	3.27E-8
^{13}CH3CH2CN	348 147	352.3	3.51E-3
CH_2DOH	348 161	38.2	2.03E-4

Table A.1. continued.

Species	Frequency (MHz)	E_{up} (K)	A_{ij} (s^{-1})
CH_3CHO $\nu = 1$	348 211	383.2	1.41E-3
CH_3CHO $\nu = 1$	348 229	400.0	1.38E-3
CH_3OCHO $\nu = 1$	348 247	267.6	1.00E-4
C_2H_5CN	348 260	343.8	3.57E-3
NH_2CDO	348 283	162.4	3.11E-3
CH_3CHO $\nu = 1$	348 288	385.2	1.41E-3
aGg'$(CH_2OH)_2$	348 326	325.8	4.16E-4
aGg'$(CH_2OH)_2$	348 331	311.2	1.04E-3
$HN^{13}C$	348 340	41.8	2.03E-3
C_2H_5CN	348 344	351.0	3.58E-3
SO_2	348 388	292.7	1.91E-4
CH_2DOH	348 427	363.3	1.27E-4
$^{33}SO_2$	348 492	110.2	3.19E-4
CH_2DOH	348 529	363.3	1.28E-4
H_2CS	348 532	105.2	6.30E-4
aGg'$(CH_2OH)_2$	348 550	329.1	6.50E-4
C_2H_5CN	348 553	351.0	3.59E-3
CH_3CHO $\nu = 1$	348 570	418.2	1.34E-3
CH_3CHO $\nu = 1$	348 578	418.2	1.34E-3
CH_2DOH	348 592	139.7	6.76E-5
CH_2DOH	348 668	219.2	2.04E-5
CH_3OH $\nu = 0$	348 682	105.8	3.19E-8
CH_2DCN	348 691	181.2	3.69E-3
CH_2DOH	348 699	329.0	1.26E-4
g-C_2H_5OH	348 720	89.6	2.33E-4
$CH_3^{13}CN$	348 854	624.3	3.05E-3
CH_3CHO $\nu = 1$	348 855	398.3	1.38E-3
CH_3OCHO $\nu = 0$	348 909	294.6	4.65E-3
CH_3CN $\nu = 0$	348 911	745.4	2.87E-3
CH_3OCHO $\nu = 0$	348 915	294.6	5.72E-4
CH_2DOH	348 939	296.9	1.24E-4
$CH_3^{13}CN$	348 954	517.3	3.20E-3
CH_2DOH	348 990	296.9	1.25E-4
C_2H_3CN	348 991	325.1	3.19E-2
CH_3OCHO $\nu = 0$	349 015	257.3	4.08E-4
NH2CHO ($\nu = 1$)	349 020	568.5	3.09E-3
CH_3CN $\nu = 0$	349 025	624.0	2.10E-3
$CH_3^{13}CN$	349 040	424.6	3.34E-3
CH_3OCHO $\nu = 0$	349 049	294.6	5.72E-4
NH_2CHO $\nu = 0$	349 053	220.7	9.00E-5
CH_3OCHO $\nu = 0$	349 066	294.6	5.82E-4
CH_3OH $\nu = 0$	349 107	260.2	4.41E-4
$CH_3^{13}CN$	349 114	346.1	3.45E-3
CH_3CN $\nu = 0$	349 125	517.0	3.21E-3
CH_2DOH	349 149	267.0	1.23E-4
$CH_3^{13}CN$	349 174	281.9	3.55E-3
CH_2DOH	349 184	267.0	1.23E-4
CH_3CN $\nu = 0$	349 212	424.7	3.34E-3
$CH_3^{13}CN$	349 222	231.9	3.62E-3
$CH_3^{13}CN$	349 254	196.2	3.67E-3
$CH_3^{13}CN$	349 274	174.8	2.38E-3
$CH_3^{13}CN$	349 280	167.6	1.47E-3
CH_3CN $\nu = 0$	349 286	346.2	2.38E-3
$NH_2^{13}CHO$	349 309	152.6	3.1E-3
CH_3CHO $\nu = 1$	349 320	369.3	1.47E-3
c-HCOOH	349 326	157.4	1.66E-3
CH_2DOH	349 334	239.1	1.21E-4

Table A.1. continued.

Species	Frequency (MHz)	E_{up} (K)	A_{ij} (s^{-1})
CH_3CN $\nu = 0$	349 346	282.0	2.45E-3
aGg'$(CH_2OH)_2$	349 355	309.2	6.03E-4
CH_2DOH	349 356	239.1	1.21E-4
C_2H_5CN	349 380	495.2	3.29E-3
CH_3CN $\nu = 0$	349 393	232.0	2.50E-3
CH_2DOH	349 411	230.3	7.95E-5
CH_3CN $\nu = 0$	349 427	196.3	2.54E-3
CH_3CN $\nu = 0$	349 447	174.9	2.56E-3
CH_3CN $\nu = 0$	349 453	167.7	2.56E-3
CH_3OH $\nu = 0$	349 470	118.8	1.92E-8
NH_2CHO $\nu = 0$	349 482	153.0	3.10E-3
CH_3OCH_3	349 487	475.7	6.54E-5
CH_2DOH	349 495	213.4	1.18E-4
CH_2DOH	349 509	213.4	1.18E-4
aGg'$(CH_2OH)_2$	349 541	294.9	8.31E-4
C_2H_5CN	349 547	425.4	3.44E-3
C_2H_5CN	349 566	618.9	3.03E-3
D_2CO	349 630	80.4	1.11E-3
CH_2DOH	349 636	189.9	1.15E-4
CH_2DOH	349 644	189.9	1.15E-4
C_2H_5CN	349 652	655.3	2.95E-3
CH_3OCHO $\nu = 1$	349 685	459.9	6.26E-4
C_2H_5CN	349 730	406.6	3.49E-3
C_2H_5CN	349 751	693.8	2.87E-3
CH_3CHO $\nu = 2$	349 752	565.7	1.40E-3
CH_2DOH	349 757	168.5	1.11E-4
CH_2DOH	349 762	168.5	1.11E-4
C_2H_5CN	349 796	353.9	3.61E-3
CH_3OCH_3	349 803	66.5	3.30E-5
CH_3OCH_3	349 806	66.5	3.30E-5
CH_3OCH_3	349 809	66.5	3.30E-5
CH_3OCH_3	349 823	326.0	1.15E-5
CH_3OCH_3	349 826	326.0	1.15E-5
CH_3OCH_3	349 828	326.0	1.15E-5
CH_3OCH_3	349 830	326.0	1.15E-5
CH_3OCHO $\nu = 1$	349 836	401.3	3.32E-5
CH_2DOH	349 862	149.2	1.07E-4
CH_2DOH	349 864	149.2	1.07E-4
aGg'$(CH_2OH)_2$	349 867	338.1	1.04E-3
CH_3CHDCN	349 907	360.9	3.63E-3
CH_2DOH	349 952	132.1	1.00E-4
g-C_2H_5OH	349 997	256.5	3.73E-4
aGg'$(CH_2OH)_2$	350 023	305.1	1.11E-3
CH_2DOH	350 027	117.1	9.06E-5
C_2H_5CN	350 039	390.1	3.54E-3
C_2H_5CN	350 051	390.1	3.54E-3
CH_3CN $v_8 = 1$	350 059	1136.0	3.01E-3
CH_2DOH	350 090	104.2	7.58E-5
$^{13}CH3OH$	350 103	16.8	3.29E-4
CH_3CHO $\nu = 0$	350 135	179.2	1.44E-3
CH_2DOH	350 141	93.5	5.04E-5
aGg'$(CH_2OH)_2$	350 142	326.2	7.96E-4
C_2H_5CN	350 145	356.1	3.65E-3
CH_3CN $v_8 = 1$	350 160	1030.0	3.13E-3
CH_3CN $v_8 = 1$	350 168	687.1	3.46E-3
CH_3CN $v_8 = 1$	350 190	1142.9	2.87E-3
$CH_3^{18}OH$	350 246	43.0	2.96E-4

Table A.1. continued.

Species	Frequency (MHz)	E_{up} (K)	A_{ij} (s^{-1})
CH_3CN $v_8 = 1$	350 247	938.3	3.23E-3
CH_3CN $v_8 = 1$	350 277	949.5	3.00E-3
CH_3OH $\nu = 1$	350 288	694.8	2.10E-4
$^{33}SO\_2\$$	350 303	89.1	3.07E-4
CH_3CN $v_8 = 1$	350 320	860.8	3.55E-3
HNCO	350 333	186.2	5.97E-4
CH_3CN $v_8 = 1$	350 352	870.2	3.14E-3
CH_3CHO $\nu = 0$	350 363	163.5	1.47E-3
g-C_2H_5OH	350 365	251.7	3.75E-4
CH_3CN $v_8 = 1$	350 380	797.5	3.39E-3
aGg'$(CH_2OH)_2$	350 402	327.7	1.91E-4
CH_3CN $v_8 = 1$	350 415	805.2	3.24E-3
^{13}CH3OH	350 422	102.6	7.03E-5
CH_3OCHO $\nu = 0$	350 442	283.9	4.91E-3
CH_3CHO $\nu = 0$	350 445	163.4	1.47E-3
CH_3CN $v_8 = 1$	350 450	713.8	3.47E-3
CH_2DOH	350 454	71.6	1.39E-4
CH_3OCHO $\nu = 0$	350 458	283.9	4.91E-3
CH_3CN $v_8 = 1$	350 465	754.4	3.33E-3
CH_3CN $v_8 = 1$	350 507	717.7	3.40E-3
C_2H_5CN	350 512	375.9	3.58E-3
t-C_2H_5OH	350 534	179.0	1.51E-4
CH_3CN $v_8 = 1$	350 552	695.4	3.45E-3
CH_2DOH	350 632	49.0	2.07E-4

Appendix B: Line properties per core (organized by species)

Table B.1. Single line detections.

Species	Transition	Frequency (MHz)	G35.20 A		G35.20 B1		G35.20 B2		G35.20 B3		G35.03 A	
			FWHM (km s^{-1})	T_{peak} (K)	*FWHM* (km s^{-1})	T_{peak} (K)	*FWHM* (km s^{-1})	T_{peak} (K)	*FWHM* (km s^{-1})	T_{peak} (K)	*FWHM* (km s^{-1})	T_{peak} (K)
2 atom												
SiO	8–7	347 330	6.18 ± 0.10	10.4 ± 0.1	6.0 ± 0.4	7.9 ± 0.2	1.7 ± 0.5	2.0 ± 0.4	3.1 ± 0.6	2.8 ± 0.3	blended	
SO	10(11)-10(10)	336 553	7.1 ± 0.8	4.0 ± 0.3	7.3 ± 0.3	5.1 ± 0.2	3.1 ± 0.6	1.7 ± 0.3	3.28 ± 0.09	6.4 ± 0.1	9.2 ± 0.3	5.7 ± 0.2
$C^{34}S$	7–6	337 400	4.7 ± 0.4	51.7 ± 8.4	2.7 ± 0.2	24.1 ± 0.7	2.4 ± 0.1	24.5 ± 0.8	2.7 ± 0.1	36.1 ± 0.6	7.6 ± 0.2	23.3 ± 0.5
$C^{17}O$	3–2	337 060	blended		1.9 ± 0.9	2.5 ± 0.6	2.3 ± 0.3	5.4 ± 0.3	2.83 ± 0.06	5.48 ± 0.08	4.6 ± 0.2	9.7 ± 0.5
3 atom												
HDO	$3_{3,1}$–$4_{2,2}$	335 396	⋆ 6.9 ± 0.3	18.4 ± 0.4	2.5 ± 0.1	8.9 ± 0.2	1.6 ± 0.2	2.6 ± 0.2	2.8 ± 0.1	19.0 ± 0.8	offset by 3 km s^{-1} or blended	
$H^{13}CO^+$	4–3	346 998	1.33 ± 0.06	7.8 ± 0.3	2.2 ± 0.1	11.4 ± 0.4	3.0 ± 0.3	14.9 ± 1.0	2.2 ± 0.2	7.9 ± 0.6	3.8 ± 0.1	9.1 ± 0.3
$HN^{13}C$	4–3	348 340	5.5 ± 0.2	9.6 ± 0.3	2.0 ± 0.1	4.2 ± 0.2	1.9 ± 0.3	4.3 ± 0.4	3.3 ± 0.2	25.9 ± 0.7	5.4 ± 0.5	4.6 ± 0.1
4 atom												
HNCO	$16_{1,16}$–$15_{1,15}$	350 333	6.5 ± 0.3	46.3 ± 1.9	6.1 ± 0.2	14.4 ± 0.3	2.7 ± 0.4	5.3 ± 0.7	3.44 ± 0.09	30.1 ± 0.5	4.55 ± 0.09	11.0 ± 0.2
CCCS	58–57	335 109	6.7 ± 0.1	3.26 ± 0.4	<3σ		<3σ		1.8 ± 0.6	0.8 ± 0.1	blended	

Notes. ⋆ Double peaked.

Table B.2. Formaldehyde.

Transition	Frequency (MHz)	G35.20 A		G35.20 B1		G35.20 B2		G35.20 B3		G35.03 A	
		FWHM (km s^{-1})	T_{peak} (K)	*FWHM* (km s^{-1})	T_{peak} (K)	*FWHM* (km s^{-1})	T_{peak} (K)	*FWHM* (km s^{-1})	T_{peak} (K)	*FWHM* (km s^{-1})	T_{peak} (K)
$H_2C^{18}O$											
$5_{1,5}$–$4_{1,4}$ o	335 815	4.9 ± 0.2	3.7 ± 0.1	2.3 ± 0.1	5.7 ± 0.2	1.6 ± 0.2	3.0 ± 0.2	2.23 ± 0.03	16.4 ± 0.1	3.4 ± 0.1	2.65 ± 0.08
$5_{4,2}$–$4_{4,1}$ p	346 984	4.4 ± 0.2	8.6 ± 0.2	2.2 ± 0.2	2.1 ± 0.2	1.7 ± 0.2	2.0 ± 0.2	2.4 ± 0.2	5.8 ± 0.1	blended	
$5_{3,3}$–$4_{3,2}$ o	347 133	6.4 ± 0.1	6.93 ± 0.09	2.2 ± 2.0	2.1 ± 2.0	2.1 ± 0.4	1.9 ± 0.2	2.46 ± 0.04	9.7 ± 0.1	blended	
$5_{3,2}$–$4_{3,1}$ o	347 144	blended		1.5 ± 0.2	3.3 ± 0.2	3.1 ± 0.5	1.1 ± 0.1	1.78 ± 0.06	6.8 ± 0.2	blended	
$5_{2,3}$–$4_{2,2}$ p	348 032	5.6 ± 0.1	5.36 ± 0.09	1.7 ± 0.2	2.6 ± 0.1	1.3 ± 0.6	1.4 ± 0.3	2.08 ± 0.05	7.2 ± 0.1	4.1 ± 0.3	2.5 ± 0.1
HDCO											
$5_{1,4}$–$4_{1,3}$	335 097	⋆ 6.6 ± 1.0	8.3 ± 0.4	2.90 ± 0.08	11.6 ± 0.2	1.77 ± 0.10	6.9 ± 0.4	2.6 ± 0.1	32.3 ± 0.6	<3σ	
D_2CO											
$13_{4,9}$–$14_{2,12}$	338 016	1.6 ± 0.2	0.48 ± 0.04	<3σ		<3σ		<3σ		<3σ	
$6_{2,5}$–$5_{2,4}$	349 630	blended		1.2 ± 0.9	0.8 ± 0.1	1.7 ± 0.3	0.54 ± 0.08	2.39 ± 0.09	5.6 ± 0.1	<3σ	

Notes. ⋄ Partially blended with other lines, ⋆ double peaked.

Table B.3. Formic Acid.

Transition	Frequency	G35.20 A		G35.20 B1		G35.20 B2		G35.20 B3		G35.03 A	
	(MHz)	*FWHM* (km s^{-1})	T_{peak} (K)	*FWHM* (km s^{-1})	T_{peak} (K)	*FWHM* (km s^{-1})	T_{peak} (K)	*FWHM* (km s^{-1})	T_{peak} (K)	*FWHM* (km s^{-1})	T_{peak} (K)
t-HCOOH											
$15_{9,6}$–$14_{9,5}$	337 429	5.4 ± 0.4	7.2 ± 0.2	blended		<3σ		1.7 ± 0.2	1.0 ± 0.1	3.9 ± 0.2	5.6 ± 0.1
$15_{10,6}$–$14_{10,5}$	337 436	4.4 ± 0.4	6.1 ± 0.2	blended		<3σ		1.9 ± 0.4	0.8 ± 0.1	5.5 ± 0.4	4.96 ± 0.09
$15_{8,7}$–$14_{8,6}$	337 444	blended		blended		<3σ		blended		5.3 ± 0.1	7.38 ± 0.09
$15_{7,8}$–$14_{7,7}$	337 492	blended		blended		blended		2.1 ± 0.8	7.2 ± 0.7	<3σ	
$15_{6,10}$–$14_{6,9}$	337 590	4.7 ± 0.4	14.1 ± 0.8	blended		<3σ		2.7 ± 0.1	2.55 ± 0.08	5.9 ± 0.2	8.5 ± 0.2
$15_{5,11}$–$14_{5,10}$	337 785	blended		blended		blended		blended		<3σ	
$15_{4,12}$–$14_{4,11}$	338 144	blended		2.99 ± 0.05	1.90 ± 0.05	blended		blended		7.0 ± 0.2	7.9 ± 0.2
$15_{3,13}$–$14_{3,12}$	338 202	4.7 ± 0.3	14.5 ± 0.3	2.2 ± 0.8	1.8 ± 0.5	1.4 ± 0.3	0.64 ± 0.10	3.2 ± 0.1	3.4 ± 0.1	6.8 ± 0.2	8.2 ± 0.2
$15_{4,11}$–$14_{4,10}$	338 249	5.3 ± 0.2	13.9 ± 0.3	1.8 ± 0.3	2.2 ± 0.7	2.2 ± 0.3	0.61 ± 0.05	⋄ 4.5 ± 0.2	5.9 ± 0.2	6.0 ± 0.2	8.3 ± 0.1
c-HCOOH											
$16_{2,15}$–$15_{2,14}$	349 326	blended		2.7 ± 0.1	2.25 ± 0.08	<3σ		1.5 ± 0.3	2.2 ± 0.3	<3σ	

Notes. ⋄ Partially blended with other lines.

Table B.4. Methanol.

Transition	Frequency (MHz)	G35.20 A *FWHM* (km s^{-1})	G35.20 A T_{peak} (K)	G35.20 B1 *FWHM* (km s^{-1})	G35.20 B1 T_{peak} (K)	G35.20 B2 *FWHM* (km s^{-1})	G35.20 B2 T_{peak} (K)	G35.20 B3 *FWHM* (km s^{-1})	G35.20 B3 T_{peak} (K)	G35.03 A *FWHM* (km s^{-1})	G35.03 A T_{peak} (K)
CH_3OH $\nu = 0$											
$11_{0,11}$–$10_{2,8}$	334 970	blended		blended		blended		1.43 ± 0.06	1.22 ± 0.04	out of window	
$2_{2,1}$–$3_{1,2}$- -	335 134	5.28 ± 0.09	70.1 ± 0.7	2.89 ± 0.10	37.27 ± 1.14	2.4 ± 0.1	28 ± 1	2.40 ± 0.04	48.7 ± 0.7	5.2 ± 0.2	26.0 ± 0.7
$16_{1,15}$–$16_{-1,16}$	335 222	6.0 ± 0.3	1.83 ± 0.06	blended		blended		1.4 ± 0.2	0.9 ± 0.1	2.3 ± 0.1	1.27 ± 0.05
$7_{3,4}$–$8_{0,8}$	335 363	blended		blended		blended		⋄ 1.2 ± 0.2	0.8 ± 0.1	<3σ	
$7_{1,7}$–$6_{1,6}$++	335 582	6.2 ± 0.1	77 ± 2	3.47 ± 0.11	48.98 ± 1.19	3.3 ± 0.2	45 ± 2	2.89 ± 0.06	55 ± 1	6.1 ± 0.1	34.5 ± 0.4
$25_{8,18}$–$26_{7,19}$- -	335 702	5.8 ± 0.1	7.3 ± 0.1	1.3 ± 0.4	0.5 ± 0.1	blended		3.1 ± 0.2	1.10 ± 0.06	<3σ	
$14_{7,8}$–$15_{6,9}$++	336 438	5.42 ± 0.08	47.8 ± 0.6	2.52 ± 0.05	19.26 ± 0.51	2.2 ± 0.1	11.1 ± 0.5	2.34 ± 0.01	27.8 ± 0.4	4.23 ± 0.09	17.3 ± 0.4
$12_{1,11}$–$12_{0,12}$-+	336 865	6.4 ± 0.2	106 ± 3	4.11 ± 0.07	90.75 ± 0.76	3.1 ± 0.1	59 ± 2	2.87 ± 0.06	72 ± 1	<3σ	
$3_{3,0}$–$4_{2,2}$	337 136	5.04 ± 0.06	52.3 ± 0.5	2.56 ± 0.09	24.08 ± 0.44	2.4 ± 0.1	18.8 ± 0.8	2.37 ± 0.02	34.1 ± 0.4	4.6 ± 1.3	16.6 ± 0.4
$20_{-6,14}$–$21_{-5,16}$	337 838	5.51 ± 0.09	21.7 ± 0.4	1.70 ± 0.08	7.55 ± 0.18	2.0 ± 0.1	2.8 ± 0.2	2.30 ± 0.05	11.4 ± 0.2	4.9 ± 0.9	9.0 ± 0.3
$7_{0,7}$–$6_{0,6}$	338 125	6.3 ± 0.5	76 ± 2	3.26 ± 0.11	50.87 ± 1.14	3.2 ± 0.2	43 ± 2	2.9 ± 0.1	56 ± 1	6.4 ± 1.8	33.0 ± 0.6
$7_{-1,7}$–$6_{-1,6}$	338 345	6.3 ± 0.5	77 ± 2	3.33 ± 0.12	50.71 ± 1.06	2.6 ± 0.1	42 ± 3	2.8 ± 0.1	57 ± 1	6.7 ± 1.6	34.2 ± 0.5
$7_{6,2}$–$6_{6,1}$	338 405	4.2 ± 0.2	53 ± 1	2.12 ± 0.22	23.13 ± 1.67	2.9 ± 0.2	26 ± 1	1.74 ± 0.06	28.9 ± 0.8	<3σ	
$7_{0,7}$–$6_{0,6}$++	338 409	4.9 ± 0.4	70 ± 7	3.91 ± 0.15	49.83 ± 1.09	2.9 ± 0.1	39.9 ± 0.9	3.25 ± 0.09	52.7 ± 1.0	8 ± 1	37.4 ± 1.0
$7_{-6,1}$–$6_{-6,0}$	338 431	6.0 ± 0.5	62 ± 2	2.69 ± 0.15	28.31 ± 0.33	2.4 ± 0.4	20.1 ± 0.8	2.37 ± 0.06	40.3 ± 0.6	5.5 ± 0.2	21.3 ± 0.6
$7_{6,1}$–$6_{6,0}$++	338 442	5.9 ± 0.3	70 ± 1	2.87 ± 0.11	34.19 ± 1.11	2.6 ± 0.5	26 ± 1	2.49 ± 0.08	45.9 ± 0.8	5.8 ± 0.2	23.4 ± 0.6
$7_{-5,2}$–$6_{-5,1}$	338 456	5.8 ± 0.2	72.0 ± 0.8	3.15 ± 0.08	37.40 ± 0.75	2.7 ± 0.7	31 ± 1	2.59 ± 0.07	48.1 ± 0.7	<3σ	
$7_{5,3}$–$6_{5,2}$	338 475	5.94 ± 0.08	70.3 ± 0.7	3.04 ± 0.04	36.37 ± 0.33	2.7 ± 0.6	30 ± 1	2.5 ± 0.1	48 ± 1	5.5 ± 0.2	24.2 ± 0.6
$7_{5,3}$–$6_{5,2}$++	338 486	6.0 ± 0.4	76 ± 2	3.16 ± 0.10	42.02 ± 1.16	2.8 ± 0.7	35 ± 1	2.64 ± 0.09	51.5 ± 0.9	6.0 ± 0.2	27.8 ± 0.6
$7_{-4,4}$–$6_{-4,3}$	338 504	6.7 ± 0.1	74.6 ± 0.9	3.16 ± 0.11	42.27 ± 1.21	3.0 ± 0.7	37 ± 2	2.5 ± 0.2	50 ± 2	5.5 ± 0.2	26.8 ± 0.5
$7_{4,0}$–$6_{4,0}$- -	338 512	5.2 ± 0.1	81.6 ± 0.9	3.50 ± 0.11	52.13 ± 1.33	2.7 ± 0.6	46 ± 1	3.0 ± 0.1	56 ± 1	6.7 ± 0.2	35.9 ± 0.5
$7_{2,6}$–$6_{2,5}$- -	338 513	blended with 338 512		blended with 338 512		blended with 338 512		blended with 338 512		blended with 338 512	
$7_{4,3}$–$6_{4,2}$	338 530	6.5 ± 0.2	75 ± 1	3.05 ± 0.09	43.24 ± 0.73	2.8 ± 0.8	36 ± 2	2.6 ± 0.1	52 ± 1	5.8 ± 0.1	29.0 ± 0.5
$7_{3,5}$–$6_{3,4}$++	338 541	5.0 ± 0.3	87 ± 2	4.34 ± 0.07	69.05 ± 0.72	4.7 ± 0.1	51 ± 1	4.2 ± 0.3	61 ± 3	7.04 ± 0.10	43.5 ± 0.4
$7_{3,4}$–$6_{3,3}$- -	338 543	3.9 ± 0.4	41 ± 4	blended with 338 541		blended with 338 541		4.4 ± 0.2	61 ± 2	blended with 338 541	
$7_{-3,5}$–$6_{-3,4}$	338 560	5.9 ± 0.4	80 ± 2	3.22 ± 0.12	45.52 ± 0.89	3.0 ± 0.89	40 ± 2	2.7 ± 0.1	54 ± 1	6.2 ± 1.6	30.2 ± 0.5
$7_{3,4}$–$6_{3,3}$	338 583	5.9 ± 0.4	81 ± 2	3.25 ± 0.11	46.95 ± 0.88	3 ± 1	41 ± 2	2.8 ± 0.1	55 ± 1	6.2 ± 1.5	31.2 ± 0.5
$7_{1,6}$–$6_{1,5}$	338 615	⋄ 5.1 ± 0.1	81 ± 2	3.25 ± 0.22	38.08 ± 3.08	2.8 ± 0.2	39 ± 2	2.6 ± 0.2	50 ± 7	8.2 ± 1.6	41.4 ± 0.5
$7_{2,5}$–$6_{2,4}$++	338 640	6.2 ± 0.3	78 ± 1	3.23 ± 0.12	48.64 ± 0.91	3 ± 1	42 ± 2	2.8 ± 0.1	55 ± 1	7 ± 1	31.4 ± 0.6
$4_{2,2}$–$4_{-1,4}$	347 370	blended		1.3 ± 0.3	0.8 ± 0.1	blended		blended		<3σ	
$5_{2,3}$–$5_{-1,5}$	347 507	blended		0.9 ± 0.2	0.7 ± 0.1	blended		2.1 ± 0.3	0.69 ± 0.07	3.4 ± 0.3	1.66 ± 0.06
$6_{2,4}$–$6_{-1,6}$	347 745	blended		blended		blended		1.7 ± 0.3	0.49 ± 0.07	2.9 ± 1.3	0.5 ± 0.1
$7_{2,5}$–$7_{-1,7}$	348 123	1.3 ± 0.3	1.2 ± 0.2	blended		blended		1.0 ± 0.4	0.6 ± 0.2	1.7 ± 0.2	1.10 ± 0.04
$8_{2,6}$–$8_{-1,8}$	348 682	4.1 ± 1.5	1.6 ± 0.1	blended		blended		1.1 ± 0.2	0.7 ± 0.1	<3σ	
$14_{1,13}$–$14_{0,14}$-+	349 107	5.3 ± 0.1	122 ± 1	3.81 ± 0.07	85.18 ± 1.30	2.8 ± 0.1	57 ± 2	2.80 ± 0.07	74 ± 2	7.9 ± 0.1	43.0 ± 0.5
$9_{2,7}$–$9_{-1,9}$	349 470	blended		1.8 ± 0.1	1.11 ± 0.06	blended		0.8 ± 0.5	0.7 ± 0.2	1.9 ± 0.2	0.79 ± 0.07
CH_3OH $\nu = 1$											
$7_{1,7}$–$6_{1,6}$++	337 297	⋄ 6.2 ± 0.1	65.2 ± 0.5	3.0 ± 0.2	29.2 ± 0.4	2.7 ± 0.5	20 ± 1	2.8 ± 0.1	38 ± 2	1 ± 1.6	15 ± 5
$7_{2,2}$–$6_{2,2}$	337 303	⋄ 3.9 ± 0.3	20.1 ± 0.8	2.43 ± 0.44	9.06 ± 1.01	1.3 ± 0.2	3.8 ± 0.5	2.22 ± 0.06	13.0 ± 0.3	4.9 ± 1.0	11.0 ± 2.7

Notes. ⋄ Partially blended with other lines, ⋆ double peaked.

Table B.4. continued.

Transition	Frequency	G35.20 A		G35.20 B1		G35.20 B2		G35.20 B3		G35.03 A	
		FWHM	T_{peak}	*FWHM*	T_{peak}	*FWHM*	T_{peak}	*FWHM*	T_{peak}	*FWHM*	T_{peak}
	(MHz)	(km s^{-1})	(K)	(km s^{-1})	(K)	(km s^{-1})	(K)	(km s^{-1})	(K)	(km s^{-1})	(K)
$7_{6,1}$–$6_{6,0}$++	337 464	5.7 ± 0.1	34.3 ± 0.5	2.1 ± 0.2	12.5 ± 0.4	2.1 ± 0.2	6.4 ± 0.3	2.36 ± 0.07	17.3 ± 0.4	5.8 ± 1.0	12.8 ± 0.3
$10_{10,1}$–$9_{9,1}$ -	337 473	5.9 ± 0.3	16.1 ± 0.5	1.64 ± 0.09	3.9 ± 0.2	2.3 ± 0.2	1.41 ± 0.09	3.2 ± 0.2	4.8 ± 0.2	5.3 ± 0.1	7.7 ± 0.1
$7_{-6,2}$–$6_{-6,1}$	337 491	5.9 ± 0.1	30.2 ± 0.6	2.5 ± 0.2	9.5 ± 0.4	2.2 ± 0.1	5.0 ± 0.3	2.65 ± 0.04	11.7 ± 0.1	6.1 ± 0.8	11.5 ± 0.3
$7_{3,5}$–$6_{3,4}$	337 519	5.3 ± 0.2	48.8 ± 0.7	2.4 ± 0.2	19.0 ± 0.4	2.3 ± 0.2	11.9 ± 0.5	2.32 ± 0.04	28.3 ± 0.3	4.7 ± 1.2	16.6 ± 0.4
$7_{5,3}$–$6_{5,2}$++	337 546	5.7 ± 0.2	48.6 ± 0.7	2.5 ± 0.1	19.2 ± 0.3	2.2 ± 0.3	12.2 ± 0.7	2.47 ± 0.07	28.2 ± 0.6	5.4 ± 1.6	15.9 ± 0.5
$7_{4,4}$–$6_{4,3}$	337 582	5.9 ± 0.2	53.4 ± 0.8	⋄ 3.3 ± 0.2	25 ± 3	⋄ 2.2 ± 0.2	12 ± 1	⋄ 3.6 ± 0.1	33 ± 1	5.8 ± 0.5	17.7 ± 1.6
$7_{-2,5}$–$6_{-2,4}$	337 605	5.1 ± 0.2	53.8 ± 0.9	2.29 ± 0.08	24.4 ± 0.7	2.5 ± 0.2	16.8 ± 0.4	2.33 ± 0.04	30.9 ± 0.5	3.4 ± 0.2	18.8 ± 0.7
$7_{-3,4}$–$6_{-3,3}$	337 611	5.0 ± 0.2	57.8 ± 1.0	2.92 ± 0.08	25.2 ± 0.5	2.2 ± 0.8	17 ± 2	2.44 ± 0.04	37.4 ± 0.5	5.5 ± 0.2	21.9 ± 0.4
$7_{2,5}$–$6_{2,4}$++	337 626	5.37 ± 0.10	64.5 ± 0.9	2.7 ± 0.1	28.6 ± 0.8	2.5 ± 0.5	21 ± 1	2.41 ± 0.08	40.7 ± 0.8	5.0 ± 0.1	21.4 ± 0.4
$7_{2,6}$–$6_{2,5}$- -	337 636	4.69 ± 0.10	56.7 ± 0.9	2.6 ± 0.1	29.5 ± 0.9	2.7 ± 0.3	21.0 ± 0.6	2.3 ± 0.2	39 ± 2	5.7 ± 0.2	23.6 ± 0.4
$7_{1,7}$–$6_{1,6}$	337 642	8.6 ± 0.2	73.9 ± 0.6	2.0 ± 0.5	38 ± 21	2 ± 1	23 ± 30	1.8 ± 0.3	31 ± 29	3.1 ± 0.9	19.0 ± 32.5
$7_{0,7}$–$6_{0,6}$	337 644	blended with 337 642		⋄ 2 ± 1	36 ± 22	⋄ 2 ± 2	23 ± 26	⋄ 2 ± 2	37 ± 34	⋄ 4 ± 3	22 ± 20
$7_{-4,3}$–$6_{-4,2}$	337 646	blended with 337 642		⋄ 2 ± 1	25 ± 14	⋄ 2 ± 2	6 ± 7	⋄ 2 ± 2	25 ± 30	⋄ 5 ± 3	16 ± 10
$7_{-5,3}$–$6_{-5,2}$	337 648	blended with 337 642		⋄ 2 ± 1	10 ± 9	blended		2 ± 1	11 ± 16	<3σ	
$7_{3,5}$–$6_{3,4}$++	337 655	4.88 ± 0.09	55.2 ± 0.7	2.7 ± 0.1	24.9 ± 0.6	2.4 ± 0.3	17.3 ± 0.6	2.44 ± 0.04	35.4 ± 0.4	4.7 ± 0.3	20.6 ± 0.6
$7_{2,6}$–$6_{2,5}$	337 671	5.4 ± 0.2	52.4 ± 0.7	2.5 ± 0.1	21.0 ± 0.8	2.3 ± 0.3	13.9 ± 0.6	2.33 ± 0.03	31.2 ± 0.3	4.9 ± 1.3	17.4 ± 0.4
$7_{4,3}$–$6_{4,2}$++	337 685	5.5 ± 0.2	55.5 ± 0.7	2.6 ± 0.1	23.1 ± 0.3	2.3 ± 0.4	14.7 ± 0.7	2.39 ± 0.03	33.1 ± 0.3	5.1 ± 1.3	19.3 ± 0.4
$7_{-1,6}$–$6_{-1,5}$	337 708	5.6 ± 0.2	50.6 ± 0.7	2.5 ± 0.1	20.2 ± 0.8	2.3 ± 0.3	12.6 ± 0.5	2.5 ± 0.1	29 ± 1	5.2 ± 1.4	17.2 ± 0.5
$7_{0,7}$–$6_{0,6}$++	337 749	5.6 ± 0.1	52.7 ± 0.6	2.7 ± 0.3	20.9 ± 0.6	2.4 ± 0.4	12.4 ± 0.8	2.50 ± 0.03	29.4 ± 0.3	5.2 ± 1.4	18.0 ± 0.5
$7_{1,6}$–$6_{1,5}$- -	337 969	5.5 ± 0.1	60.8 ± 0.6	2.75 ± 0.07	27.6 ± 0.6	2.4 ± 0.4	19.5 ± 0.8	2.45 ± 0.04	38.6 ± 0.4	5.1 ± 1.5	20.2 ± 0.5
$19_{3,17}$–$19_{2,18}$	347 448	5.5 ± 0.1	27.6 ± 0.6	1.9 ± 0.1	9.2 ± 0.5	2.0 ± 0.2	4.1 ± 0.4	2.36 ± 0.06	9.8 ± 0.2	<3σ	
$15_{3,13}$–$16_{4,13}$	350 288	5.5 ± 0.2	48.5 ± 0.8	2.2 ± 0.1	16.0 ± 0.7	2.0 ± 0.2	7.9 ± 0.7	2.25 ± 0.04	24.3 ± 0.3	5.4 ± 0.1	18.0 ± 0.4
CH_3OH $\nu = 2$											
$7_{1,2}$–$6_{1,2}$++	336 606	6.0 ± 0.1	19.2 ± 0.4	1.6 ± 0.2	5.4 ± 0.3	1.7 ± 0.3	2.6 ± 0.2	2.28 ± 0.07	7.8 ± 0.1	5.2 ± 0.2	7.7 ± 0.2
$7_{6,-2}$–$6_{6,-2}$	336 970	5.7 ± 0.2	8.0 ± 0.2	blended		blended		2.8 ± 0.1	1.85 ± 0.07	5.7 ± 0.2	2.19 ± 0.07
$7_{3,2}$–$6_{3,2}$ - -	337 022	5.4 ± 0.5	4.1 ± 0.2	0.8 ± 0.2	0.8 ± 0.1	1.0 ± 0.4	0.6 ± 0.2	1.3 ± 0.2	1.2 ± 0.2	3.5 ± 0.2	2.08 ± 0.08
$7_{2,2}$–$6_{2,2}$ ++	337 030	5.6 ± 0.2	10.2 ± 0.1	1.6 ± 0.1	2.51 ± 0.08	1.6 ± 0.2	1.2 ± 0.1	2.23 ± 0.09	3.2 ± 0.1	5.4 ± 0.1	4.62 ± 0.06
$7_{4,2}$–$6_{4,2}$	337 066	blended		2 ± 1	0.7 ± 0.3	0.9 ± 0.4	0.6 ± 0.2	2.8 ± 0.2	1.56 ± 0.08	blended	
$7_{5,2}$–$6_{5,2}$	337 079	blended		1.2 ± 0.2	0.67 ± 0.08	0.86 ± 0.09	0.54 ± 0.03	1.7 ± 0.2	0.8 ± 0.1	4.3 ± 1.1	2.2 ± 0.1
$7_{5,2}$–$6_{5,2}$ ++	337 099	⋆ 6.6 ± 0.2	7.5 ± 0.2	1.2 ± 0.2	1.9 ± 0.1	1.9 ± 0.3	0.8 ± 0.1	2.0 ± 0.1	2.7 ± 0.2	3.4 ± 0.4	2.60 ± 0.05
$7_{1,2}$–$6_{1,2}$	337 114	6.3 ± 0.2	9.1 ± 0.2	1.29 ± 0.05	2.15 ± 0.05	1.7 ± 0.1	1.30 ± 0.05	2.0 ± 0.2	3.0 ± 0.2	3.3 ± 0.2	4.32 ± 0.09
$7_{6,2}$–$6_{6,2}$ - -	337 118	blended with 337 114		1.8 ± 0.7	0.6 ± 0.2	1.7 ± 0.6	0.5 ± 0.1	2.5 ± 0.3	0.70 ± 0.07	2.1 ± 0.4	2.3 ± 0.7
$7_{6,2}$–$6_{6,2}$	337 159	⋆ 5.5 ± 0.2	4.8 ± 0.2	1.1 ± 0.2	1.2 ± 0.1	1.5 ± 0.6	0.7 ± 0.2	2.1 ± 0.1	1.8 ± 0.1	3.6 ± 0.3	2.37 ± 0.10
$7_{4,2}$–$6_{4,2}$ - -	337 175	⋆ 6.2 ± 0.2	8.7 ± 0.2	1.38 ± 0.07	2.41 ± 0.07	1.8 ± 0.4	0.9 ± 0.1	2.3 ± 0.2	3.0 ± 0.2	4.4 ± 0.3	4.10 ± 0.10
$7_{0,2}$–$6_{0,2}$	337 186	5.8 ± 0.2	13.4 ± 0.3	1.49 ± 0.04	3.96 ± 0.07	2.2 ± 0.2	1.5 ± 0.1	2.7 ± 0.2	5.1 ± 0.2	4.0 ± 0.6	6.6 ± 1.8
$7_{5,2}$–$6_{5,2}$ - -	337 198	5.6 ± 0.1	15.8 ± 0.3	3.2 ± 0.2	7.2 ± 0.4	3.0 ± 0.5	2.0 ± 0.3	3.3 ± 0.1	8.8 ± 0.3	5.7 ± 0.4	6.5 ± 0.2
$7_{3,-2}$–$6_{3,-2}$	337 252	5.7 ± 0.1	26.0 ± 0.5	1.83 ± 0.08	9.5 ± 0.2	2.0 ± 0.2	4.4 ± 0.2	2.35 ± 0.08	12.2 ± 0.4	4.7 ± 0.7	10.0 ± 0.2
$7_{4,2}$–$6_{4,2}$ ++	337 274	blended		1.73 ± 0.09	9.9 ± 0.2	2.08 ± 0.09	5.0 ± 0.2	2.25 ± 0.07	13.8 ± 0.4	4.3 ± 0.2	11.6 ± 0.2
$7_{-2,2}$–$6_{-2,2}$	337 279	blended		1.4 ± 0.2	5.3 ± 0.5	1.6 ± 0.1	3.5 ± 0.2	2.3 ± 0.1	7.8 ± 0.4	2.8 ± 0.3	7.2 ± 0.5
$7_{0,2}$–$6_{0,2}$	337 284	6.5 ± 0.2	39.7 ± 0.8	2.3 ± 0.3	14.3 ± 0.7	2.1 ± 0.2	8.4 ± 0.4	2.47 ± 0.05	20.3 ± 0.4	5.9 ± 0.2	14.8 ± 0.2
$7_{-1,2}$–$6_{-1,2}$	337 312	5.5 ± 0.1	33.7 ± 0.6	2.0 ± 0.1	12.6 ± 0.3	2.1 ± 0.2	6.9 ± 0.3	2.27 ± 0.04	17.4 ± 0.3	5.8 ± 2.0	11.4 ± 0.6
$7_{1,-2}$–$6_{1,-2}$	337 878	5.87 ± 0.09	17.8 ± 0.4	1.72 ± 0.08	5.7 ± 0.2	1.77 ± 0.06	2.3 ± 0.1	2.26 ± 0.07	7.2 ± 0.2	6.2 ± 0.8	7.9 ± 0.2

Table B.4. continued.

Transition	Frequency (MHz)	G35.20 A *FWHM* (km s^{-1})	G35.20 A T_{peak} (K)	G35.20 B1 *FWHM* (km s^{-1})	G35.20 B1 T_{peak} (K)	G35.20 B2 *FWHM* (km s^{-1})	G35.20 B2 T_{peak} (K)	G35.20 B3 *FWHM* (km s^{-1})	G35.20 B3 T_{peak} (K)	G35.03 A *FWHM* (km s^{-1})	G35.03 A T_{peak} (K)
$CH_3^{18}OH$ $\nu = 0$											
$13_{1,12}$–$13_{0,13}$	335 775	⋆ 5.4 ± 0.2	7.8 ± 0.3	1.70 ± 0.09	3.8 ± 0.2	1.30 ± 0.11	1.6 ± 0.1	2.27 ± 0.09	4.3 ± 0.1	<3σ	
$8_{1,7}$–$7_{2,5}$	336 100	⋄⋆ 5.3 ± 0.9	3.9 ± 0.5	⋄ 1.3 ± 0.3	0.83 ± 0.10	<3σ	⋄ 1.8 ± 0.1	1.9 ± 0.1	<3σ		
$4_{0,4}$–$3_{1,3}$	336 743	⋄ 8.9 ± 1.0	4.8 ± 0.2	3.4 ± 0.2	1.6 ± 0.2	<3σ		2.7 ± 0.2	1.46 ± 0.07	<3σ	
$8_{3,6}$–$9_{2,8}$	347 865	⋆ 6.2 ± 0.3	6.4 ± 0.2	1.21 ± 0.19	0.9 ± 0.1	1.78 ± 0.24	0.9 ± 0.1	2.9 ± 0.2	1.41 ± 0.08	<3σ	
$15_{1,14}$–$15_{0,15}$	348 053	blended		1.46 ± 0.15	2.6 ± 0.2	1.45 ± 0.06	1.33 ± 0.05	2.0 ± 0.2	3.1 ± 0.2	<3σ	
$4_{1,3}$–$3_{0,3}$	350 246	blended		2.15 ± 0.26	2.3 ± 0.2	1.89 ± 0.29	1.0 ± 0.1	blended		<3σ	
^{13}CH3OH $\nu = 0$											
$12_{1,11}$–$12_{0,12}$-+	335 560	5.04 ± 0.10	48.3 ± 0.8	2.4 ± 0.1	19.8 ± 0.5	2.2 ± 0.1	13.0 ± 0.6	2.26 ± 0.04	29.4 ± 0.5	4.6 ± 0.1	16.1 ± 0.3
$14_{1,13}$–$14_{0,14}$-+	347 188	5.3 ± 0.2	47.9 ± 1.2	2.05 ± 0.08	18.9 ± 0.6	2.1 ± 0.1	11.2 ± 0.6	2.31 ± 0.03	30.6 ± 0.4	4.6 ± 0.1	14.1 ± 0.2
$13_{4,9}$–$14_{3,11}$	347 788	5.0 ± 0.2	9.1 ± 0.2	1.5 ± 0.2	2.2 ± 0.2	1.8 ± 0.2	1.2 ± 0.1	2.18 ± 0.10	3.4 ± 0.1	2.5 ± 0.3	2.4 ± 0.2
$21_{3,19}$–$20_{4,16}$++	347 848	blended		blended		blended		2.1 ± 0.2	1.16 ± 0.07	2.2 ± 0.8	1.7 ± 0.3
$11_{0,11}$–$10_{1,9}$	348 100	⋄ 5.1 ± 0.4	20.1 ± 0.3	1.8 ± 0.1	9.8 ± 0.6	1.9 ± 0.1	5.6 ± 0.3	2.15 ± 0.05	14.7 ± 0.3	4.0 ± 0.1	7.1 ± 0.2
$19_{2,17}$–$18_{1,18}$ ++	348 942	blended		blended		blended		blended		<3σ	
$21_{3,18}$–$20_{4,17}$- -	349 996	blended		blended		blended		blended		<3σ	
$1_{1,1}$–$0_{0,0}$++	350 103	⋆ 4.9 ± 0.2	26.8 ± 0.9	2.03 ± 0.08	12.7 ± 0.4	1.9 ± 0.2	9.1 ± 0.6	2.10 ± 0.03	19.6 ± 0.3	3.9 ± 0.1	8.3 ± 0.2
$8_{1,7}$–$7_{2,5}$	350 422	blended		1.51 ± 0.10	6.7 ± 0.5	2.12 ± 0.03	5.23 ± 0.07	3.5 ± 0.2	15.8 ± 0.6	blended	
CH_2DOH											
$18_{2,17}$–$17_{3,14}$	335 796	blended		1.9 ± 0.5	0.64 ± 0.06	1.3 ± 0.7	0.5 ± 0.1	2.1 ± 0.2	1.9 ± 0.1	<3σ	
$8_{1,7}$–$7_{0,7}$	335 997	3.1 ± 0.8	3.0 ± 1.9	1.8 ± 0.1	2.23 ± 0.07	1.1 ± 0.2	0.8 ± 0.1	2.10 ± 0.09	2.7 ± 0.1	<3σ	
$19_{2,18}$–$19_{1,19}$	336 325	blended		1.1 ± 0.1	0.64 ± 0.06	blended		3.1 ± 0.3	0.97 ± 0.08	<3σ	
$9_{0,9}$–$8_{1,8}$	337 349	blended		⋄ 2.5 ± 0.2	6.6 ± 0.3	1.5 ± 0.3	2.0 ± 0.3	⋄ 2.2 ± 0.1	9.4 ± 0.3	<3σ	
$12_{2,11}$–$11_{3,9}$	337 977	blended		1.0 ± 0.2	1.1 ± 0.2	1.56 ± 0.07	0.49 ± 0.02	2.0 ± 0.1	1.32 ± 0.06	<3σ	
$9_{1,8}$–$8_{2,6}$	338 463	blended		2.0 ± 1.5	1.7 ± 1.0	2.1 ± 3.3	1.7 ± 1.3	2.0 ± 0.8	2.2 ± 0.4	<3σ	
$20_{4,17}$–$20_{3,17}$	346 924	⋄ 1.3 ± 0.2	4.5 ± 0.7	blended		blended		3.8 ± 0.1	1.52 ± 0.03	<3σ	
$20_{4,16}$–$20_{3,18}$	347 222	⋄ 2.3 ± 0.4	4.2 ± 1.4	<3σ		<3σ		2.0 ± 0.5	1.4 ± 0.1	<3σ	
$19_{4,16}$–$19_{3,16}$	347 371	⋄ 3.1 ± 1.5	2.3 ± 0.7	2.0 ± 0.2	0.82 ± 0.08	blended		2.1 ± 0.4	0.6 ± 0.1	<3σ	
$19_{4,15}$–$19_{3,17}$	347 610	blended		2.15 ± 2.06	1.0 ± 0.1	1.0 ± 0.4	0.5 ± 0.2	blended		<3σ	
$18_{4,15}$–$18_{3,15}$	347 767	blended		1.1 ± 0.3	0.6 ± 0.2	0.9 ± 0.1	0.59 ± 0.06	1.8 ± 0.2	0.85 ± 0.07	<3σ	
$18_{4,14}$–$18_{3,16}$	347 953	5.43 ± 0.09	4.48 ± 0.05	1.9 ± 0.3	0.7 ± 0.1	blended		2.1 ± 0.3	0.7 ± 0.1	<3σ	
$4_{1,3}$–$4_{0,4}$	348 161	blended		1.9 ± 0.1	8.4 ± 0.4	1.6 ± 0.3	4.2 ± 1.4	2.36 ± 0.04	16.1 ± 0.3	5.3 ± 0.2	0.93 ± 0.06
$16_{4,13}$–$16_{3,13}$	348 427	2.0 ± 0.3	3.2 ± 0.3	1.5 ± 0.1	2.1 ± 0.1	blended		1.8 ± 0.3	1.8 ± 0.3	<3σ	
$16_{4,12}$–$16_{3,14}$	348 529	blended		blended		2.0 ± 0.6	5.1 ± 1.1	blended		<3σ	
$10_{1,10}$–$9_{2,8}$	348 592	blended		1.8 ± 0.2	1.00 ± 0.09	1.1 ± 0.3	0.8 ± 0.2	2.2 ± 0.4	1.0 ± 0.1	<3σ	
$13_{1,12}$–$12_{2,11}$	348 668	partially blended		1.1 ± 0.4	0.8 ± 0.1	1.4 ± 0.2	0.91 ± 0.04	1.0 ± 0.2	0.8 ± 0.2	<3σ	
$15_{4,12}$–$15_{3,12}$	348 699	blended		1.52 ± 0.09	1.72 ± 0.09	1.6 ± 0.3	0.9 ± 0.1	1.7 ± 0.2	2.3 ± 0.2	<3σ	
$14_{4,11}$–$14_{3,11}$	348 939	blended		1.32 ± 0.07	2.3 ± 0.1	blended		2.2 ± 0.1	2.4 ± 0.1	<3σ	
$14_{4,10}$–$14_{3,12}$	348 990	blended		1.3 ± 0.2	2.3 ± 0.2	1.3 ± 0.2	0.9 ± 0.1	blended		<3σ	
$13_{4,10}$–$13_{3,10}$	349 149	⋄⋆ 6.1 ± 0.3	4.3 ± 0.2	1.3 ± 0.1	2.3 ± 0.2	1.0 ± 0.2	1.2 ± 0.2	2.10 ± 0.09	3.1 ± 0.1	<3σ	
$13_{4,9}$–$13_{3,11}$	349 184	⋄⋆ 6.1 ± 0.4	4.4 ± 0.1	1.43 ± 0.06	2.42 ± 0.09	1.0 ± 0.4	1.0 ± 0.4	1.9 ± 0.1	3.4 ± 0.2	<3σ	
$12_{4,9}$–$12_{3,9}$	349 334	2.6 ± 0.2	6.6 ± 0.3	1.8 ± 0.2	2.7 ± 0.3	2.7 ± 0.1	6.8 ± 0.2	blended		<3σ	
$12_{4,8}$–$12_{3,10}$	349 356	blended		1.84 ± 0.07	4.1 ± 0.1	1.3 ± 0.5	1.1 ± 0.3	2.19 ± 0.06	3.73 ± 0.09	<3σ	

Table B.4. continued.

Transition	Frequency	G35.20 A		G35.20 B1		G35.20 B2		G35.20 B3		G35.03 A	
		FWHM	T_{peak}	*FWHM*	T_{peak}	*FWHM*	T_{peak}	*FWHM*	T_{peak}	*FWHM*	T_{peak}
	(MHz)	(km s^{-1})	(K)	(km s^{-1})	(K)	(km s^{-1})	(K)	(km s^{-1})	(K)	(km s^{-1})	(K)
$13_{2,12}$–$13_{1,12}$	349 411	blended		1.8 ± 0.3	3.8 ± 0.3	1.3 ± 0.3	1.7 ± 0.2	1.91 ± 0.07	4.2 ± 0.1	<3σ	
$11_{4,8}$–$11_{3,8}$	349 495	⋆ 6.3 ± 0.3	7.9 ± 0.3	1.62 ± 0.09	3.4 ± 0.2	1.2 ± 0.2	1.6 ± 0.1	2.7 ± 0.1	4.9 ± 0.2	<3σ	
$11_{4,7}$–$11_{3,9}$	349 509	⋆ 5.8 ± 0.4	5.5 ± 0.3	1.70 ± 0.09	3.7 ± 0.2	1.7 ± 0.6	1.2 ± 0.2	1.97 ± 0.08	4.4 ± 0.2	<3σ	
$10_{4,7}$–$10_{3,7}$	349 636	⋆ 5.3 ± 0.2	9.7 ± 0.3	1.7 ± 0.1	4.5 ± 0.3	1.2 ± 0.2	1.7 ± 0.1	2.13 ± 0.04	5.51 ± 0.08	<3σ	
$10_{4,6}$–$10_{3,8}$	349 644	⋆ 6.6 ± 0.2	6.7 ± 0.3	1.43 ± 0.07	4.0 ± 0.2	1.2 ± 0.2	2.0 ± 0.3	1.89 ± 0.06	5.4 ± 0.2	<3σ	
$9_{4,6}$–$9_{3,6}$	349 757	⋄ 2.6 ± 0.3	10.4 ± 0.8	1.7 ± 0.2	3.6 ± 0.4	1.6 ± 0.3	1.7 ± 0.2	2.12 ± 0.07	5.8 ± 0.1	<3σ	
$9_{4,5}$–$9_{3,7}$	349 762	⋄ 3.9 ± 0.6	6.8 ± 0.3	1.7 ± 0.1	4.1 ± 0.2	0.9 ± 0.3	1.6 ± 0.5	1.98 ± 0.06	5.5 ± 0.1	<3σ	
$8_{4,5}$–$8_{3,5}$	349 862	blended 349 864		1.4 ± 0.2	3.9 ± 0.4	1.5 ± 0.1	2.3 ± 0.1	3.6 ± 0.2	7.3 ± 0.3	<3σ	
$8_{4,4}$–$8_{3,6}$	349 864	blended with 349 862		1.7 ± 0.2	4.7 ± 0.2	0.9 ± 0.3	1.2 ± 0.2	blended with 349 862		<3σ	
$7_{4,4}$–$7_{3,4}$	349 952	⋆ 6.2 ± 0.2	14.2 ± 0.4	2.07 ± 0.03	7.6 ± 0.1	1.8 ± 0.1	3.2 ± 0.2	2.31 ± 0.04	10.1 ± 0.2	<3σ	
$6_{4,3}$–$6_{3,3}$	350 027	⋆ 5.4 ± 0.4	13.8 ± 0.8	1.67 ± 0.04	7.2 ± 0.2	1.7 ± 0.2	3.0 ± 0.2	2.11 ± 0.04	10.3 ± 0.2	<3σ	
$5_{4,2}$–$5_{3,2}$	350 090	⋆ 6.3 ± 0.6	10.8 ± 0.6	1.81 ± 0.09	6.2 ± 0.3	1.4 ± 0.2	2.8 ± 0.3	2.07 ± 0.02	8.07 ± 0.07	<3σ	
$4_{4,1}$–$4_{3,1}$	350 141	blended		1.71 ± 0.08	3.6 ± 0.1	2.1 ± 0.4	1.7 ± 0.2	3.7 ± 0.1	5.7 ± 0.1	<3σ	
$6_{2,5}$–$5_{1,5}$	350 454	blended		1.5 ± 0.2	3.4 ± 0.2	1.3 ± 0.1	1.13 ± 0.08	1.9 ± 0.1	3.8 ± 0.2	<3σ	
$5_{1,4}$–$5_{0,5}$	350 632	⋆ 5.5 ± 0.4	13.3 ± 0.7	1.92 ± 0.09	8.4 ± 0.3	1.7 ± 0.2	4.7 ± 0.4	2.07 ± 0.04	12.1 ± 0.2	<3σ	

Table B.5. Acetaldehyde.

Transition	Frequency (MHz)	G35.20 A *FWHM* (km s^{-1})	G35.20 A T_{peak} (K)	G35.20 B1 *FWHM* (km s^{-1})	G35.20 B1 T_{peak} (K)	G35.20 B2 *FWHM* (km s^{-1})	G35.20 B2 T_{peak} (K)	G35.20 B3 *FWHM* (km s^{-1})	G35.20 B3 T_{peak} (K)	G35.03 A *FWHM* (km s^{-1})	G35.03 A T_{peak} (K)
CH_3CHO $\nu = 0$											
$18_{1,4}$–$17_{1,4}$	334 980	⋆ 4.8 ± 0.3	2.07 ± 0.07	0.8 ± 0.1	0.55 ± 0.09	0.9 ± 0.2	0.5 ± 0.1	1.4 ± 0.4	1.0 ± 0.1	<3σ	
$18_{0,18}$–$17_{0,17}$E	335 318	5.1 ± 0.1	8.9 ± 0.2	2.0 ± 0.2	3.3 ± 0.2	2.3 ± 0.1	2.0 ± 0.1	1.7 ± 0.1	3.7 ± 0.2	4.2 ± 0.2	2.42 ± 0.10
$18_{0,18}$–$17_{0,17}$A	335 358	5.38 ± 0.09	12.8 ± 0.2	2.2 ± 0.5	3.8 ± 0.3	1.7 ± 0.2	1.7 ± 0.2	2.5 ± 0.1	5.6 ± 0.1	<3σ	
$18_{7,11}$–$17_{7,10}$E	346 934	blended		blended		1.4 ± 0.3	1.55 ± 0.10	2.5 ± 0.1	2.8 ± 0.2	3.1 ± 1.4	5.8 ± 0.9
$18_{7,12}$–$17_{7,11}$A	346 957	⋄ 3.3 ± 0.4	8.4 ± 0.8	1.54 ± 0.08	1.46 ± 0.06	2.3 ± 0.2	1.47 ± 0.10	2.7 ± 0.1	8.3 ± 0.3	<3σ	
$18_{6,12}$–$17_{6,11}$A	347 071	5.6 ± 0.2	9.2 ± 0.2	1.8 ± 0.1	3.2 ± 0.2	1.7 ± 0.4	1.7 ± 0.3	2.6 ± 0.1	5.1 ± 0.1	4.0 ± 0.2	2.6 ± 0.1
$18_{6,12}$–$17_{6,11}$E	347 090	6.2 ± 0.5	6.2 ± 0.1	1.7 ± 0.2	1.2 ± 0.1	1.3 ± 0.4	1.2 ± 0.3	2.9 ± 0.1	2.63 ± 0.08	4.9 ± 0.3	1.94 ± 0.10
$18_{6,13}$–$17_{6,12}$E	347 133	blended		1.5 ± 0.9	2.3 ± 4.2	2.4 ± 0.3	1.8 ± 0.1	2.46 ± 0.05	9.7 ± 0.1	<3σ	
$18_{5,14}$–$17_{5,13}$A	347 288	⋆ 4.6 ± 0.3	5.3 ± 0.3	1.6 ± 0.2	2.6 ± 0.5	1.7 ± 0.2	1.23 ± 0.10	2.26 ± 0.08	3.6 ± 0.1	3.1 ± 0.3	1.84 ± 0.04
$18_{5,13}$–$17_{5,12}$A	347 295	⋆ 7.2 ± 0.8	6.1 ± 0.1	2.16 ± 0.07	2.72 ± 0.07	1.6 ± 0.1	1.27 ± 0.09	2.3 ± 0.1	3.5 ± 0.1	<3σ	
$18_{5,13}$–$17_{5,12}$E	347 345	blended		1.3 ± 0.4	2.1 ± 0.6	1.7 ± 0.2	1.4 ± 0.1	2.6 ± 0.3	3.53 ± 0.07	3.4 ± 0.3	2.8 ± 0.1
$18_{5,14}$–$17_{5,13}$E	347 349	blended		blended		blended		2.87 ± 0.05	5.86 ± 0.09	4.0 ± 0.2	4.57 ± 0.09
$18_{3,16}$–$17_{3,15}$A	347 519	5.3 ± 0.2	8.4 ± 0.2	2.1 ± 0.2	3.4 ± 0.2	2.2 ± 0.3	1.3 ± 0.1	2.2 ± 0.1	5.1 ± 0.1	4.0 ± 0.2	2.21 ± 0.06
$18_{3,16}$–$17_{3,15}$E	347 563	⋆ 3.6 ± 0.4	7.5 ± 0.5	1.8 ± 0.2	3.2 ± 0.3	⋄ 1.4 ± 0.3	2.0 ± 0.3	2.16 ± 0.08	5.6 ± 0.1	<3σ	
$18_{4,15}$–$17_{4,14}$A	347 650	6.2 ± 0.4	10.1 ± 0.3	1.9 ± 0.2	3.2 ± 0.3	2.0 ± 0.3	1.6 ± 0.2	2.4 ± 0.2	5.0 ± 0.2	3.7 ± 0.5	3.3 ± 0.1
$18_{4,15}$–$17_{4,14}$E	347 756	⋆ 5.8 ± 0.1	18.5 ± 0.3	2.7 ± 0.2	4.6 ± 0.2	blended		2.3 ± 0.2	6.2 ± 0.5	<3σ	
$18_{4,14}$–$17_{4,13}$E	347 830	6.2 ± 0.6	6.4 ± 0.2	1.93 ± 0.10	2.3 ± 0.1	⋄ 1.9 ± 0.3	1.5 ± 0.2	2.2 ± 0.1	4.2 ± 0.2	3.0 ± 0.6	1.59 ± 0.08
$18_{4,14}$–$17_{4,13}$A	347 838	blended		1.3 ± 0.3	2.2 ± 0.3	1.6 ± 0.3	1.7 ± 0.3	1.6 ± 0.1	5.5 ± 0.2	<3σ	
$18_{3,15}$–$17_{3,14}$A	350 135	⋄ 6.8 ± 0.2	17.5 ± 0.2	2.4 ± 0.1	5.3 ± 0.2	1.9 ± 0.5	2.5 ± 2.0	3.0 ± 0.1	8.0 ± 0.1	5.4 ± 0.2	5.1 ± 0.1
$18_{1,17}$–$17_{1,16}$E	350 363	blended		1.8 ± 0.3	4.8 ± 0.6	blended		1.5 ± 0.2	4.6 ± 0.6	<3σ	
$18_{1,17}$–$17_{1,16}$A	350 445	blended		2.1 ± 0.2	5.8 ± 0.8	1.3 ± 0.2	2.1 ± 0.3	blended		<3σ	
CH_3CHO $\nu = 1$											
$18_{0,18}$–$17_{0,17}$ A	335 382	partially blended		2.5 ± 0.2	0.60 ± 0.08	<3σ		1.9 ± 0.2	1.1 ± 0.1	<3σ	
$18_{0,18}$–$17_{0,17}$ E	336 416	3.4 ± 0.5	1.46 ± 0.09	1.2 ± 0.3	0.8 ± 0.2	<3σ		<3σ		<3σ	
$18_{5,13}$–$17_{5,12}$E	347 217	blended		blended		<3σ		2.4 ± 0.3	5.8 ± 1.0	<3σ	
$18_{5,14}$–$17_{5,13}$E	347 252	3.0 ± 0.6	1.77 ± 0.09	<3σ		<3σ		1.7 ± 0.3	1.14 ± 0.08	<3σ	
$18_{7,11}$–$17_{7,10}$A	347 459	<3σ		<3σ		<3σ		2.1 ± 0.2	0.83 ± 0.07	<3σ	
$18_{8,11}$–$19_{7,12}$A	347 645	2.0 ± 1.0	1.1 ± 0.5	<3σ		<3σ		2.1 ± 0.4	0.8 ± 0.1	<3σ	
$18_{9,10}$–$17_{9,9}$	347 819	<3σ		<3σ		<3σ		<3σ		<3σ	
$18_{6,13}$–$17_{6,12}$ A	348 088	blended		blended		<3σ		2.5 ± 0.1	1.43 ± 0.06	4.1 ± 0.7	1.8 ± 0.1
$18_{3,16}$–$17_{3,15}$A	348 211	5.8 ± 0.1	4.86 ± 0.09	<3σ		1.1 ± 0.3	0.9 ± 0.2	2.3 ± 0.3	2.0 ± 0.1	5.5 ± 0.4	1.26 ± 0.06
$18_{4,15}$–$17_{4,14}$E	348 229	blended		1.4 ± 0.2	1.0 ± 0.1	1.7 ± 0.2	1.01 ± 0.08	1.4 ± 0.4	0.9 ± 0.1	<3σ	
$18_{3,15}$–$17_{3,14}$E	348 288	blended		1.9 ± 0.2	0.93 ± 0.08	1.8 ± 0.2	0.92 ± 0.06	0.8 ± 0.2	0.49 ± 0.07	<3σ	
$18_{5,14}$–$17_{5,13}$A	348 570	3.8 ± 1.4	2.7 ± 0.6	2.3 ± 0.2	0.93 ± 0.08	1.4 ± 0.3	0.59 ± 0.03	2.6 ± 0.4	0.9 ± 0.2	4.4 ± 0.3	0.97 ± 0.05
$18_{5,13}$–$17_{5,12}$A	348 578	⋄ 3.7 ± 4.6	1.2 ± 2.4	⋄ 1.6 ± 0.3	0.60 ± 0.06	<3σ		⋄ 1.25 ± 1.28	0.4 ± 0.2	<3σ	
$18_{4,15}$–$17_{4,14}$A	348 855	blended		<3σ		<3σ		2.8 ± 0.4	0.8 ± 0.2	<3σ	
$18_{1,17}$–$17_{1,16}$A	349 320	5.3 ± 0.2	4.03 ± 0.10	1.6 ± 0.2	1.0 ± 0.1	<3σ		1.9 ± 0.2	1.4 ± 0.1	3.9 ± 0.2	1.72 ± 0.04
	349 650	<3σ		<3σ		<3σ		<3σ		3.0 ± 0.4	0.81 ± 0.06
CH_3CHO $\nu = 2$											
$17_{9,9}$–$16_{9,8}$ A	335 224	6.2 ± 0.7	1.87 ± 0.08	<3σ		<3σ		<3σ		<3σ	
$18_{1,18}$–$17_{1,17}$E	336 025	blended		<3σ		blended		1.2 ± 7.1	0.9 ± 0.1	<3σ	
$18_{1,18}$–$17_{1,17}$ A	337 082	7.3 ± 0.3	5.6 ± 0.1	<3σ		<3σ		3.4 ± 0.6	0.85 ± 0.05	4.1 ± 0.6	2.4 ± 0.2
$18_{2,17}$–$17_{2,16}$ A	347 657	⋄ 2.4 ± 1.0	2.4 ± 0.5	<3σ		<3σ		<3σ		<3σ	
$18_{3,15}$–$17_{3,14}$ A	349 752	⋄ 2.4 ± 0.2	8.6 ± 0.3	0.7 ± 0.7	0.6 ± 0.5	<3σ		2.4 ± 0.7	0.9 ± 0.1	<3σ	

Notes. ⋄ Partially blended with other lines, ⋆ double peaked.

Table B.6. Methyl formate.

Transition	Frequency (MHz)	G35.20 A *FWHM* (km s^{-1})	G35.20 A T_{peak} (K)	G35.20 B1 *FWHM* (km s^{-1})	G35.20 B1 T_{peak} (K)	G35.20 B2 *FWHM* (km s^{-1})	G35.20 B2 T_{peak} (K)	G35.20 B3 *FWHM* (km s^{-1})	G35.20 B3 T_{peak} (K)	G35.03 A *FWHM* (km s^{-1})	G35.03 A T_{peak} (K)
CH_3OCHO $\nu = 0$											
$15_{6,10}$–$14_{5,10}$E	335 145	blended		⋄ 2.0 ± 0.2	0.62 ± 0.02	<3σ		<3σ		blended	
$28_{4,24}$–$27_{5,23}$E	335 158	blended		⋄ 2.2 ± 0.5	0.7 ± 0.1	<3σ		blended		blended	
$28_{4,24}$–$27_{5,23}$A	335 183	6.0 ± 0.1	3.26 ± 0.05	2.3 ± 0.5	0.77 ± 0.09	<3σ		<3σ		4.4 ± 0.2	2.42 ± 0.09
$13_{2,11}$–$12_{1,12}$A	335 336	blended		<3σ		<3σ		<3σ		<3σ	
$15_{6,9}$–$14_{5,10}$A	335 403	blended		1.90 ± 0.11	0.85 ± 0.04	1.1 ± 0.3	0.5 ± 0.1	blended		<3σ	
$15_{6,9}$–$14_{5,10}$E	335 454	3.1 ± 1.1	1.3 ± 0.6	<3σ		<3σ		<3σ		blended	
$26_{5,22}$–$25_{4,21}$A	335 828	5.6 ± 0.8	2.6 ± 0.2	1.9 ± 0.2	0.87 ± 0.06	<3σ		1.8 ± 0.2	0.82 ± 0.08	2.5 ± 0.1	1.27 ± 0.06
$26_{5,22}$–$25_{4,21}$E	335 839	blended		3.0 ± 0.2	0.79 ± 0.06	<3σ		1.6 ± 1.9	0.6 ± 0.6	blended	
$27_{9,19}$–$26_{9,17}$E	335 900	blended		1.9 ± 0.7	0.5 ± 0.1	<3σ		<3σ		<3σ	
$27_{9,19}$–$26_{9,18}$A	336 028	⋄ 7.3 ± 0.1	24.4 ± 0.3	⋄ 1.58 ± 0.06	3.88 ± 0.07	⋄ 2.5 ± 0.1	2.8 ± 0.1	⋄ 2.9 ± 0.2	4.6 ± 0.1	⋄ 4.3 ± 0.3	6.7 ± 0.1
$27_{9,19}$–$26_{9,18}$E	336 032	blended with 336 028		⋄ 1.63 ± 0.06	3.99 ± 0.07	⋄ 1.1 ± 0.2	1.2 ± 0.2	⋄ 2.5 ± 0.2	4.1 ± 0.1	⋄ 3.9 ± 0.5	6.3 ± 0.6
$27_{9,18}$–$26_{9,17}$E	336 086	blended		blended		3.66 ± 0.09	7.8 ± 0.1	blended		<3σ	
$27_{9,18}$–$26_{9,17}$A	336 111	5.4 ± 0.1	15.0 ± 0.3	1.8 ± 0.2	3.9 ± 0.3	1.8 ± 0.2	1.8 ± 0.1	2.58 ± 0.09	4.1 ± 0.1	5.0 ± 0.1	4.64 ± 0.10
$27_{9,18}$–$26_{9,18}$E	336 219	blended		<3σ		<3σ		2.7 ± 0.3	0.52 ± 0.05	<3σ	
$27_{6,22}$–$26_{6,21}$E	336 351	⋄ 6.8 ± 0.1	26.9 ± 0.5	⋄ 1.7 ± 0.1	3.9 ± 0.2	⋄ 2.29 ± 0.07	2.80 ± 0.06	⋄ 1.9 ± 0.1	5.7 ± 0.3	⋄ 3.6 ± 0.3	4.1 ± 0.2
$26_{5,21}$–$25_{5,20}$E	336 355	blended with 336 351		⋄ 1.9 ± 0.1	5.6 ± 0.2	⋄ 1.66 ± 0.06	2.91 ± 0.07	⋄ 2.9 ± 0.2	6.3 ± 0.2	⋄ 3.8 ± 0.2	6.8 ± 0.2
$27_{6,22}$–$26_{6,21}$A	336 368	⋄★ 5.0 ± 0.6	14.9 ± 1.3	1.4 ± 0.2	4.6 ± 0.5	2.1 ± 0.2	2.4 ± 0.2	1.99 ± 0.06	4.9 ± 0.1	3.8 ± 0.3	5.1 ± 0.2
$26_{5,21}$–$25_{5,20}$A	336 374	⋄★ 5.7 ± 0.6	18.0 ± 0.9	1.81 ± 0.09	4.9 ± 0.2	1.7 ± 0.2	3.6 ± 0.2	2.2 ± 0.2	6.4 ± 0.4	4.5 ± 0.4	5.3 ± 0.2
$26_{6,20}$–$25_{6,19}$E	336 889	★ 5.0 ± 0.2	16.2 ± 0.5	1.4 ± 0.1	4.9 ± 0.3	1.8 ± 0.2	2.8 ± 0.2	2.16 ± 0.06	5.9 ± 0.1	4.7 ± 0.3	4.8 ± 0.2
$26_{6,20}$–$25_{6,19}$A	336 918	5.8 ± 0.2	17.6 ± 0.5	1.72 ± 0.07	4.8 ± 0.2	2.0 ± 0.1	3.0 ± 0.1	2.34 ± 0.04	5.60 ± 0.08	5.6 ± 0.3	5.4 ± 0.2
$27_{8,20}$–$26_{8,19}$E	337 490	5.9 ± 0.1	30.2 ± 0.6	2.5 ± 0.2	9.5 ± 0.5	2.22 ± 0.07	5.0 ± 0.1	2.1 ± 0.8	7 ± 0.6	<3σ	
$27_{8,20}$–$26_{8,19}$A	337 504	★ 5.1 ± 0.2	14.6 ± 0.4	1.57 ± 0.09	4.1 ± 0.2	1.9 ± 0.4	2.2 ± 0.4	2.26 ± 0.04	4.63 ± 0.08	4.6 ± 0.2	3.9 ± 0.1
$27_{8,19}$–$26_{8,18}$E	338 338	5.6 ± 0.3	22.2 ± 0.7	1.4 ± 0.2	4.4 ± 0.4	blended		1.74 ± 0.02	4.92 ± 0.06	<3σ	
$27_{8,19}$–$26_{8,18}$A	338 356	★ 6.0 ± 0.3	14.6 ± 0.5	1.5 ± 0.1	4.2 ± 0.3	1.7 ± 0.3	2.3 ± 0.3	2.32 ± 0.05	4.67 ± 0.09	5.9 ± 0.3	4.5 ± 0.1
$27_{7,21}$–$26_{7,20}$E	338 396	⋄ 7.6 ± 0.5	17.8 ± 0.5	1.4 ± 0.1	4.2 ± 0.3	1.8 ± 0.1	2.5 ± 0.2	2.00 ± 0.10	4.1 ± 0.1	<3σ	
$27_{7,21}$–$26_{7,20}$A	338 414	7.3 ± 1.2	23.4 ± 3.2	blended		1.5 ± 0.2	1.8 ± 0.2	1.9 ± 1.2	5.2 ± 1.5	<3σ	
$27_{5,22}$–$26_{5,21}$E	347 478	★ 7.2 ± 0.5	19.6 ± 1.5	1.7 ± 0.1	5.6 ± 0.3	1.71 ± 0.07	3.9 ± 0.1	2.17 ± 0.05	6.7 ± 0.1	5.2 ± 0.3	6.6 ± 0.1
$27_{5,22}$–$26_{5,21}$A	347 494	★ 5.6 ± 1.3	19.1 ± 1.5	1.59 ± 0.05	5.9 ± 0.2	2.10 ± 0.09	3.4 ± 0.1	2.14 ± 0.04	7.4 ± 0.1	5.1 ± 0.3	5.03 ± 0.10
$16_{6,10}$–$15_{5,11}$A	347 590	★ 7.1 ± 0.8	3.7 ± 0.2	3.0 ± 0.2	1.46 ± 0.08	1.1 ± 0.4	0.8 ± 0.2	1.4 ± 0.2	1.2 ± 0.1	<3σ	
$16_{6,10}$–$15_{5,11}$E	347 599	★ 2.8 ± 2.0	2.7 ± 4.3	2.3 ± 0.2	1.26 ± 0.09	1.5 ± 0.4	0.7 ± 0.1	<3σ		<3σ	
$28_{10,18}$–$27_{10,17}$E	347 605	★ 6.3 ± 0.2	11.2 ± 0.3	1.4 ± 0.2	3.2 ± 0.3	1.6 ± 0.1	2.4 ± 0.2	2.10 ± 0.06	3.72 ± 0.09	5.3 ± 0.4	3.1 ± 0.1
$28_{10,19}$–$27_{10,18}$A	347 617	★ 5.8 ± 0.3	11.3 ± 0.4	1.24 ± 0.08	3.7 ± 0.2	1.8 ± 0.1	2.0 ± 0.1	2.02 ± 0.07	3.52 ± 0.10	3.5 ± 0.1	3.13 ± 0.10
$28_{10,19}$–$27_{10,18}$E	347 628	★ 5.4 ± 0.2	20.5 ± 0.7	1.7 ± 0.1	5.5 ± 0.4	1.7 ± 0.3	3.6 ± 0.5	2.26 ± 0.04	7.4 ± 0.1	4.5 ± 0.3	4.9 ± 0.2
$29_{4,25}$–$28_{5,24}$E	347 818	blended		1.12 ± 0.04	1.04 ± 0.03	1.4 ± 0.2	0.55 ± 0.09	<3σ		<3σ	
$28_{6,23}$–$27_{6,22}$E	348 050	5.0 ± 1.0	12.2 ± 2.0	1.49 ± 0.06	4.3 ± 0.1	1.8 ± 0.1	3.0 ± 0.2	2.26 ± 0.07	5.6 ± 0.1	6.0 ± 0.2	4.4 ± 0.1
$28_{6,23}$–$27_{6,22}$A	348 066	5.6 ± 0.2	17.7 ± 0.5	1.56 ± 0.04	4.9 ± 0.1	1.7 ± 0.1	2.8 ± 0.1	2.0 ± 0.1	5.5 ± 0.2	4.6 ± 0.3	4.4 ± 0.2
$28_{9,20}$–$27_{9,19}$E	348 909	blended with 348 915		2.1 ± 0.2	3.8 ± 0.3	2.2 ± 0.2	2.7 ± 0.2	2.2 ± 0.1	5.1 ± 0.4	5.9 ± 0.2	6.5 ± 0.1
$28_{9,20}$–$27_{9,19}$A	348 915	⋄★ 8.0 ± 0.1	27.4 ± 0.4	⋄ 2.5 ± 0.2	4.0 ± 0.3	⋄ 1.2 ± 0.2	1.8 ± 0.2	⋄ 2.2 ± 0.1	3.8 ± 0.2	⋄ 5.9 ± 0.2	6.8 ± 0.2
$28_{5,24}$–$27_{4,23}$A	349 015	blended		0.8 ± 0.3	0.9 ± 0.2	0.7 ± 0.2	0.6 ± 0.1	<3σ		<3σ	

Notes. ⋄ Partially blended with other lines, ★ double peaked.

Table B.6. continued.

Transition	Frequency (MHz)	G35.20 A *FWHM* (km s^{-1})	G35.20 A T_{peak} (K)	G35.20 B1 *FWHM* (km s^{-1})	G35.20 B1 T_{peak} (K)	G35.20 B2 *FWHM* (km s^{-1})	G35.20 B2 T_{peak} (K)	G35.20 B3 *FWHM* (km s^{-1})	G35.20 B3 T_{peak} (K)	G35.03 A *FWHM* (km s^{-1})	G35.03 A T_{peak} (K)
$28_{5,24}$–$27_{4,23}$E	349 019	blended		<3σ							
blended		blended		<3σ							
$28_{9,19}$ − $27_{9,18}$E	349 049	⋆ 6.9 ± 0.3	12.6 ± 0.4	1.5 ± 0.1	3.9 ± 0.3	1.6 ± 0.3	2.0 ± 0.3	2.24 ± 0.07	4.00 ± 0.09	4.0 ± 0.4	3.5 ± 0.2
$28_{9,19}$–$27_{9,18}$A	349 066	⋆ 6.3 ± 0.3	13.1 ± 0.5	1.50 ± 0.07	4.2 ± 0.2	1.4 ± 0.2	2.1 ± 0.2	2.23 ± 0.07	4.26 ± 0.12	4.8 ± 0.2	3.6 ± 0.1
$26_{7,19}$–$26_{5,22}$E	350 306	blended		blended		<3σ		<3σ		<3σ	
$28_{8,21}$–$27_{8,20}$E	350 442	blended		⋄ 1.61 ± 0.07	4.5 ± 0.1	⋄ 3.1 ± 0.2	2.74 ± 0.08	blended		<3σ	
$28_{8,21}$–$27_{8,20}$A	350 458	blended		2.02 ± 0.09	4.3 ± 0.2	1.4 ± 0.2	1.9 ± 0.2	2.09 ± 0.09	4.89 ± 0.17	4.7 ± 0.4	3.6 ± 0.2
CH_3OCHO $\nu = 1$											
$27_{7,21}$–$26_{7,20}$A	335 016	5.6 ± 0.2	4.15 ± 0.10	1.3 ± 0.1	1.5 ± 0.1	<3σ		1.6 ± 0.2	0.72 ± 0.07	2.1 ± 0.3	0.99 ± 0.10
$15_{6,10}$–$14_{5,10}$E	335 208	3.9 ± 0.3	1.17 ± 0.09	<3σ		<3σ		<3σ		<3σ	
$27_{8,20}$–$26_{8,19}$E	335 392	blended		in abs feature		2.6 ± 0.3	3.0 ± 0.2	blended		4.0 ± 0.5	1.24 ± 0.06
$27_{7,21}$–$26_{7,20}$E	335 961	5.4 ± 0.2	4.0 ± 0.2	1.8 ± 0.3	0.8 ± 0.1	<3σ		1.8 ± 0.2	1.04 ± 0.10	2.3 ± 0.2	1.2 ± 0.1
$28_{5,24}$–$27_{5,23}$A	338 393	blended with 338 396		blended with 338 396		blended with 338 396		1.3 ± 0.3	1.3 ± 0.2	<3σ	
$28_{7,22}$–$27_{7,21}$A	347 568	1.1 ± 0.2	2.4 ± 0.4	1.0 ± 0.2	1.5 ± 0.2	0.8 ± 0.9	0.7 ± 0.2	2.2 ± 0.3	1.0 ± 0.1	<3σ	
$27_{6,21}$–$26_{6,20}$E	347 698	blended		1.5 ± 0.2	1.5 ± 0.2	<3σ		1.59 ± 0.07	1.59 ± 0.06	3.0 ± 0.4	2.24 ± 0.09
$25_{13,12}$–$25_{12,13}$E	348 053	⋄ 4.5 ± 1.0	9.6 ± 2.0	<3σ		<3σ		⋄ 2.2 ± 0.1	5.7 ± 0.2	<3σ	
$28_{8,21}$–$27_{8,20}$E	348 084	6.8 ± 0.2	9.2 ± 0.2	1.86 ± 0.08	1.87 ± 0.07	2.50 ± 0.27	0.67 ± 0.05	2.8 ± 0.1	1.76 ± 0.08	5.5 ± 0.3	2.22 ± 0.06
$9_{9,1}$–$8_{8,1}$E	348 247	5.5 ± 1.4	1.3 ± 0.1	<3σ		<3σ		<3σ		<3σ	
$29_{5,25}$–$28_{5,24}$E	349 685	5.5 ± 0.2	5.7 ± 0.1	1.27 ± 0.10	1.21 ± 0.08	0.5 ± 1.3	0.6 ± 1.3	2.1 ± 0.3	1.3 ± 0.1	3.5 ± 0.2	1.26 ± 0.06
$18_{13,5}$–$18_{12,6}$E	349 836	2.2 ± 0.3	1.1 ± 0.1	<3σ		<3σ		<3σ		<3σ	

Table B.7. Dimethyl ether.

Transition	Frequency (MHz)	G35.20 A *FWHM* (km s^{-1})	G35.20 A T_{peak} (K)	G35.20 B1 *FWHM* (km s^{-1})	G35.20 B1 T_{peak} (K)	G35.20 B2 *FWHM* (km s^{-1})	G35.20 B2 T_{peak} (K)	G35.20 B3 *FWHM* (km s^{-1})	G35.20 B3 T_{peak} (K)	G35.03 A *FWHM* (km s^{-1})	G35.03 A T_{peak} (K)
CH_3OCH_3 $\nu = 0$											
$21_{2,19}$–$20_{3,18}$AA	337 421	⋆ 5.4 ± 0.2	13.2 ± 0.4	2.05 ± 0.05	10.8 ± 0.2	1.7 ± 0.2	3.2 ± 0.3	2.53 ± 0.04	22.5 ± 0.3	4.7 ± 0.2	6.1 ± 0.2
$7_{4,4}$–$6_{3,3}$ EA	337 712	blended		⋄ 1.5 ± 1.2	2.2 ± 1.7	<3σ		⋄ 2.40 ± 0.04	5.35 ± 0.07	<3σ	
$7_{4,4}$–$6_{3,3}$ EE	337 722	⋆ 6.8 ± 3.4	10.5 ± 1.9	1.89 ± 0.06	7.9 ± 0.2	1.6 ± 0.2	3.3 ± 0.3	2.25 ± 0.05	19.8 ± 0.4	4.1 ± 0.1	4.57 ± 0.08
$7_{4,3}$–$6_{3,3}$ EA	337 731	⋆ 6.7 ± 1.7	16.4 ± 6.8	2.45 ± 0.05	11.3 ± 0.2	2.1 ± 0.2	3.3 ± 0.3	3.00 ± 0.08	24.8 ± 0.6	5.5 ± 0.2	6.5 ± 0.1
$7_{4,4}$–$6_{3,4}$ EA	337 770	⋆ 4.4 ± 1.4	2.5 ± 0.5	1.2 ± 0.2	2.5 ± 0.3	1.3 ± 0.6	0.6 ± 0.2	1.8 ± 0.1	7.5 ± 0.5	<3σ	
$7_{4,3}$–$6_{3,4}$ EE	337 779	⋆ 5.1 ± 0.3	13.7 ± 0.4	2.5 ± 0.1	9.7 ± 0.3	2.2 ± 0.3	3.0 ± 0.3	2.73 ± 0.08	22.5 ± 0.6	5.0 ± 0.1	6.05 ± 0.08
$7_{4,3}$–$6_{3,4}$ EE	337 787	6.0 ± 0.1	29.4 ± 0.4	2.32 ± 0.04	15.1 ± 0.1	2.2 ± 0.2	4.9 ± 0.4	2.45 ± 0.09	27.0 ± 1.0	6.5 ± 0.1	14.1 ± 0.2
$7_{4,4}$–$6_{3,4}$ EE	337 790	blended with 337 787		2.0 ± 0.1	4.2 ± 0.1	in abs feature		2.8 ± 0.4	7.0 ± 0.8	<3σ	
$35_{3,33}$–$35_{2,34}$	347 985	2.5 ± 1.0	2.7 ± 0.9	<3σ		<3σ		1.53 ± 0.06	1.46 ± 0.03	<3σ	
$35_{3,32}$–$35_{2,33}$EE	347 989	2.5 ± 3.1	1.6 ± 0.8	<3σ		<3σ		1.56 ± 0.06	2.01 ± 0.04	<3σ	
$35_{3,33}$–$35_{2,34}$AA	347 992	2.5 ± 1.2	1.7 ± 0.6	<3σ		<3σ		1.3 ± 0.1	1.04 ± 0.05	<3σ	
$32_{2,31}$–$32_{1,32}$ EE	349 487	blended		<3σ		<3σ		2.2 ± 0.2	2.1 ± 0.2	<3σ	
$11_{2,9}$–$10_{1,10}$AE	349 803	blended with 349 806		1.4 ± 0.1	2.1 ± 0.1	1.3 ± 0.3	0.9 ± 0.2	1.70 ± 0.07	8.8 ± 0.3	<3σ	
$11_{2,9}$–$10_{1,10}$EE	349 806	⋄⋆ 7.8 ± 0.2	7.6 ± 0.2	⋄ 1.9 ± 0.1	3.9 ± 0.1	⋄ 0.9 ± 0.2	0.7 ± 0.1	⋄ 2.4 ± 0.1	12.7 ± 0.2	<3σ	
$11_{2,9}$–$10_{1,10}$AA	349 809	blended with 349 806		1.46 ± 0.09	3.29 ± 0.14	in abs feature		2.1 ± 0.1	8.5 ± 0.2	<3σ	

Notes. ⋄ Partially blended with other lines, ⋆ double peaked.

Table B.8. Ethanol.

Transition	Frequency (MHz)	G35.20 A *FWHM* (km s^{-1})	G35.20 A T_{peak} (K)	G35.20 B1 *FWHM* (km s^{-1})	G35.20 B1 T_{peak} (K)	G35.20 B2 *FWHM* (km s^{-1})	G35.20 B2 T_{peak} (K)	G35.20 B3 *FWHM* (km s^{-1})	G35.20 B3 T_{peak} (K)	G35.03 A *FWHM* (km s^{-1})	G35.03 A T_{peak} (K)
t-C_2H_5OH											
$24_{1,23}$–$23_{2,21}$	335 192	⋄ 4 ± 2	1.2 ± 0.5	<3σ		<3σ		<3σ		2.5 ± 0.2	1.00 ± 0.09
$23_{7,16}$–$23_{6,17}$	335 441	★ 5.1 ± 0.2	6.4 ± 0.2	1.6 ± 0.2	1.98 ± 0.08	1.9 ± 0.5	0.6 ± 0.2	2.3 ± 0.1	1.78 ± 0.08	2.8 ± 0.2	1.8 ± 0.1
$23_{7,17}$–$23_{6,18}$	335 631	★ 5.5 ± 0.2	7.0 ± 0.2	1.9 ± 0.2	2.2 ± 0.1	1.3 ± 0.7	1.1 ± 0.2	2.2 ± 0.2	1.8 ± 0.1	3.6 ± 0.2	2.16 ± 0.10
$13_{3,11}$–$12_{2,10}$	335 950	★ 5.0 ± 0.2	10.3 ± 0.4	2.1 ± 0.2	3.9 ± 0.2	1.9 ± 0.2	1.8 ± 0.2	1.9 ± 0.3	4.2 ± 0.2	3.1 ± 0.2	2.79 ± 0.09
$22_{7,15}$–$22_{6,16}$	336 158	5.6 ± 0.6	4.1 ± 0.2	1.6 ± 0.2	2.6 ± 0.2	1.7 ± 0.4	1.3 ± 0.1	1.5 ± 0.4	1.8 ± 1.0	2.7 ± 0.3	2.7 ± 0.2
$22_{7,16}$–$22_{6,17}$	336 270	⋄ 6.3 ± 0.1	10.9 ± 0.2	2.6 ± 0.3	3.3 ± 0.3	1.6 ± 0.9	1.5 ± 0.3	3.0 ± 0.6	6.9 ± 0.4	4.9 ± 0.1	3.66 ± 0.06
$19_{2,18}$–$18_{1,17}$	336 626	5.6 ± 0.1	18.6 ± 0.4	<3σ		<3σ		<3σ		4.0 ± 0.2	5.6 ± 0.2
$21_{7,14}$–$21_{6,15}$	336 767	★ 5.3 ± 0.2	7.9 ± 0.2	1.9 ± 0.1	2.6 ± 0.1	1.3 ± 0.7	0.9 ± 0.2	2.1 ± 0.1	2.32 ± 0.07	3.9 ± 0.2	2.9 ± 0.1
$21_{7,15}$–$21_{6,16}$	336 832	★ 6.1 ± 0.2	8.9 ± 0.2	edge of window		edge of window		edge of window		<3σ	
$20_{7,14}$–$20_{6,15}$	337 323	6.4 ± 0.5	9.7 ± 0.5	1.33 ± 0.01	2.86 ± 0.01	1.3 ± 0.2	1.7 ± 0.3	2.6 ± 0.2	2.8 ± 0.1	5.4 ± 0.7	5.09 ± 0.08
$19_{7,12}$–$19_{6,13}$	337 727	blended		1.4 ± 0.1	2.2 ± 0.2	1.2 ± 0.4	1.3 ± 0.5	blended		2.1 ± 0.2	2.3 ± 0.2
$18_{7,11}$–$18_{6,12}$	338 099	★ 6.8 ± 0.4	13.2 ± 0.3	1.5 ± 0.2	3.3 ± 0.2	1.6 ± 0.3	1.7 ± 0.4	2.5 ± 0.2	3.7 ± 0.1	6.0 ± 0.3	4.1 ± 0.1
$18_{7,12}$–$18_{6,13}$	338 110	★ 7.0 ± 0.4	15.0 ± 0.3	1.9 ± 0.2	3.5 ± 0.1	1.8 ± 0.2	1.3 ± 0.2	3.0 ± 0.4	3.3 ± 0.3	5.4 ± 0.4	4.51 ± 0.09
$17_{7,10}$–$17_{6,11}$	338 411	blended		blended		blended		blended		<3σ	
$17_{7,11}$–$17_{6,12}$	338 416	blended		<3σ		<3σ		<3σ		<3σ	
$16_{7,9}$–$16_{6,10}$	338 672	blended with 338 674		1.7 ± 0.1	3.6 ± 0.2	2.2 ± 0.1	1.77 ± 0.09	2.2 ± 0.4	3.3 ± 0.2	5.3 ± 0.1	4.40 ± 0.10
$16_{7,10}$–$16_{6,11}$	338 674	★ 6.0 ± 0.1	17.4 ± 0.3	1.8 ± 0.4	4.1 ± 0.9	1.0 ± 0.3	1.2 ± 0.2	2.2 ± 0.3	3.4 ± 0.3	<3σ	
$21_{0,21}$–$20_{1,20}$	346 963	6.2 ± 0.2	26.2 ± 0.4	2.4 ± 0.1	8.8 ± 0.4	1.8 ± 0.4	3.5 ± 0.3	2.6 ± 0.2	8.4 ± 0.2	5.6 ± 0.1	8.8 ± 0.1
$14_{3,12}$–$13_{2,11}$	347 351	★ 5.6 ± 0.1	17.1 ± 0.4	3.1 ± 0.1	6.5 ± 0.2	1.9 ± 0.5	1.8 ± 0.4	2.9 ± 0.1	5.9 ± 0.1	3.8 ± 0.2	4.5 ± 0.1
$21_{1,21}$–$20_{0,20}$	347 446	blended		1.9 ± 0.1	9.3 ± 0.4	2.0 ± 0.5	4.1 ± 0.4	2.3 ± 0.2	9.9 ± 0.3	4.5 ± 0.1	8.0 ± 0.2
$22_{2,20}$–$21_{3,19}$	347 975	★ 6.9 ± 0.2	11.0 ± 0.1	1.9 ± 0.1	3.2 ± 0.2	1.5 ± 0.3	1.5 ± 0.2	2.6 ± 0.2	3.0 ± 0.2	<3σ	
$20_{2,19}$–$19_{1,18}$	350 534	★ 4.8 ± 0.2	16.1 ± 0.5	1.8 ± 0.2	6.1 ± 0.3	1.7 ± 0.4	3.0 ± 0.4	2.08 ± 0.09	5.3 ± 0.2	3.1 ± 0.2	4.1 ± 0.2
g-C_2H_5OH											
$19_{3,16}$–$18_{3,15}$, vt = 0–0	336 030	blended		⋄ 1.34 ± 0.04	4.0 ± 0.2	blended		blended		<3σ	
$19_{3,16}$–$18_{3,15}$, vt = 1–1	336 572	6.1 ± 0.2	10.7 ± 0.3	1.8 ± 0.1	3.4 ± 0.1	1.1 ± 0.4	1.7 ± 0.4	2.4 ± 0.2	3.3 ± 0.1	4.1 ± 0.2	3.4 ± 0.1
$19_{2,17}$–$18_{2,16}$, vt = 1–1	336 795	★ 5.3 ± 0.1	13.7 ± 0.3	2.1 ± 0.2	4.0 ± 0.2	1.7 ± 0.9	1.9 ± 0.3	2.3 ± 0.2	4.4 ± 0.2	4.2 ± 0.1	4.6 ± 0.1
$19_{2,17}$–$18_{2,16}$, vt = 0–0	337 801	★ 5.9 ± 0.2	7.5 ± 0.2	1.72 ± 0.04	2.45 ± 0.05	1.0 ± 0.2	1.0 ± 0.2	2.33 ± 0.08	2.28 ± 0.07	3.7 ± 0.1	2.61 ± 0.03
$20_{6,15}$–$19_{6,14}$, vt = 1–1	346 929	★ 6.6 ± 0.7	11.0 ± 0.4	2.1 ± 0.1	3.6 ± 0.3	1.5 ± 0.3	1.4 ± 0.3	2.13 ± 0.09	3.1 ± 0.1	<3σ	
$20_{6,14}$–$19_{6,13}$, vt = 1–1	346 939	⋄ 6.8 ± 1.0	13.0 ± 0.7	1.9 ± 0.1	2.5 ± 0.1	1.2 ± 0.2	1.7 ± 0.2	2.1 ± 1.1	3.1 ± 0.9	4.5 ± 0.7	9.6 ± 0.2
$20_{6,15}$–$19_{6,14}$, vt = 0–0	347 147	★ 5.2 ± 0.2	10.9 ± 0.3	1.53 ± 0.08	3.2 ± 0.1	0.8 ± 0.4	0.7 ± 0.3	2.5 ± 0.2	3.6 ± 0.1	3.64 ± 0.07	2.63 ± 0.04
$20_{6,14}$–$19_{6,13}$, vt = 0–0	347 158	★ 5.4 ± 0.2	11.2 ± 0.2	1.7 ± 0.2	3.4 ± 0.1	1.18 ± 0.07	1.71 ± 0.08	2.34 ± 0.08	3.0 ± 0.1	3.52 ± 0.09	2.94 ± 0.06
$20_{5,16}$–$19_{5,15}$, vt = 1–1	347 474	<3σ		1.1 ± 0.6	2.4 ± 0.4	2.3 ± 0.3	1.2 ± 0.2	1.8 ± 0.2	2.4 ± 0.3	4.6 ± 0.5	2.7 ± 0.3
$20_{5,15}$–$19_{5,15}$, vt = 0–0	347 670	⋄★ 5.5 ± 1.0	13.7 ± 0.3	1.9 ± 0.2	3.5 ± 0.2	1.8 ± 0.2	1.7 ± 0.1	2.30 ± 0.08	3.72 ± 0.09	4.8 ± 0.2	4.6 ± 0.1
$20_{5,15}$–$19_{5,14}$, vt = 1–1	347 675	⋄★ 5.5 ± 1.0	9.5 ± 0.4	1.7 ± 0.1	3.5 ± 0.2	1.2 ± 0.3	1.8 ± 0.3	2.0 ± 0.2	2.8 ± 0.2	3.9 ± 0.1	2.91 ± 0.05
$16_{4,12}$–$15_{3,12}$, vt = 0–1	347 693	★ 5.5 ± 1.2	7.7 ± 0.2	1.6 ± 0.1	2.0 ± 0.1	1.0 ± 0.3	1.2 ± 0.3	2.2 ± 0.1	1.7 ± 0.1	4.9 ± 0.4	2.13 ± 0.07
$20_{4,17}$–$19_{4,16}$, vt = 1–1	347 755	<3σ		±	±	2.7 ± 0.2	2.2 ± 0.2	3.0 ± 0.2	6.4 ± 0.2	5.5 ± 0.2	4.30 ± 0.10
$20_{5,15}$–$19_{5,14}$, vt = 0–0	347 887	★ 5.2 ± 0.2	12.1 ± 0.4	2.1 ± 0.1	3.8 ± 0.1	1.7 ± 0.3	1.9 ± 0.3	2.0 ± 0.1	3.4 ± 0.2	3.7 ± 0.1	3.00 ± 0.10
$20_{4,17}$–$19_{4,16}$, vt = 0–0	347 916	5.4 ± 0.4	22.5 ± 2.7	1.6 ± 0.1	4.2 ± 0.2	1.7 ± 0.2	1.2 ± 0.1	2.3 ± 0.2	4.0 ± 0.2	<3σ	
$4_{4,0}$–$3_{3,0}$, vt = 1–0	348 720	5.5 ± 0.2	13.6 ± 0.3	2.0 ± 0.2	4.3 ± 0.2	1.4 ± 0.2	2.3 ± 0.2	2.3 ± 0.1	4.4 ± 0.2	3.6 ± 0.1	3.25 ± 0.10
$4_{4,1}$–$3_{3,1}$, vt = 1–0	348 721	blended with 348 720		blended with 348 720		blended with 348 720		blended with 348 720		<3σ	
$20_{4,16}$–$19_{4,15}$, vt = 1–1	349 997	5.3 ± 0.1	12.2 ± 0.2	<3σ		<3σ		2.33 ± 0.09	3.3 ± 0.1	4.1 ± 0.1	3.46 ± 0.09
$20_{4,16}$–$19_{4,15}$, vt = 0–0	350 365	blended		⋄ 1.9 ± 0.1	5.4 ± 0.4	2.6 ± 0.8	2.9 ± 0.4	blended		4.7 ± 0.1	5.4 ± 0.1

Notes. ⋄ Partially blended with other lines, ★ double peaked.

Table B.9. Ethylene glycol.

Transition	Frequency (MHz)	G35.20 A *FWHM* (km s^{-1})	G35.20 A T_{peak} (K)	G35.20 B1 *FWHM* (km s^{-1})	G35.20 B1 T_{peak} (K)	G35.20 B2 *FWHM* (km s^{-1})	G35.20 B2 T_{peak} (K)	G35.20 B3 *FWHM* (km s^{-1})	G35.20 B3 T_{peak} (K)	G35.03 A *FWHM* (km s^{-1})	G35.03 A T_{peak} (K)
aGg' $(CH_2OH)_2$											
$32_{6,27}$ $\nu = 1$–$31_{6,26}$ $\nu = 0$	335 030	5.7 ± 0.2	4.6 ± 0.1	<3σ		<3σ		<3σ		3.9 ± 0.1	2.72 ± 0.09
$33_{9,25}$ $\nu = 0$–$32_{9,24}$ $\nu = 1$	335 180	6.1 ± 0.2	3.23 ± 0.07	<3σ		<3σ		<3σ		3.6 ± 0.2	2.15 ± 0.10
$32_{11,21}$ $\nu = 1$–$31_{11,20}$ $\nu = 0$	335 357	blended		<3σ		<3σ		<3σ		3.78 ± 0.06	6.48 ± 0.09
$33_{9,24}$ $\nu = 0$–$32_{9,23}$ $\nu = 1$	335 397	blended		<3σ		<3σ		<3σ		4.7 ± 0.3	2.38 ± 0.09
$33_{5,29}$ $\nu = 1$–$32_{4,28}$ $\nu = 1$	335 657	2.7 ± 0.1	0.82 ± 0.03	<3σ		<3σ		<3σ		2.6 ± 0.4	1.1 ± 0.1
$34_{5,30}$ $\nu = 0$–$33_{5,29}$ $\nu = 1$	335 739	6.1 ± 0.1	7.2 ± 0.1	<3σ		<3σ		<3σ		4.2 ± 0.1	3.57 ± 0.10
$33_{8,26}$ $\nu = 0$–$32_{8,25}$ $\nu = 1$	335 906	6.7 ± 0.3	3.11 ± 0.09	<3σ		<3σ		<3σ		3.80 ± 0.10	2.46 ± 0.05
$32_{10,23}$ $\nu = 1$–$31_{10,22}$ $\nu = 0$	336 012	4.5 ± 0.2	3.04 ± 0.08	<3σ		<3σ		<3σ		3.7 ± 0.4	1.9 ± 0.2
$34_{4,30}$ $\nu = 0$–$33_{4,29}$ $\nu = 1$	336 223	5.5 ± 0.2	3.5 ± 0.1	<3σ		<3σ		<3σ		4.0 ± 0.2	2.40 ± 0.09
$34_{3,32}$ $\nu = 1$–$33_{3,31}$ $\nu = 0$	336 323	7.3 ± 0.3	6.6 ± 0.2	<3σ		<3σ		<3σ		5.1 ± 0.1	4.18 ± 0.06
$33_{7,27}$ $\nu = 0$–$32_{7,26}$ $\nu = 1$	336 334	4.3 ± 0.2	3.15 ± 0.09	<3σ		<3σ		<3σ		3.0 ± 0.1	2.16 ± 0.08
$37_{1,37}$ $\nu = 0$–$36_{1,36}$ $\nu = 1$	336 756	4.0 ± 0.3	6.9 ± 0.5	<3σ		<3σ		<3σ		3.6 ± 0.1	4.5 ± 0.1
$31_{6,25}$ $\nu = 1$–$30_{6,24}$ $\nu = 0$	336 828	blended		<3σ		<3σ		<3σ		5.3 ± 0.3	3.4 ± 0.1
$32_{9,24}$ $\nu = 1$–$31_{9,23}$ $\nu = 0$	336 939	4.1 ± 0.2	3.6 ± 0.1	<3σ		<3σ		<3σ		4.7 ± 0.2	2.75 ± 0.06
$33_{8,25}$ $\nu = 0$–$32_{8,24}$ $\nu = 1$	337 082	blended		<3σ		<3σ		<3σ		3.8 ± 0.2	3.0 ± 0.1
$32_{9,23}$ $\nu = 1$–$31_{9,22}$ $\nu = 0$	337 094	blended		<3σ		<3σ		<3σ		<3σ	
$32_{7,26}$ $\nu = 1$–$31_{7,25}$ $\nu = 0$	337 571	blended		<3σ		<3σ		<3σ		<3σ	
$33_{5,28}$ $\nu = 0$–$32_{5,27}$ $\nu = 1$	337 816	4.7 ± 0.7	4.5 ± 2.0	<3σ		<3σ		<3σ		<3σ	
$35_{4,32}$ $\nu = 0$–$34_{4,31}$ $\nu = 1$	338 214	blended		<3σ		<3σ		<3σ		4.2 ± 0.6	2.7 ± 0.3
$32_{8,25}$ $\nu = 1$–$31_{8,24}$ $\nu = 0$	338 221	3.86 ± 0.10	3.45 ± 0.05	<3σ		<3σ		<3σ		2.8 ± 0.4	2.1 ± 0.2
$35_{3,32}$ $\nu = 0$–$34_{3,31}$ $\nu = 1$	338 240	3.9 ± 0.8	6.1 ± 0.2	<3σ		<3σ		<3σ		4.7 ± 0.4	3.2 ± 0.1
$36_{4,33}$ $\nu = 0$–$35_{4,32}$ $\nu = 1$	347 361	4.6 ± 0.3	4.6 ± 0.2	<3σ		<3σ		<3σ		2.94 ± 0.07	2.74 ± 0.05
$36_{3,33}$ $\nu = 0$–$35_{3,32}$ $\nu = 1$	347 378	4.9 ± 0.2	4.5 ± 0.1	<3σ		<3σ		<3σ		3.5 ± 0.2	2.29 ± 0.07
$32_{6,26}$ $\nu = 1$–$31_{6,25}$ $\nu = 0$	347 387	blended		<3σ		<3σ		<3σ		3.49 ± 0.08	3.00 ± 0.06
$33_{9,25}$ $\nu = 1$–$32_{9,24}$ $\nu = 0$	347 487	blended		<3σ		<3σ		<3σ		3.0 ± 0.3	3.2 ± 0.2
$33_{7,27}$ $\nu = 1$–$32_{7,26}$ $\nu = 0$	347 732	⋄ 4.28 ± 0.09	6.1 ± 0.1	<3σ		<3σ		<3σ		4.1 ± 0.3	4.2 ± 0.6
$33_{9,24}$ $\nu = 1$–$32_{9,23}$ $\nu = 0$	347 738	4.27 ± 0.09	5.83 ± 0.07	<3σ		<3σ		<3σ		3.7 ± 0.2	2.88 ± 0.07
$17_{9,8}$ $\nu = 1$–$16_{8,9}$ $\nu = 1$	347 813	blended		<3σ		<3σ		<3σ		2.9 ± 0.3	0.82 ± 0.05
$17_{9,8}$ $\nu = 0$–$16_{8,9}$ $\nu = 0$	347 821	blended		<3σ		<3σ		<3σ		2.3 ± 0.1	1.14 ± 0.06
$15_{10,5}$ $\nu = 0$–$14_{9,6}$ $\nu = 0$	347 963	4.6 ± 0.4	4.1 ± 0.2	<3σ		<3σ		<3σ		3.8 ± 0.4	1.84 ± 0.08
$34_{8,27}$ $\nu = 0$–$33_{8,25}$ $\nu = 0$	348 326	⋄ 4.3 ± 0.5	3.9 ± 0.2	<3σ		<3σ		<3σ		<3σ	
$36_{1,35}$ $\nu = 1$–$35_{1,34}$ $\nu = 0$	348 331	⋄ 4.3 ± 0.5	9.0 ± 0.2	<3σ		<3σ		<3σ		<3σ	
$35_{6,30}$ $\nu = 0$–$34_{6,29}$ $\nu = 1$	348 550	5.7 ± 0.2	9.8 ± 0.3	<3σ		<3σ		<3σ		4.9 ± 0.2	2.56 ± 0.07
$33_{8,26}$ $\nu = 1$–$32_{8,25}$ $\nu = 0$	349 355	blended		<3σ		<3σ		<3σ		5.0 ± 0.4	1.73 ± 0.04
$34_{5,30}$ $\nu = 1$–$33_{5,29}$ $\nu = 0$	349 445	blended		<3σ		<3σ		<3σ		<3σ	
$33_{5,28}$ $\nu = 1$–$32_{5,27}$ $\nu = 0$	349 541	blended		<3σ		<3σ		<3σ		6.4 ± 2.3	2.18 ± 0.08
$37_{3,35}$ $\nu = 0$–$36_{3,34}$ $\nu = 1$	349 867	blended		<3σ		<3σ		<3σ		2.94 ± 0.10	4.2 ± 0.1
$34_{4,30}$ $\nu = 1$–$33_{4,29}$ $\nu = 0$	350 023	blended		<3σ		<3σ		<3σ		3.35 ± 0.10	2.35 ± 0.06
$34_{8,26}$ $\nu = 0$–$33_{8,25}$ $\nu = 1$	350 142	blended		<3σ		<3σ		<3σ		5.2 ± 0.7	2.44 ± 0.09
$37_{1,36}$ $\nu = 0$–$36_{2,35}$ $\nu = 0$	350 402	blended		<3σ		<3σ		<3σ		2.4 ± 0.0754	1.43 ± 0.02

Notes. ⋄ Partially blended with other lines.

Table B.10. Formamide.

Transition	Frequency	G35.20 A		G35.20 B1		G35.20 B2		G35.20 B3		G35.03 A	
	(MHz)	*FWHM* (km s^{-1})	T_{peak} (K)	*FWHM* (km s^{-1})	T_{peak} (K)	*FWHM* (km s^{-1})	T_{peak} (K)	*FWHM* (km s^{-1})	T_{peak} (K)	*FWHM* (km s^{-1})	T_{peak} (K)
NH_2CHO $v = 0$											
$16_{2,15}$–$15_{2,14}$	336 136	5.8 ± 0.2	30.8 ± 0.8	5.0 ± 0.1	8.0 ± 0.1	2.8 ± 0.4	2.3 ± 0.1	3.17 ± 0.09	8.2 ± 0.1	4.63 ± 0.09	15.4 ± 0.3
$16_{1,16}$–$15_{0,15}$	336 161	8.5 ± 0.2	9.4 ± 0.2	3.2 ± 0.6	1.54 ± 0.07	<3σ		2.7 ± 0.2	5.6 ± 0.3	4.3 ± 0.2	4.24 ± 0.10
$28_{2,26}$–$28_{1,27}$	347 729	blended		<3σ		<3σ		4.1 ± 0.5	0.85 ± 0.05	<3σ	
	349 053	blended		<3σ		<3σ		2.0 ± 0.2	1.66 ± 0.09	<3σ	
$16_{2,14}$–$15_{2,13}$	349 482	5.4 ± 0.2	33.4 ± 1.0	5.4 ± 0.1	8.3 ± 0.2	2.2 ± 0.2	1.9 ± 0.1	3.4 ± 0.1	7.2 ± 0.2	5.0 ± 0.1	12.9 ± 0.3
NH_2CHO $v12 = 1$											
	349 020	blended		<3σ		2.3 ± 0.3	0.92 ± 0.09	<3σ		<3σ	
NH_2CDO											
$16_{4,13}$–$15_{4,12}$	335 234	10.7 ± 0.5	2.81 ± 0.07	<3σ		<3σ		<3σ		<3σ	
$18_{1,18}$–$17_{1,17}$	348 283	blended		<3σ		<3σ		1.4 ± 0.4	0.6 ± 0.1	<3σ	
$18_{0,18}$–$17_{0,17}$	348 730	blended		<3σ		<3σ		<3σ		<3σ	
$NH_2^{13}CHO$											
	335 403	⋄ 3.6 ± 0.6	3.9 ± 0.4	1.9 ± 0.1	0.84 ± 0.05	1.1 ± 0.2	0.54 ± 0.09	2.2 ± 0.3	1.4 ± 0.2	<3σ	
	349 309	5.7 ± 0.2	3.6 ± 0.1	1.21 ± 0.09	0.78 ± 0.04	0.9 ± 0.2	0.7 ± 0.2	2.2 ± 0.2	1.3 ± 0.1	<3σ	
$NH_2CH^{18}O$											
$18_{0,18}$–$17_{0,17}$	347 589	⋄ 6 ± 2	3 ± 2	1.2 ± 0.4	0.6 ± 0.1	1.85 ± 0.2	0.8 ± 0.2	1.4 ± 0.4	1.2 ± 0.2	<3σ	
$17_{1,16}$–$16_{1,15}$	348 029	blended		<3σ		2.6 ± 0.5	0.66 ± 0.07	<3σ		<3σ	

Notes. ⋄ Partially blended with other lines.

Table B.11. Methyl cyanide.

Transition	Frequency (MHz)	G35.20 A *FWHM* (km s^{-1})	G35.20 A T_{peak} (K)	G35.20 B1 *FWHM* (km s^{-1})	G35.20 B1 T_{peak} (K)	G35.20 B2 *FWHM* (km s^{-1})	G35.20 B2 T_{peak} (K)	G35.20 B3 *FWHM* (km s^{-1})	G35.20 B3 T_{peak} (K)	G35.03 A *FWHM* (km s^{-1})	G35.03 A T_{peak} (K)
CH_3CN $v = 0$											
19_9–18_9	348 911	⋆ 8.0 ± 0.2	27.3 ± 0.4	blended		blended		2.0 ± 0.2	8 ± 1	<3σ	
19_8–18_8	349 025	⋆ 7.8 ± 0.2	19.1 ± 0.5	1.5 ± 0.2	3.0 ± 0.2	1.6 ± 0.3	1.2 ± 0.2	2.22 ± 0.06	12.2 ± 0.4	7.6 ± 0.1	8.2 ± 0.1
19_7–18_7	349 125	⋆ 6.3 ± 0.2	26.6 ± 0.8	2.1 ± 0.1	6.3 ± 0.3	1.6 ± 0.2	2.6 ± 0.3	2.58 ± 0.08	22.0 ± 0.5	5.97 ± 0.09	10.9 ± 0.2
19_6–18_6	349 212	⋆ 6.6 ± 0.3	47.0 ± 1.0	3.2 ± 0.3	18 ± 1	1.8 ± 0.2	8.4 ± 1.0	2.82 ± 0.06	39.9 ± 0.8	4.4 ± 0.2	13.6 ± 0.5
19_5–18_5	349 286	⋆ 7.0 ± 0.3	48.9 ± 1.8	3.2 ± 0.2	18.4 ± 1.0	1.9 ± 0.2	8.9 ± 0.6	2.70 ± 0.03	41.7 ± 0.3	5.6 ± 0.5	19.4 ± 0.3
19_4–18_4	349 346	⋆ 6.3 ± 0.2	54.8 ± 1.6	3.2 ± 0.2	24 ± 1	2.3 ± 0.2	14.7 ± 1.2	2.89 ± 0.03	47.7 ± 0.5	7.1 ± 0.2	21.9 ± 0.6
19_3–18_3	349 393	6.2 ± 0.2	62.3 ± 1.8	3.3 ± 0.1	26.6 ± 1.0	3.35 ± 0.08	25.9 ± 0.5	3.14 ± 0.06	38.8 ± 0.5	6.2 ± 0.3	25.4 ± 0.9
19_2–18_2	349 427	6.5 ± 0.2	65.0 ± 1.4	3.5 ± 0.2	32 ± 2	2.8 ± 0.2	23.4 ± 1.3	3.01 ± 0.05	53.1 ± 0.8	7.6 ± 0.2	26.6 ± 0.5
19_1–18_1	349 447	⋄ 6.7 ± 0.2	68.0 ± 0.8	⋄ 3.3 ± 0.2	38 ± 2	⋄ 2.7 ± 0.2	26.7 ± 1.6	⋄ 2.94 ± 0.03	50.3 ± 0.4	⋄ 6.9 ± 0.5	30.2 ± 0.5
19_0–18_0	349 453	⋄ 5.0 ± 0.3	64.5 ± 1.5	⋄ 3.3 ± 0.2	40 ± 2	⋄ 2.7 ± 0.2	24.9 ± 1.5	⋄ 3.10 ± 0.04	54.5 ± 0.6	⋄ 5.1 ± 0.3	27.6 ± 1.1
CH_3CN $v_8 = 1$, $F = 19$–18											
$19_{10,2}$–$18_{10,2}$	349 975	blended		<3σ		<3σ		<3σ		<3σ	
$19_{7,1}$–$18_{7,1}$	350 059	⋄ 3.1 ± 0.8	1.6 ± 1.7	<3σ		<3σ		1.4 ± 0.7	0.6 ± 0.1	3.2 ± 0.3	0.91 ± 0.08
$19_{6,1}$–$18_{6,1}$	350 160	7.5 ± 1.7	3.9 ± 0.4	<3σ		<3σ		1.5 ± 0.2	1.6 ± 0.1	<3σ	
$19_{1,2}$–$18_{-1,2}$	350 168	6.5 ± 0.2	15.7 ± 0.5	3.1 ± 0.3	2.6 ± 0.2	1.3 ± 0.3	0.9 ± 0.2	2.6 ± 0.1	11.2 ± 0.4	<3σ	
$19_{8,2}$–$18_{8,2}$	350 190	7.0 ± 0.3	3.07 ± 0.06	<3σ		<3σ		⋄ 1.4 ± 0.9	0.8 ± 0.9	4.6 ± 0.2	1.27 ± 0.03
$19_{5,1}$–$18_{5,1}$	350 247	8.2 ± 0.2	10.1 ± 0.3	blended		<3σ		3.33 ± 0.08	4.44 ± 0.09	<3σ	
$19_{7,2}$–$18_{7,2}$	350 277	⋄ 7.0 ± 1.2	7.2 ± 0.7	blended		<3σ		2.38 ± 0.06	3.16 ± 0.07	<3σ	
$19_{4,1}$–$18_{4,1}$	350 320	blended		blended		<3σ		2.12 ± 0.09	3.5 ± 0.1	<3σ	
$19_{6,1}$–$18_{6,1}$	350 352	5.1 ± 1.0	6.7 ± 0.3	<3σ		<3σ		2.5 ± 0.1	2.8 ± 0.1	5.4 ± 0.3	2.93 ± 0.09
$19_{3,1}$–$18_{3,1}$	350 380	7.3 ± 0.1	10.1 ± 0.2	blended		<3σ		2.3 ± 0.1	5.7 ± 0.1	6.0 ± 0.2	4.19 ± 0.10
$19_{5,2}$–$18_{5,2}$	350 415	blended		1.9 ± 0.3	0.9 ± 0.1	1.1 ± 0.1	0.72 ± 0.07	2.33 ± 0.07	5.0 ± 0.1	<3σ	
$19_{2,1}$–$18_{2,1}$	350 423	blended		blended		blended		blended		<3σ	
$19_{0,2}$–$18_{0,2}$	350 445	blended		blended		blended		blended		<3σ	
$19_{1,1}$–$18_{1,1}$	350 450	blended		blended		<3σ		2.5 ± 0.2	9.8 ± 0.4	<3σ	
$19_{4,2}$–$18_{4,2}$	350 465	4.9 ± 0.3	16.0 ± 1.2	3.7 ± 0.3	2.9 ± 0.1	2.3 ± 0.5	0.9 ± 0.2	2.46 ± 0.05	11.9 ± 0.2	5.9 ± 0.2	7.7 ± 0.1
$19_{3,2}$–$18_{3,2}$	350 507	8.2 ± 0.2	15.6 ± 0.3	⋄ 3.7 ± 0.4	1.79 ± 0.10	1.8 ± 0.2	1.6 ± 0.2	2.59 ± 0.07	9.3 ± 0.2	6.6 ± 0.1	6.19 ± 0.05
$19_{2,2}$–$18_{2,2}$	350 552	6.9 ± 0.2	17.4 ± 0.3	⋄ 3.5 ± 0.2	2.61 ± 0.07	blended		2.8 ± 0.1	10.5 ± 0.4	6.4 ± 0.1	6.96 ± 0.08
$CH_3^{13}CN$											
19_8–18_8	348 854	blended		<3σ		<3σ		1 ± 2	0.7 ± 0.2	<3σ	
19_7–18_7	348 954	blended		<3σ		<3σ		2.2 ± 0.4	0.64 ± 0.08	<3σ	
19_6–18_6	349 040	blended		<3σ		<3σ		2.1 ± 0.2	3.2 ± 0.3	<3σ	
19_5–18_5	349 114	blended		blended		<3σ		2.5 ± 0.1	2.9 ± 0.1	<3σ	
19_4–18_4	349 174	⋄⋆ 6.2 ± 0.3	8.0 ± 0.1	2.3 ± 0.4	1.6 ± 0.2	<3σ		2.95 ± 0.03	5.67 ± 0.05	<3σ	
19_3–18_3	349 222	blended		2.5 ± 0.3	4.1 ± 0.4	1.3 ± 0.4	1.3 ± 0.2	2.48 ± 0.05	12.5 ± 0.2	4.9 ± 1.1	5.0 ± 0.5
19_2–18_2	349 254	⋆ 5.7 ± 0.2	9.0 ± 0.3	1.7 ± 0.4	1.5 ± 0.3	1.4 ± 0.3	1.1 ± 0.2	2.46 ± 0.09	10.4 ± 0.2	5.2 ± 0.2	3.3 ± 0.1
19_1–18_1	349 274	blended		1.6 ± 0.2	1.8 ± 0.2	1.4 ± 0.5	0.9 ± 0.3	2.6 ± 0.1	11.7 ± 0.4	5.5 ± 0.5	4.4 ± 0.3
19_0–18_0	349 280	blended		blended		blended		3.1 ± 0.3	10.4 ± 0.3	5.5 ± 0.5	6.7 ± 0.3

Notes. ⋄ Partially blended with other lines, ⋆ double peaked.

Table B.11. continued.

Transition	Frequency (MHz)	G35.20 A *FWHM* (km s^{-1})	G35.20 A T_{peak} (K)	G35.20 B1 *FWHM* (km s^{-1})	G35.20 B1 T_{peak} (K)	G35.20 B2 *FWHM* (km s^{-1})	G35.20 B2 T_{peak} (K)	G35.20 B3 *FWHM* (km s^{-1})	G35.20 B3 T_{peak} (K)	G35.03 A *FWHM* (km s^{-1})	G35.03 A T_{peak} (K)
					CH_2DCN						
$20_{7,13}$–$19_{7,12}$	346 968	blended		<3σ		<3σ		blended		<3σ	
$20_{0,20}$–$19_{0,19}$	347 043	5.8 ± 0.3	7.1 ± 0.3	1.5 ± 0.3	1.0 ± 0.2	1 ± 1	0.54 ± 0.09	3.01 ± 0.08	10.0 ± 0.2	<3σ	
$20_{5,15}$–$19_{5,14}$	347 110	7.5 ± 0.2	3.8 ± 0.1	0.9 ± 0.2	0.52 ± 0.09	<3σ		2.4 ± 0.1	5.6 ± 0.2	<3σ	
$20_{4,16}$–$19_{4,15}$	347 166	blended		1.4 ± 0.5	0.5 ± 0.3	<3σ		2.7 ± 0.1	7.4 ± 0.3	<3σ	
$20_{3,18}$–$19_{3,17}$	347 216	blended		1.6 ± 0.2	0.61 ± 0.04	<3σ		4.2 ± 0.1	7.8 ± 0.2	<3σ	
$20_{3,17}$–$19_{3,16}$	347 219	blended		1.09 ± 0.06	1.26 ± 0.04	<3σ		blended with 347 216		<3σ	
$20_{2,18}$–$19_{2,17}$	347 388	5.7 ± 0.1	8.7 ± 0.2	1.2 ± 0.1	0.75 ± 0.06	<3σ		2.59 ± 0.08	7.6 ± 0.2	3.49 ± 0.09	3.00 ± 0.06
$20_{1,19}$–$19_{1,18}$	348 691	⋄ 2.84 ± 0.07	3.9 ± 0.1	1.6 ± 0.3	1.1 ± 0.2	<3σ		2.36 ± 0.09	7.7 ± 0.3	<3σ	

Table B.12. Vinyl cyanide.

Transition	Frequency (MHz)	G35.20 A *FWHM* (km s^{-1})	G35.20 A T_{peak} (K)	G35.20 B1 *FWHM* (km s^{-1})	G35.20 B1 T_{peak} (K)	G35.20 B2 *FWHM* (km s^{-1})	G35.20 B2 T_{peak} (K)	G35.20 B3 *FWHM* (km s^{-1})	G35.20 B3 T_{peak} (K)	G35.03 A *FWHM* (km s^{-1})	G35.03 A T_{peak} (K)
					C_2H_3CN						
$36_{2,35}$–$35_{2,34}$	337 040	⋄ 4.0 ± 0.3	3.4 ± 0.2	blended		<3σ		2.38 ± 0.09	1.96 ± 0.06	8.1 ± 3.1	1.25 ± 0.10
$35_{3,32}$–$34_{3,31}$	337 051	blended		blended		<3σ		2.0 ± 0.9	0.9 ± 0.3	2.5 ± 0.2	2.8 ± 0.1
$37_{1,37}$–$36_{1,36}$	338 214	⋄ 7.2 ± 0.3	5.4 ± 0.1	<3σ		<3σ		2.8 ± 0.1	2.49 ± 0.09	<3σ	
$35_{2,33}$–$34_{2,32}$	338 278	4.31 ± 0.09	3.90 ± 0.03	<3σ		<3σ		2.32 ± 0.08	2.09 ± 0.06	5.7 ± 0.8	1.12 ± 0.06
$37_{0,37}$–$36_{0,36}$	338 448	blended		<3σ		<3σ		⋄ 1.3 ± 0.9	2.4 ± 1.2	<3σ	
$36_{3,33}$–$35_{3,32}$	346 943	blended		<3σ		<3σ		⋄ 2.0 ± 0.5	2.7 ± 0.5	<3σ	
$38_{1,38}$–$37_{1,37}$	347 232	5.3 ± 0.2	4.03 ± 0.07	<3σ		<3σ		2.7 ± 0.1	2.23 ± 0.08	<3σ	
$38_{0,38}$–$37_{0,37}$	347 434	6.1 ± 1.1	6.3 ± 0.5	<3σ		<3σ		2.8 ± 0.2	2.6 ± 0.1	5.5 ± 0.4	2.00 ± 0.07
$53_{5,48}$–$53_{4,49}$	347 685	blended		<3σ		<3σ		⋄ 1.35 ± 0.08	0.61 ± 0.02	<3σ	
$36_{2,34}$–$35_{2,33}$	347 759	blended		blended		<3σ		3.2 ± 0.4	1.8 ± 0.1	<3σ	
$38_{1,38}$–$37_{0,37}$	348 637	blended		<3σ		<3σ		blended		<3σ	
$37_{1,36}$–$36_{1,35}$	348 991	4.8 ± 0.1	6.2 ± 0.1	<3σ		<3σ		⋄ 2.31 ± 0.05	4.71 ± 0.09	<3σ	
$49_{4,46}$–$49_{3,47}$	350 364	<3σ		blended		blended		blended		<3σ	

Notes. ⋄ Partially blended with other lines.

Table B.13. Ethyl cyanide.

Transition	Frequency (MHz)	G35.20 A *FWHM* (km s^{-1})	G35.20 A T_{peak} (K)	G35.20 B1 *FWHM* (km s^{-1})	G35.20 B1 T_{peak} (K)	G35.20 B2 *FWHM* (km s^{-1})	G35.20 B2 T_{peak} (K)	G35.20 B3 *FWHM* (km s^{-1})	G35.20 B3 T_{peak} (K)	G35.03 A *FWHM* (km s^{-1})	G35.03 A T_{peak} (K)
C_2H_5CN $\nu = 0$											
$55_{8,48}$–$55_{7,49}$	335 274	<3σ		<3σ		<3σ		1.65 ± 0.22	0.72 ± 0.08	<3σ	
$9_{6,4}$–$8_{5,3}$	335 321	blended		blended		<3σ		blended		<3σ	
$52_{8,44}$–$52_{7,45}$	335 895	2.89 ± 0.29	1.14 ± 0.04	<3σ		<3σ		<3σ		<3σ	
$20_{4,17}$–$19_{3,16}$	336 614	blended		<3σ		<3σ		1.59 ± 0.18	0.50 ± 0.05	<3σ	
$38_{3,36}$–$37_{3,35}$	337 347	blended		blended		blended		2.76 ± 0.07	4.05 ± 0.09	<3σ	
$37_{4,33}$–$36_{4,32}$	337 445	5.3 ± 0.1	14.5 ± 0.2	2.7 ± 0.1	1.71 ± 0.06	<3σ		2.77 ± 0.07	4.05 ± 0.09	<3σ	
$37_{3,34}$–$36_{3,33}$	338 142	blended		blended		1.9 ± 0.2	1.08 ± 0.0854	2.87 ± 0.06	5.49 ± 0.10	<3σ	
$20_{8,12}$–$20_{7,13}$	346 925	blended		<3σ		<3σ		3.66 ± 0.11	1.54 ± 0.03	<3σ	
$12_{8,4}$–$12_{7,5}$	346 970	blended		1.11 ± 0.09	0.83 ± 0.06	<3σ		blended		<3σ	
$16_{8,9}$–$16_{7,10}$	346 976	blended		<3σ		<3σ		2.84 ± 0.11	3.10 ± 0.08	<3σ	
$15_{8,7}$–$15_{7,8}$	346 979	blended		<3σ		1.5 ± 0.2	1.2 ± 0.1	2.69 ± 0.15	2.20 ± 0.09	<3σ	
$38_{3,35}$–$37_{3,34}$	346 983	blended		blended		blended		blended		<3σ	
$39_{2,37}$–$38_{2,36}$	348 260	5.7 ± 0.1	9.0 ± 0.1	<3σ		<3σ		2.96 ± 0.16	3.96 ± 0.17	4.6 ± 0.8	1.39 ± 0.07
$40_{2,39}$–$39_{2,38}$	348 344	blended		blended		<3σ		blended		4.8 ± 1.6	2.1 ± 0.1
$40_{1,39}$–$39_{1,38}$	348 553	5.4 ± 0.2	10.0 ± 0.2	1.1 ± 0.1	0.76 ± 0.06	<3σ		2.08 ± 0.17	4.24 ± 0.28	5.1 ± 0.2	2.55 ± 0.08
$39_{12,28}$–$38_{12,27}$	349 380	5.8 ± 1.0	5.8 ± 0.6	1.1 ± 0.2	1.02 ± 0.07	<3σ		2.21 ± 0.26	1.97 ± 0.18	<3σ	
$39_{9,31}$–$38_{9,30}$	349 547	5.5 ± 0.5	7.5 ± 2.0	<3σ		<3σ		2.47 ± 0.13	3.42 ± 0.15	<3σ	
$39_{16,23}$–$38_{16,22}$	349 566	4.65 ± 0.06	3.79 ± 0.05	<3σ		<3σ		<3σ		<3σ	
$39_{17,22}$–$38_{17,21}$	349 652	4.7 ± 0.7	2.9 ± 0.2	<3σ		<3σ		<3σ		<3σ	
$39_{8,32}$–$38_{8,31}$	349 730	5.3 ± 0.1	7.4 ± 0.2	1.2 ± 0.2	1.0 ± 0.1	<3σ		2.37 ± 0.08	3.67 ± 0.10	<3σ	
$39_{18,21}$–$38_{18,20}$	349 751	4.1 ± 0.6	3.6 ± 0.1	<3σ		<3σ		<3σ		<3σ	
$39_{4,36}$–$38_{4,35}$	349 796	4.86 ± 0.04	6.73 ± 0.08	<3σ		<3σ		2.26 ± 0.10	3.09 ± 0.11	4.9 ± 0.7	0.97 ± 0.04
$39_{20,19}$–$38_{20,18}$	349 981	blended		<3σ		<3σ		<3σ		<3σ	
$39_{7,33}$–$38_{7,32}$	350 039	4.9 ± 0.1	5.1 ± 0.1	1.0 ± 0.5	0.5 ± 0.2	blended		2.04 ± 0.10	2.87 ± 0.11	3.6 ± 1.0	0.95 ± 0.10
$39_{7,32}$–$38_{7,31}$	350 051	5.5 ± 0.3	5.6 ± 0.1	<3σ		<3σ		2.21 ± 0.12	2.36 ± 0.11	3.0 ± 0.4	1.36 ± 0.07
$41_{1,41}$–$40_{1,40}$	350 140	blended		blended		<3σ		blended		<3σ	
$41_{0,41}$–$40_{0,40}$	350 145	blended		⋄ 1.4 ± 0.2	1.2 ± 0.1	<3σ		⋄ 2.02 ± 0.24	2.54 ± 0.13	⋄ 3.9 ± 0.1	2.53 ± 0.04
$39_{6,34}$–$38_{6,33}$	350 512	blended		1.0 ± 0.2	0.9 ± 0.1	1.3 ± 0.2	0.71 ± 0.08	2.17 ± 0.21	2.59 ± 0.19	<3σ	
CH_3CHDCN											
$40_{0,40}$–$39_{1,39}$	335 229	⋄ 1.8 ± 0.2	1.6 ± 0.1	<3σ		<3σ		<3σ		<3σ	
$40_{1,40}$–$39_{1,39}$	335 237	⋄ 2.0 ± 0.7	2.4 ± 2.0	<3σ		<3σ		<3σ		<3σ	
$40_{0,40}$–$39_{1,39}$	335 239	⋄ 2.3 ± 0.7	2.4 ± 0.2	<3σ		<3σ		<3σ		<3σ	
$40_{1,40}$–$39_{0,39}$	335 246	2.4 ± 0.3	0.93 ± 0.06	<3σ		<3σ		<3σ		<3σ	
$38_{14,25}$–$37_{14,24}$	335 427	⋄ 1.83 ± 0.07	1.44 ± 0.02	<3σ		<3σ		<3σ		<3σ	
$38_{13,26}$–$37_{13,25}$	335 430	⋄ 2.05 ± 0.07	2.00 ± 0.01	<3σ		<3σ		<3σ		<3σ	
$38_{4,35}$–$37_{4,34}$	335 511	⋄ 2.7 ± 0.5	1.27 ± 0.06	<3σ		<3σ		<3σ		<3σ	
$38_{11,27}$–$37_{11,26}$	335 513	⋄ 1.9 ± 0.3	1.0 ± 0.1	<3σ		<3σ		<3σ		<3σ	
$43_{9,34}$–$43_{8,35}$	335 989	2.1 ± 0.5	0.9 ± 0.2	<3σ		<3σ		<3σ		<3σ	
$38_{7,32}$–$37_{7,31}$	336 425	⋄ 5.5 ± 0.1	3.30 ± 0.04	<3σ		<3σ		<3σ		<3σ	

Notes. ⋄ Partially blended with other lines.

Table B.13. continued.

Transition	Frequency	G35.20 A		G35.20 B1		G35.20 B2		G35.20 B3		G35.03 A	
		FWHM	T_{peak}	*FWHM*	T_{peak}	*FWHM*	T_{peak}	*FWHM*	T_{peak}	*FWHM*	T_{peak}
	(MHz)	(km s^{-1})	(K)	(km s^{-1})	(K)	(km s^{-1})	(K)	(km s^{-1})	(K)	(km s^{-1})	(K)
$36_{7,29}$–$35_{7,28}$	336 453	3.8 ± 0.2	2.54 ± 0.07	<3σ		<3σ		<3σ		<3σ	
$38_{6,33}$–$37_{6,32}$	336 971	blended		<3σ		<3σ		<3σ		<3σ	
$38_{6,32}$–$37_{6,31}$	337 336	blended		<3σ		<3σ		<3σ		<3σ	
$40_{3,38}$–$39_{3,37}$	347 816	1.83 ± 0.04	2.28 ± 0.02	<3σ		<3σ		<3σ		<3σ	
$41_{2,40}$–$40_{2,39}$	349 907	5.4 ± 0.1	1.85 ± 0.05	<3σ		<3σ		<3σ		<3σ	
$CH_3^{13}CH_2CN$											
$38_{8,31}$–$38_{7,32}$	335 362	<3σ		<3σ		<3σ		1.2 ± 0.2	0.77 ± 0.09	<3σ	
$38_{3,36}$–$37_{3,35}$	335 369	4.2 ± 2.4	1.5 ± 0.1	<3σ		<3σ		<3σ		<3σ	
$39_{1,38}$–$38_{1,37}$	337 951	6.5 ± 0.3	2.32 ± 0.07	<3σ		<3σ		<3σ		<3σ	
$^{13}CH_3CH_2CN$											
$40_{2,38}$–$39_{2,37}$	348 147	3 ± 1	2.45 ± 0.08	<3σ		<3σ		<3σ		<3σ	

Table B.14. Cyanoacetylene.

Transition	Frequency (MHz)	G35.20 A *FWHM* (km s^{-1})	G35.20 A T_{peak} (K)	G35.20 B1 *FWHM* (km s^{-1})	G35.20 B1 T_{peak} (K)	G35.20 B2 *FWHM* (km s^{-1})	G35.20 B2 T_{peak} (K)	G35.20 B3 *FWHM* (km s^{-1})	G35.20 B3 T_{peak} (K)	G35.03 A *FWHM* (km s^{-1})	G35.03 A T_{peak} (K)
HC_3N $\nu = 0$											
37–36	336 520	7.4 ± 0.1	27.6 ± 0.4	4.53 ± 0.10	17.0 ± 0.3	⋄ 1.6 ± 0.1	6.5 ± 0.4	3.32 ± 0.04	47.2 ± 0.5	blended	
HC_3N $v6 = 1$											
37 $_1$–36 $_{-1}$	337 070	blended		<3σ		<3σ		2.4 ± 0.1	2.64 ± 0.08	<3σ	
37 $_{-1}$–36 $_1$	337 335	5.3 ± 0.8	3.1 ± 0.3	<3σ		<3σ		2.2 ± 0.1	2.1 ± 0.1	<3σ	
HC_3N $v7 = 1$											
37 $_1$–36 $_{-1}$	337 344	blended		⋄ 1.8 ± 0.5	1.7 ± 0.4	⋄ 1.4 ± 0.1	1.20 ± 0.07	⋄ 2.84 ± 0.05	19.2 ± 0.2	blended	
37 $_{-1}$–36 $_1$	337 825	⋄ 5.3 ± 0.5	9.3 ± 1.4	⋄ 3.9 ± 0.4	3.08 ± 0.09	<3σ		⋄ 2.83 ± 0.08	18.8 ± 0.4	blended	
38 $_1$–37 $_{-1}$	346 949	6.2 ± 1.4	13.6 ± 1.3	3.8 ± 0.2	2.5 ± 0.1	0.9 ± 0.3	0.7 ± 0.2	2.8 ± 0.1	22.6 ± 0.8	6.3 ± 1.1	10.8 ± 0.3
HC_3N $v7 = 2$											
37 $_2$–36 $_{-2}$	338 646	blended		<3σ		<3σ		2.53 ± 0.05	3.57 ± 0.06	<3σ	
38 $_0$–37 $_0$	347 663	5.2 ± 1.2	5.3 ± 0.4	<3σ		<3σ		2.62 ± 0.09	3.4 ± 0.1	<3σ	
38 $_{-2}$–37 $_2$	347 791	blended		<3σ		<3σ		⋄ 1.94 ± 0.09	3.5 ± 0.1	<3σ	
38 $_2$–37 $_{-2}$	347 924	blended		<3σ		<3σ		2.36 ± 0.08	3.4 ± 0.1	<3σ	
$HC^{13}CCN$ $\nu = 0$											
37–36	335 092	⋆ 5.0 ± 0.4	13.4 ± 0.9	blended		⋄ 3.4 ± 0.4	3.43 ± 0.10	blended		<3σ	
$HCC^{13}CN$ $\nu = 0$											
37–36	335 124	blended		<3σ		<3σ		2.3 ± 0.3	6.9 ± 0.7	<3σ	
$H^{13}CCCN$ $v7 = 1$											
37 $_{-1}$–36 $_1$	335 760	4.1 ± 0.2	1.29 ± 0.05	<3σ		<3σ		1.8 ± 0.2	0.60 ± 0.04	3.1 ± 0.3	1.36 ± 0.10
37 $_1$–36 $_{-1}$	336 227	5.6 ± 0.2	3.4 ± 0.1	<3σ		<3σ		1.4 ± 0.2	0.77 ± 0.07	4.3 ± 0.3	2.36 ± 0.09
$HC^{13}CCN$ $v7 = 1$											
37 $_1$–36 $_{-1}$	335 883	4.3 ± 0.5	1.22 ± 0.09	<3σ		<3σ		2.7 ± 0.2	0.97 ± 0.07	<3σ	
$HCC^{13}CN$ $v7 = 1$											
37 $_1$–36 $_{-1}$	335 930	5.3 ± 0.2	7.0 ± 0.2	1.9529 ± 0.3336	1.16 ± 0.1159	<3σ		2.81 ± 0.08	2.17 ± 0.05	3.3 ± 0.1	4.5 ± 0.2
37 $_{-1}$–36 $_1$	336 410	blended		<3σ		<3σ		2.0 ± 0.2	0.65 ± 0.05	<3σ	
$HCC^{13}CN$ $v6 = 1$											
37 $_{-1}$–36 $_1$	335 921	1.8 ± 0.6	1.2 ± 0.4	<3σ		<3σ		<3σ		<3σ	

Notes. ⋄ Partially blended with other lines, ⋆ double peaked.

Table B.15. Thioformaldehyde.

Transition	Frequency (MHz)	G35.20 A *FWHM* (km s^{-1})	G35.20 A T_{peak} (K)	G35.20 B1 *FWHM* (km s^{-1})	G35.20 B1 T_{peak} (K)	G35.20 B2 *FWHM* (km s^{-1})	G35.20 B2 T_{peak} (K)	G35.20 B3 *FWHM* (km s^{-1})	G35.20 B3 T_{peak} (K)	G35.03 A *FWHM* (km s^{-1})	G35.03 A T_{peak} (K)
H_2CS $\nu = 0$											
$10_{1,10}$–$9_{1,9}$ o	338 083	5.9 ± 0.1	51.7 ± 0.9	2.7 ± 0.1	27.3 ± 1.0	2.4 ± 0.1	28 ± 1	2.54 ± 0.06	44.3 ± 0.9	6.6 ± 0.1	21.0 ± 0.3
$10_{1,9}$–$9_{1,8}$ o	348 532	5.8 ± 0.1	59.2 ± 1.3	2.6 ± 0.1	31 ± 1	2.3 ± 0.1	31 ± 1	2.5806 ± 0.0374	52.1 ± 0.7	6.33 ± 0.09	21.3 ± 0.3
$H_2C^{33}S$											
$10_{1,10}$–$9_{1,9}$	335 160	7.5 ± 0.2	3.91 ± 0.09	1.6 ± 0.5	0.4 ± 0.1	1.5 ± 0.6	0.4 ± 0.2	2.5 ± 0.2	1.47 ± 0.08	<3σ	
$H_2C^{34}S$											
$10_{0,10}$–$9_{0,9}$	337 125	blended		1.2 ± 0.7	0.7 ± 0.4	1.5 ± 0.2	1.0 ± 0.1	1.9 ± 0.1	2.5 ± 0.1	<3σ	
$10_{4,6}$–$9_{4,5}$	337 460	blended		in abs feature		1.5 ± 0.4	0.55 ± 0.09	blended		<3σ	
$10_{2,9}$–$9_{2,8}$	337 475	⋄ 6.3 ± 0.3	16.0 ± 0.3	⋄ 1.66 ± 0.08	3.8 ± 0.2	⋄ 1.7 ± 0.1	3.8 ± 0.2	⋄ 3.1 ± 0.2	4.9 ± 0.2	<3σ	
$10_{3,8}$–$9_{3,7}$	337 555	blended		2.0 ± 0.2	0.78 ± 0.05	1.7 ± 0.5	0.6 ± 0.2	2.03 ± 0.04	2.35 ± 0.03	<3σ	
$10_{3,7}$–$9_{3,6}$	337 559	blended		2.16 ± 0.09	1.55 ± 0.04	1.3 ± 0.1	0.54 ± 0.04	2.37 ± 0.06	2.26 ± 0.03	<3σ	
$10_{2,8}$–$9_{2,7}$	337 933	blended		1.2 ± 0.5	0.8 ± 0.2	1.8 ± 0.5	0.7 ± 0.1	2.3 ± 0.1	2.4 ± 0.1	<3σ	

Notes. ⋄ Partially blended with other lines.

Table B.16. Sulfur dioxide.

Transition	Frequency (MHz)	G35.20 A *FWHM* (km s^{-1})	G35.20 A T_{peak} (K)	G35.20 B1 *FWHM* (km s^{-1})	G35.20 B1 T_{peak} (K)	G35.20 B2 *FWHM* (km s^{-1})	G35.20 B2 T_{peak} (K)	G35.20 B3 *FWHM* (km s^{-1})	G35.20 B3 T_{peak} (K)	G35.03 A *FWHM* (km s^{-1})	G35.03 A T_{peak} (K)
SO_2 $\nu = 0$											
$23_{3,21}$–$23_{2,22}$	336 089	7.7 ± 0.2	24.1 ± 0.5	7.8 ± 0.1	19.2 ± 0.3	3.4 ± 0.2	8.0 ± 0.4	4.1 ± 0.1	24.4 ± 0.7	10.0 ± 0.3	21.0 ± 0.5
$16_{7,9}$–$17_{6,12}$	336 670	8.8 ± 0.3	6.8 ± 0.2	7.3 ± 0.2	6.0 ± 0.1	2.4 ± 0.1	3.2 ± 0.2	3.4 ± 0.1	11.0 ± 0.3	8.4 ± 0.2	10.1 ± 0.1
$18_{4,14}$–$18_{3,15}$	338 306	8.0 ± 0.2	22.8 ± 0.5	7.6 ± 0.2	25.4 ± 0.6	4.0 ± 0.3	7.5 ± 0.5	3.84 ± 0.07	31.2 ± 0.5	9.8 ± 0.1	25.2 ± 0.2
$20_{1,19}$–$19_{2,18}$	338 612	5.6 ± 0.5	28.5 ± 1.6	7.5 ± 0.4	27.7 ± 1.9	4.1 ± 0.6	15.3 ± 0.9	3.8 ± 1.0	32 ± 2	10.0 ± 0.3	39.4 ± 0.9
$24_{2,22}$–$23_{3,21}$	348 388	7.7 ± 0.1	18.3 ± 0.3	7.9 ± 0.2	18.9 ± 0.4	3.2 ± 0.3	5.5 ± 0.4	3.41 ± 0.09	30.2 ± 0.7	9.6 ± 0.2	20.3 ± 0.3
$^{33}SO_2$											
$12_{4,8}$–$12_{3,9}$	348 492	blended		blended		blended		3.1 ± 0.3	2.0 ± 0.1	<3σ	
$10_{4,6}$–$10_{3,7}$	350 303	5.5 ± 0.2	12.0 ± 0.4	3.0 ± 0.1	2.46 ± 0.09	2.5 ± 0.4	1.2 ± 0.2	2.7 ± 0.1	4.00 ± 0.10	5.9 ± 0.2	3.12 ± 0.05
$^{34}SO_2$											
$13_{2,12}$–$12_{1,11}$	338 320	6.4 ± 0.2	3.69 ± 0.05	6.7 ± 0.1	4.08 ± 0.06	1.9 ± 0.4	1.7 ± 0.3	3.2 ± 0.1	8.2 ± 0.2	7.8 ± 0.3	5.97 ± 0.08

Appendix C: XCLASS fit errors

In this section we give the error values on each of our XCLASS fit results. They are rarely symmetrical, so they are reported in the format, value, lower error (−), and upper error (+), except for column density, which is listed as value, lower limit (value-error), and upper limit (value+error). The errors were calculated using the interval nested sampling (INS) error estimator algorithm in XCLASS.

Table C.1. Error values for G35.20 A.

Catalog entry	Source size	Error left	Error right	T_{ex}	Error left	Error right	N_{col}	Lower limit	Upper limit
CH3OH; $v = 0$	0.6	0.2	0.3	164	18	36	3.52E+18	6.88E+17	7.00E+18
CH3OH; $v12 = 1$	0.5	0.1	0.2	218	24	32	4.79E+18	9.77E+17	3.00E+19
CH3OH; $v12 = 2$	0.39	0.09	0.11	227	18	73	3.78E+18	7.93E+17	1.00E+19
C-13-H3OH; $v = 0$;	1.0	0.3	0.2	121	70	39	1.62E+17	4.27E+16	3.00E+17
CH3O-18-H; $v = 0$;	1.1	0.2	0.1	121	62	49	4.42E+16	1.35E+16	7.00E+16
CH3CN; $v = 0$;	0.45	0.10	0.15	208	23	32	3.91E+16	1.16E+16	3.00E+17
CH3CN; $v8 = 1$;	0.6	0.1	0.2	359	54	41	3.22E+16	1.10E+16	6.00E+16
CH2DCN; $v = 0$;	0.5	0.2	0.3	82	12	63	4.14E+15	1.16E+15	8.00E+15
CH3C-13-N; $v = 0$;	1.0	0.4	0.0	263	73	37	5.00E+14	1.19E+14	8.00E+14
CH3OCHO; $v = 0$;	0.98	0.20	0.02	103	17	77	8.10E+16	1.03E+16	1.00E+17
CH3OCH3; $v = 0$;	0.34	0.09	0.62	229	43	71	3.67E+17	4.13E+16	8.00E+17
CH3CHO; $v = 0$;	0.4	0.3	0.2	234	8	66	1.69E+16	6.78E+14	8.00E+16
CH3CHO; $v15 = 1$;	1.102	0.576	0.002	278	38	22	5.45E+15	1.09E+14	1.00E+16
CH3CHO; $v15 = 2$;	0.7	0.6	0.5	295	92	5	4.33E+15	3.88E+13	1.00E+16
HC(O)NH2; $v = 0$;	0.7	0.2	0.8	98	9	62	7.58E+15	2.34E+15	3.00E+16
C2H5OH; $v = 0$;	0.8	0.2	0.4	281	35	19	7.13E+16	2.23E+16	8.00E+17
H2CS; $v = 0$;	1.3	0.2	0.3	165	14	65	1.41E+16	4.10E+15	3.00E+16
SO2; $v = 0$;	1.36	0.10	0.30	260	52	40	1.74E+16	4.43E+15	1.50E+17
C2H5CN; $v = 0$;	0.9	0.3	0.3	125	15	35	1.53E+16	2.56E+15	3.00E+16
CH3CHDCN	0.6	0.1	0.3	97	4	63	2.90E+15	4.64E+14	5.00E+15
C2H3CN; $v = 0$;	0.6	0.5	0.3	77	6	53	1.28E+16	3.46E+15	3.50E+16
HCCCN; $v = 0$;	1.2	0.3	0.003	176	41	61	1.69E+15	7.47E+14	2.00E+16
HCCCN; $v6 = 1$;	0.6	0.1	0.3	200	22	68	3.08E+15	1.04E+15	8.00E+15
HCCCN; $v7 = 1$;	0.37	0.08	0.23	251	35	49	5.31E+15	1.22E+15	9.00E+15
HCCCN; $v7 = 2$;	0.20	0.03	0.40	350	51	105	2.22E+15	3.93E+14	7.00E+15
aGg'-(CH2OH)2; $v = 0$;	0.6	0.2	0.6	172	27	28	3.47E+16	9.06E+15	6.00E+17
HCOOH	0.6	0.5	0.2	103	37	97	1.37E+16	3.42E+15	3.00E+17
H2CO-18; $v = 0$;	0.6	0.2	0.4	188	53	66	8.51E+14	3.56E+14	5.00E+15

Table C.2. Error values for G35.20 B1.

Catalog entry	Source size	Error left	Error right	T_{ex}	Error left	Error right	N_{col}	Lower limit	Upper limit
CH3OH; $v = 0$	0.3	0.2	0.2	234	35	63	6.99E+17	2.16E+17	5.00E+18
CH3OH; $v12 = 1$	0.36	0.06	0.12	153	3	25	1.07E+18	3.34E+17	5.00E+19
CH3OH; $v12 = 2$	0.18	0.01	0.22	154	1	46	2.23E+18	6.90E+17	6.80E+18
C-13-H3OH; $v = 0$;	0.3	0.2	0.2	113	41	36	3.87E+16	1.57E+16	1.50E+17
CH3O-18-H; $v = 0$;	0.3	0.1	0.2	82	19	35	1.45E+16	8.20E+15	1.20E+17
CH3CN; $v = 0$;	0.32	0.09	0.16	129	78	20	7.24E+15	5.45E+15	1.32E+16
CH3CN; $v8 = 1$;	0.29	0.04	0.11	283	43	17	3.50E+15	2.94E+15	7.00E+16
CH2DCN; $v = 0$;	0.1	0.0	0.3	180	59	101	3.00E+13	1.77E+13	2.05E+15
CH3C-13-N; $v = 0$;	0.7	0.2	0.3	262	34	38	2.01E+14	5.59E+13	8.00E+14
CH3OCHO; $v = 0$;	0.5	0.1	0.2	285	79	15	4.49E+16	5.63E+15	1.00E+17
CH3OCH3; $v = 0$;	0.22	0.02	0.28	156	8	34	3.76E+17	1.05E+17	6.00E+17
CH3CHO; $v = 0$;	0.25	0.06	0.50	100	0	30	1.11E+16	1.12E+15	3.39E+16
CH3CHO; $v15 = 1$;	0.25	0.15	0.08	150	26	25	8.94E+14	1.99E+13	1.16E+16
CH3CHO; $v15 = 2$;	⋆								
HC(O)NH2; $v = 0$;	0.3	0.2	0.2	50	0	100	5.67E+15	2.15E+15	7.00E+16
C2H5OH; $v = 0$;	0.7	0.2	0.3	78	24	63	6.03E+15	4.39E+15	1.00E+17
H2CS; $v = 0$;	2.0	0.2	0.5	230	35	61	3.29E+15	1.48E+15	7.00E+16
SO2; $v = 0$;	1.44	0.09	0.95	279	36	21	3.28E+16	8.15E+15	6.00E+17
C2H5CN; $v = 0$;	⋆								
C2H3CN; $v = 0$;	⋆								
HCCCN; $v = 0$;	0.9	0.2	0.3	119	43	70	9.29E+14	5.50E+14	8.00E+15
HCCCN; $v6 = 1$;	⋆								
HCCCN; $v7 = 1$;	0.8	0.2	0.2	219	49	45	5.84E+14	3.39E+14	6.00E+14
HCCCN; $v7 = 2$;	⋆								
H2CO-18; $v = 0$;	0.3	0.1	0.3	41	1	61	5.66E+14	3.46E+14	7.00E+15
HCOOH	0.3	0.2	0.2	156	30	99	1.11E+15	2.79E+14	7.00E+16

Notes. Star (⋆) indicates a catalog entry that was not modeled.

Table C.3. Error values for G35.20 B2.

Catalog entry	Source size	Error left	Error right	T_{ex}	Error left	Error right	N_{col}	Lower limit	Upper limit
CH3OH; $v = 0$	0.36	0.05	0.84	136	5	164	5.25E+17	1.75E+17	5.00E+19
CH3OH; $v12 = 1$	0.32	0.05	0.38	145	0	155	6.18E+17	2.24E+17	5.00E+19
CH3OH; $v12 = 2$	0.15	0.03	0.24	152	0	148	1.06E+18	2.77E+17	5.00E+19
C-13-H3OH; $v = 0$;	1.1	0.2	0.1	97	34	36	7.99E+15	4.94E+15	1.00E+18
CH3O-18-H; $v = 0$;	0.9	0.3	0.2	75	26	40	1.36E+15	1.34E+15	2.00E+17
CH3CN; $v = 0$;	0.62	0.08	0.08	132	7	10	1.30E+15	1.20E+15	1.74E+15
CH3CN; $v8 = 1$;	⋆								
CH2DCN; $v = 0$;	⋆								
CH3C-13-N; $v = 0$;	0.44	0.19	0.07	55	5	66	1.40E+14	7.24E+13	1.00E+16
CH3OCHO; $v = 0$;	0.5	0.1	0.2	64	14	59	2.02E+16	3.10E+15	1.00E+17
CH3OCH3; $v = 0$;	0.4	0.1	0.3	67	17	62	1.30E+16	3.94E+15	1.00E+18
CH3CHO; $v = 0$;	0.26	0.08	0.35	88	38	40	2.28E+15	1.89E+14	1.00E+17
CH3CHO; $v15 = 1$;	⋆								
CH3CHO; $v15 = 2$;	⋆								
HC(O)NH2; $v = 0$;	0.6	0.2	0.3	45	30	55	2.32E+14	2.01E+14	4.79E+16
C2H5OH; $v = 0$;	0.12	0.02	0.31	297	247	0	1.01E+15	1.01E+15	4.17E+16
H2CS; $v = 0$;	1.0	0.0	1.0	50	0	183	1.18E+15	5.01E+14	1.00E+17
SO2; $v = 0$;	2.42	0.69	0.08	114	66	48	6.58E+15	2.25E+15	1.00E+18
C2H5CN; $v = 0$;	⋆								
C2H3CN; $v = 0$;	⋆								
HCCCN; $v = 0$;	0.8	0.3	0.3	122	44	99	1.96E+14	1.58E+14	1.00E+16
HCCCN; $v6 = 1$;	⋆								
HCCCN; $v7 = 1$;	⋆								
HCCCN; $v7 = 2$;	⋆								
H2CO-18; $v = 0$;	0.32	0.02	0.98	29	2	183	1.51E+15	6.71E+14	1.00E+16

Notes. Star (⋆) indicates a catalog entry that was not modeled.

Table C.4. Error values for G35.20 B3

Catalog entry	Source size	Error left	Error right	T_{ex}	Error left	Error right	N_{col}	Lower limit	Upper limit
CH3OH; $v = 0$	0.35	0.04	0.02	155	6	36	6.23E+17	5.55E+17	8.13E+17
CH3OH; $v12 = 1$	0.36	0.02	0.07	189	14	14	9.81E+17	7.62E+17	1.12E+18
CH3OH; $v12 = 2$	0.20	0.02	0.02	172	5	20	1.80E+18	1.32E+18	2.33E+18
C-13-H3OH; $v = 0$;	1.20	0.06	0.03	89	10	9	1.63E+16	1.20E+16	1.93E+16
CH3O-18-H; $v = 0$;	1.20	0.01	0.00	111	43	18	5.75E+15	4.17E+15	1.21E+16
CH3CN; $v = 0$;	0.35	0.06	0.04	208	30	30	6.46E+15	5.21E+15	1.06E+16
CH3CN; $v8 = 1$;	0.8	0.2	0.2	213	47	27	1.30E+15	5.69E+14	1.00E+18
CH2DCN; $v = 0$;	0.8	0.2	0.2	90	5	203	1.12E+15	2.40E+14	1.00E+16
CH3C-13-N; $v = 0$;	0.7	0.1	0.3	118	14	156	5.44E+14	1.97E+14	1.00E+16
CH3OCHO; $v = 0$;	0.59	0.28	0.01	67	5	2	2.74E+16	2.36E+16	4.30E+16
CH3OCH3; $v = 0$;	0.49	0.10	0.23	97	4	13	1.66E+17	6.31E+16	4.37E+17
CH3CHO; $v = 0$;	1.16	0.05	0.05	170	49	33	2.14E+15	1.90E+15	2.68E+15
CH3CHO; $v15 = 1$;	0.56	0.05	0.21	224	114	74	1.44E+15	8.65E+14	2.19E+15
CH3CHO; $v15 = 2$;	0.12	0.02	0.03	102	1	2	8.07E+14	2.46E+13	1.40E+16
HC(O)NH2; $v = 0$;	0.3	0.1	0.5	53	8	19	1.62E+15	9.12E+14	1.66E+16
C2H5OH; $v = 0$;	0.43	0.03	0.06	178	35	87	1.29E+16	1.02E+16	1.51E+16
H2CS; $v = 0$;	0.9	0.1	1.1	87	23	123	6.05E+15	1.99E+15	1.00E+17
SO2; $v = 0$;	1.3	0.2	1.2	288	73	12	3.92E+16	8.92E+15	1.00E+18
C2H5CN; $v = 0$;	0.8	0.2	0.2	90	0	16	1.29E+15	8.51E+14	2.00E+15
C2H3CN; $v = 0$;	0.8	0.3	0.1	207	77	49	7.29E+14	4.08E+14	1.00E+16
HCCCN; $v = 0$;	1.2	0.6	0.0	251	11	13	1.76E+15	1.64E+15	1.93E+15
HCCCN; $v6 = 1$;	0.4	0.3	0.3	256	34	34	2.43E+15	1.53E+15	3.54E+15
HCCCN; $v7 = 1$;	0.98	0.17	0.02	288	27	32	2.12E+15	1.85E+15	2.25E+15
HCCCN; $v7 = 2$;	0.35	0.06	0.35	473	10	4	1.31E+15	9.70E+14	1.65E+15
HCOOH	0.4	0.3	0.5	173	38	22	3.82E+15	1.70E+15	1.00E+16
H2CO-18; $v = 0$;	1.09	0.06	0.06	125	18	18	4.18E+14	3.78E+14	4.74E+14

Table C.5. Error values for G35.03 A.

Catalog entry	Source size	Error left	Error right	T_{ex}	Error left	Error right	N_{col}	Lower limit	Upper limit
CH3OH; $v = 0$	0.40	0.09	0.71	142	18	68	1.80E+18	3.99E+17	1.00E+19
CH3OH; $v12 = 1$	0.30	0.06	0.62	239	40	61	2.64E+18	6.01E+17	1.00E+19
CH3OH; $v12 = 2$	0.20	0.05	0.52	192	19	108	5.06E+18	9.95E+17	1.00E+19
C-13-H3OH; $v = 0$;	0.6	0.1	0.6	120	24	51	5.00E+16	1.58E+16	1.00E+18
CH3O-18-H; $v = 0$;	1.2	0.3	0.3	130	21	41	9.99E+15	3.48E+15	1.00E+16
CH3CN; $v = 0$;	0.30	0.06	0.40	186	21	114	3.04E+16	1.04E+16	1.00E+19
CH3CN; v8=1;	0.30	0.05	0.20	216	19	54	3.57E+16	1.35E+16	1.29E+19
CH2DCN; $v = 0$;	⋆								
CH3C-13-N; $v = 0$;	0.35	0.08	0.55	70	1	80	1.44E+15	3.48E+14	1.00E+18
CH3OCHO; $v = 0$;	0.2	0.1	0.2	100	21	66	2.29E+15	2.13E+15	1.00E+18
CH3OCH3; $v = 0$;	0.7	0.2	0.1	150	39	56	8.27E+16	2.45E+16	2.68E+17
CH3CHO; $v = 0$;	0.5	0.3	0.3	120	21	77	1.29E+15	8.11E+14	1.00E+18
CH3CHO; $v15 = 1$;	0.5	0.3	0.3	220	53	91	1.29E+15	9.55E+14	1.00E+17
CH3CHO; $v15 = 2$;	⋆								
HC(O)NH2; $v = 0$;	0.8	0.2	0.4	43	1	78	4.68E+15	1.74E+15	1.86E+16
C2H5OH; $v = 0$;	0.4	0.1	0.7	150	29	150	4.88E+16	1.56E+16	4.88E+17
H2CS; $v = 0$;	1.7	0.4	0.3	96	3	105	3.65E+15	1.40E+15	2.51E+16
SO2; $v = 0$;	1.2	0.2	0.8	281	72	19	7.47E+16	1.55E+16	5.01E+17
C2H5CN; $v = 0$;	0.5	0.1	0.3	78	7	70	4.98E+15	1.20E+15	2.07E+16
HCCCN; $v = 0$;	0.6	0.2	0.2	140	27	61	2.28E+15	9.95E+14	1.00E+16
HCCCN; $v7 = 1$;	0.8	0.2	0.2	194	21	32	5.87E+15	1.87E+15	1.84E+16
HCOOH	0.7	0.3	0.2	100	48	82	5.00E+15	1.70E+15	1.00E+16
aGg'-(CH2OH)2; $v = 0$;	0.70	0.10	0.50	100	3	50	2.81E+16	4.99E+15	1.00E+17
H2CO-18; $v = 0$;	0.50	0.03	0.20	52	0	128	2.10E+14	1.56E+14	1.00E+15

Notes. Star (⋆) indicates a catalog entry that was not modeled.

Appendix D: XCLASS analysis details

D.1. S-bearing

We detected two S-bearing species with more than one transition in our sources.

- Sulfur dioxide (SO_2) – as a species with extended emission, the source size ranges from 1.2″ at G35.03 to 2.4″ at B2. The column densities for this species are relatively consistent at 0.6–4.3 × 10^{16} cm^{-2} across G35.20 and 7.5 × 10^{16} cm^{-2} at G35.03. The T_{ex} values are from 114 K in B2 to 288 K in B3. The fits were based on 24 different transitions within the spectral window, five of which were measured in the survey (others were not present or within the noise).
- Thioformaldehyde (H_2CS) – this species was observed to have fairly extended emission so the source size ranged from 0.9″ for B3 to 2.5″ for B1. The T_{ex} range is on the cooler side at 50 K for B2, less than 100 K for B1, B3, and G35.03, and 165 K at A. A had the highest column density at 1.4 × 10^{16} cm^{-2}, where the others ranged from 1.2–6.1 × 10^{15} cm^{-2}.

D.2. O-bearing organics

- Formaldehyde (H_2CO) – only the isotopologues $H_2C^{18}O$, HDCO, and D_2CO were in the spectral range of these observations. See Appendix D.6.
- Formic acid (HCOOH) – this species was detected at all peaks, but it was not modeled for B2 because the emission lines were only just above 3σ.
- Methanol (CH_3OH) – the $\nu = 0$ state of CH_3OH was modeled to a maximum source size of 1″, so the source size fits were 0.4–0.6″. The temperature range was from 132–268 K. The column densities for this species ranged from 0.3–4.8×10^{18} cm^{-2}. The vibrationally excited states and isotopologues were modeled separately as their spatial extents are different from the main state and are likely part of different gas; see Appendices C.5 and C.6.
- Acetaldehyde (CH_3CHO) – the $\nu = 0$ state was modeled separately from the vibrationally excited states (see subsection D.5). This species was observed to have a fairly compact emitting region, so the source size was limited to 1.5″. The best-fit source sizes were 0.3–1.2″ with relatively high excitation temperatures between 193 K and 300 K. The column densities ranged from 1.5–17 × 10^{15} cm^{-2}.
- Methyl formate (CH_3OCHO) – only the $\nu = 0$ state was fit as the $\nu = 1$ transitions were not in the XCLASS database. The emission from this species was fairly compact so the model was allowed a maximum source size of 1.2″. The final source sizes were 0.2–1.0″ and column densities ranged from 1.9–29 × 10^{16} cm^{-2}. Generally the T_{ex} values were high (182–295 K for B1, B2, and B3), but the excitation temperatures of A and G35.03 were 103 K and 151 K, respectively.
- Dimethyl ether (CH_3OCH_3) – there was a lot of variation between the sources for this species. The source size was very compact for A, B1, and B2 (0.3, 0.4, and 0.5″, respectively), but more extended for B3 and G35.03 at 0.8″. The temperature differences were also large. The T_{ex} for B3 was 90 K, 170, and 180 K for B2 and B1, 229 K at A, and 260 K at G35.03. The column densities were lower for B2 (1.6 × 10^{16} cm^{-2}) and higher for the other peaks (8.8 × 10^{16}–9.7 × 10^{17} cm^{-2}).
- Ethanol (C_2H_5OH) – the trans- and gauche- transitions for ethanol were modeled from a single JPL database entry. The temperatures varied widely with best-fit values of 88 K for B1 and 120 K for B2, and much higher values of 260, 281, and 300 K for B3, A and G35.03, respectively. The column densities ranged between 0.6 and 7.1 × 10^{16} cm^{-2} range with the lowest at B1 and B2 and the highest at A. The source sizes were 0.4–0.8″.
- Ethylene glycol (($CH_2OH)_2$) – this species was only modeled for G35.20 core A and for G35.03 as it was not detected in any part of core B. In G35.20 core A and G35.03, the best-fit source sizes are 0.6″ and 0.2″, respectively, and the T_{ex} was 172 K for G35.20 and 75 K in G35.03. The column densities were 3.5 × 10^{16} cm^{-2} in G35.20 core A and 7.8 × 10^{16} cm^{-2} in G35.03.

D.3. N-bearing organics

- Cyanoacetylene (HC_3N) – the $\nu = 0$ state was modeled for all regions and the isotopologue $HC^{13}CCN$ $\nu = 0$ was coupled with HC_3N $\nu = 0$ to improve the uncertainty (from fitting one transition to fitting two). The fit for $HCC^{13}CN$ $\nu = 0$ was also coupled for B3, as this is the only location where this species was detected. When fits of species are coupled together they share the same temperature and source size, but the isotope ratio (and therefore the column density) vary. See Appendix C.5 for excited states. The column densities for this species ranged from 2.1 × 10^{14} cm^{-2} at B2 to 2.2 × 10^{15} cm^{-2} at G35.03. The source sizes were fairly consistent, ranging between 0.9 and 1.2″ and the T_{ex} range was 132–208 K.
- Methyl cyanide (CH_3CN) – the $\nu = 0$ state was modeled for all regions, but the isotopologues were not coupled with the main species because their spatial extents were dramatically different. The modeled source sizes for this species were quite compact, i.e., 0.3–0.6″; the temperature range was 124–235 K. The range of column densities was 1.8–7.2 × 10^{16} cm^{-2}. See Appendices D.5 and D.6 for excited states and isotopologues.
- Vinyl cyanide (C_2H_3CN) – the results for vinyl cyanide are very different for the two regions where it was detected. G35.20 A has a source size of 0.6″, an excitation temperature of 77 K, and a column density of 1.3 × 10^{16} cm^{-2}. On the other end of this source, B3 has a size of 0.8″, a T_{ex} of 207 K, and a column density of 7.3 × 10^{14} cm^{-2}.
- Ethyl cyanide (C_2H_5CN) – this species was only modeled for G35.20 core A, region B3, and G35.03 core A. The temperatures for this species were all low compared to many of the other species. At B3, the T_{ex} was 50 K, at A it was 71 K, and at G35.03 it was 78 K. Column densities were 5.0–45 × 10^{15} cm^{-2} with the highest value at B3 and the source sizes were somewhat similar at 0.3″ for B3, 0.5″ for G35.03, and 0.6″ for A.

D.4. H-, N-, and O-bearing organics

- Isocyanic acid (HNCO) – the fit was based on a single strong transition so some assumptions were made. The source size was fixed based on the 3σ level emission and the column density was modeled at temperatures of 50 K and 100 K. These temperatures are reasonable for a more extended emitting region, as the bulk of the emission is not likely to come from very near the heating source. The resulting column densities are between 2.2 × 10^{15} cm^{-2} and 2.0 × 10^{16} cm^{-2} at

50 K and range from 9.4×10^{14} cm^{-2} to 7.5×10^{16} cm^{-2} at 100 K.

– Formamide (NH_2CHO) – the $v = 0$ transitions were fit with the $NH_2{}^{13}CHO$ transitions coupled with the same parameters except abundance. The temperatures for this species were comparatively low, ranging from 43–100 K. The best-fit source sizes were between 0.5″ (at B1) and 0.8″ at G35.03. The range of column densities is 0.3–7.6×10^{15} cm^{-2}.

D.5. Vibrationally excited transitions

High energy transitions were modeled uncoupled to the main state as those in our sources are observed to emit from a much smaller area than lower energy transitions (see Figs. 3 and 4) and many are not observed in B1 or B2. Vibrationally excited emission from HC_3N is only found toward cores A and B3 and weakly toward B1. See Fig. 8.

– Methanol (CH_3OH) – the $v_{12} = 1$ and $v_{12} = 2$ excited states were modeled separately on the assumption that the different excited states are emitted in different gas, since the spatial extent of each excited state grows more compact with increased energy (see Sect. 2.3 and Sánchez-Monge et al. 2014, Fig. 6). The source sizes for the $v_{12} = 2$ are more compact than the $v_{12} = 1$ states and generally have a higher temperature. The range of column densities between the two states are similar at 0.3–4.8×10^{18} cm^{-2} for $v_{12} = 1$ and 1.9–5.1×10^{18} cm^{-2} for $v_{12} = 2$.
– Cyanoacetylene (HC_3N) – each of the vibrational states ($v_6 = 1$, $v_7 = 1$, $v_7 = 2$) were modeled separately and the source size was more compact with higher excitation. No vibrationally excited states were modeled for B2, as they were not detected in the observations and only the $v_7 = 1$ state was modeled for B1 and G35.03. The $v_6 = 1$ state was modeled for A and B3 and was coupled with $HCC^{13}CN$ with the $^{12}C/^{13}C$ isotope ratio fixed at 50. The resulting temperatures based on these 2–3 transitions was 200 K at A and 365 K at B3 with source sizes of 0.6 and 0.4″. Both peaks had similar column densities at 3.1 and 2.7×10^{15} cm^{-2}, only slightly more than those of the $v = 0$ state. The $v_7 = 1$ state was also modeled coupled with the three different ^{13}C isotopologues for A and B3 with the isotope ratio fixed at 50. The $v_7 = 1$ source size is more compact for all modeled sources, but still somewhat extended at 0.8–1.0″. The excitation temperatures are 25–80 K higher than the $v = 0$ state, ranging from 194 K at G35.03 to 283 K for both A and B3. The abundances of the $v_7 = 1$ state are similar to those of the $v = 0$ state, but for A, the abundance is about 0.45; for B1 and B3 the abundances are almost equal, and for G35.03, the $v_7 = 1$ abundance is about twice the abundance of the $v = 0$ state. The $v_7 = 2$ state was only modeled for A and B3 where the emission becomes very compact, i.e., 0.1 and 0.3″, the temperature is very hot, i.e., 420–450 K, and the abundances are 1.3 and 0.7 times higher than the $v = 0$ state.
– Methyl cyanide – CH_3CN $v_8 = 1$ was modeled separately since its spatial distribution was significantly different from that of the $v = 0$ transitions. The $v_8 = 1$ emission was not modeled for region B2 since it was not detected to a significant degree. Temperatures for this species are generally high, ranging from 215–360 K with compact source sizes of 0.3–0.6″. The column densities for this excited species are 0.4–3.6×10^{16} cm^{-2}, which are similar to those of the $v = 0$ state.
– Acetaldehyde (CH_3CHO) – the $v_{15} = 1$ and $v_{15} = 2$ excited states were modeled as more compact emission sources than the $v = 0$ state. Fits were made for the $v_{15} = 1$ state for all sources except B2, but only for A and B3 for the $v_{15} = 2$ state. In all sources the temperature increases with increasing excitation and the source size decreases. The column densities for both excited states range from 3.5–9.8×10^{15} cm^{-2} though the column density for the $v_{15} = 2$ state at B3 is 5.2×10^{16} cm^{-2}.

D.6. Isotopologues and deuteration

– Formaldehyde (H_2CO) – only the isotopologues HDCO, D_2CO, and $H_2C^{18}O$ were in the spectral range of these observations. These were modeled separately where the $H_2C^{18}O$ fit was based on six transitions and the HDCO fit was based on a single transition. For $H_2C^{18}O$ the size ranges from 0.24–0.75″ and the temperatures are 26 K for B2 to 275 K for A. The range of column densities is 0.4–4.6×10^{15} cm^{-2}. The abundances for HDCO are also on the order of 0.15–1.6×10^{15} cm^{-2} at 50 K and 0.3–16 $\times$ 10^{14} cm^{-2} at 100 K with the source size fixed at 1.5″. D_2CO was not fitted as only single weak lines were detected.
– Methanol – $CH_3{}^{18}OH$ and $^{13}CH_3OH$ were modeled uncoupled to the main isotopologue because their spatial extents differ somewhat from the main isotopologue. The isotope ratios reached were 20–80 for $CH_3OH/^{13}CH_3OH$ and 180–320 for $CH_3OH/CH_3{}^{18}OH$ at peaks B2, B3, and G35.03. The isotope ratios are less ideal for G35.30N A and B1 at 40 and 80, respectively, but the source size is also significantly different. Deuterated methanol (CH_2DOH) was not modeled because it was not in the XCLASS database, so analysis for this species was completed using Cassis.
– Methyl cyanide – $CH_3{}^{13}CN$, and CH_2DCN were modeled separately from the $v = 0$ emission because of their differing spatial distribution. The CH_2DCN was not modeled for region B2 since it was not detected to a significant degree.
– Ethyl cyanide – CH_3CHDCN was only detected at G35.20 A and was modeled for that location.

Appendix E: Line ID xclass fits

Presented below are the spectra of each peak with the original data, the full XCLASS fit, and fits of selected species alone in different colors.

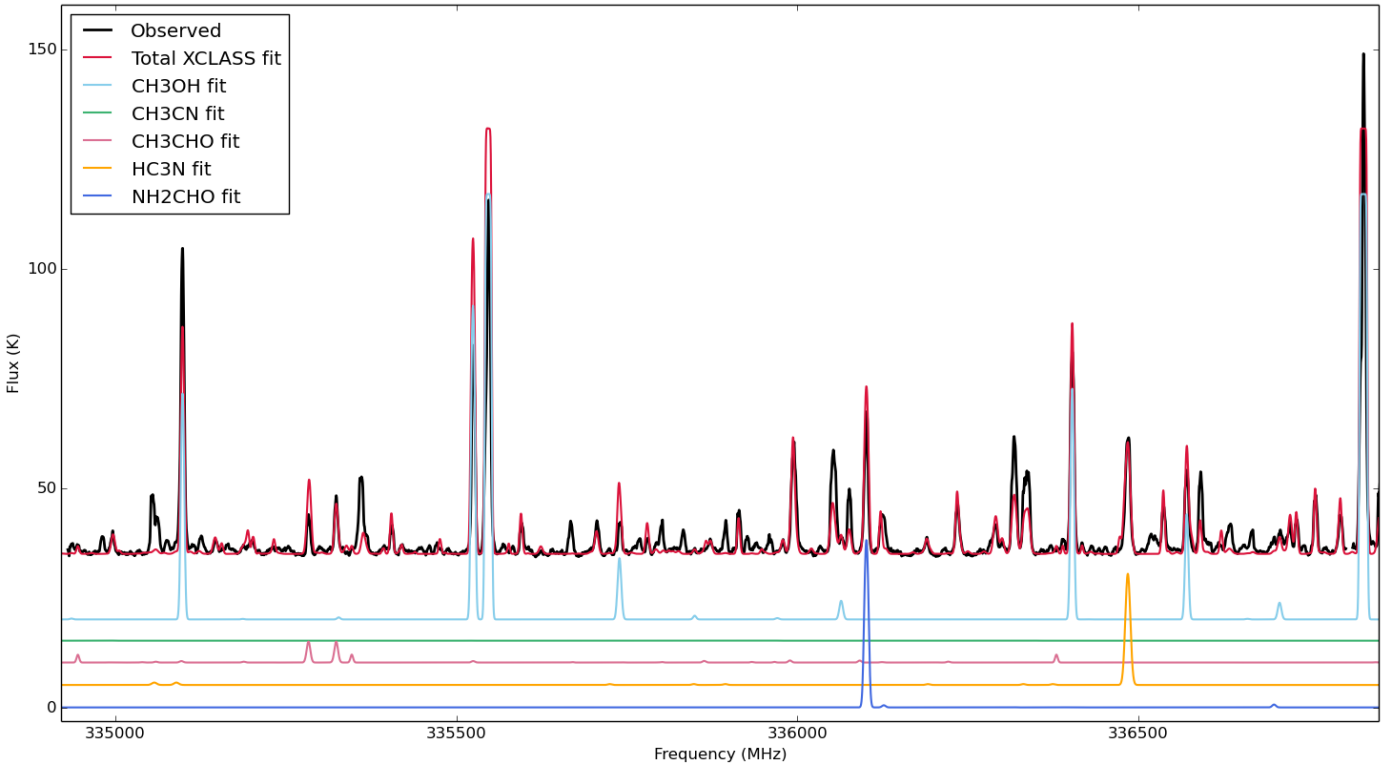

Fig. E.1. G35.20 peak A spectral window 1 (334.9–336.8 GHz), XCLASS total fit, plus selected species.

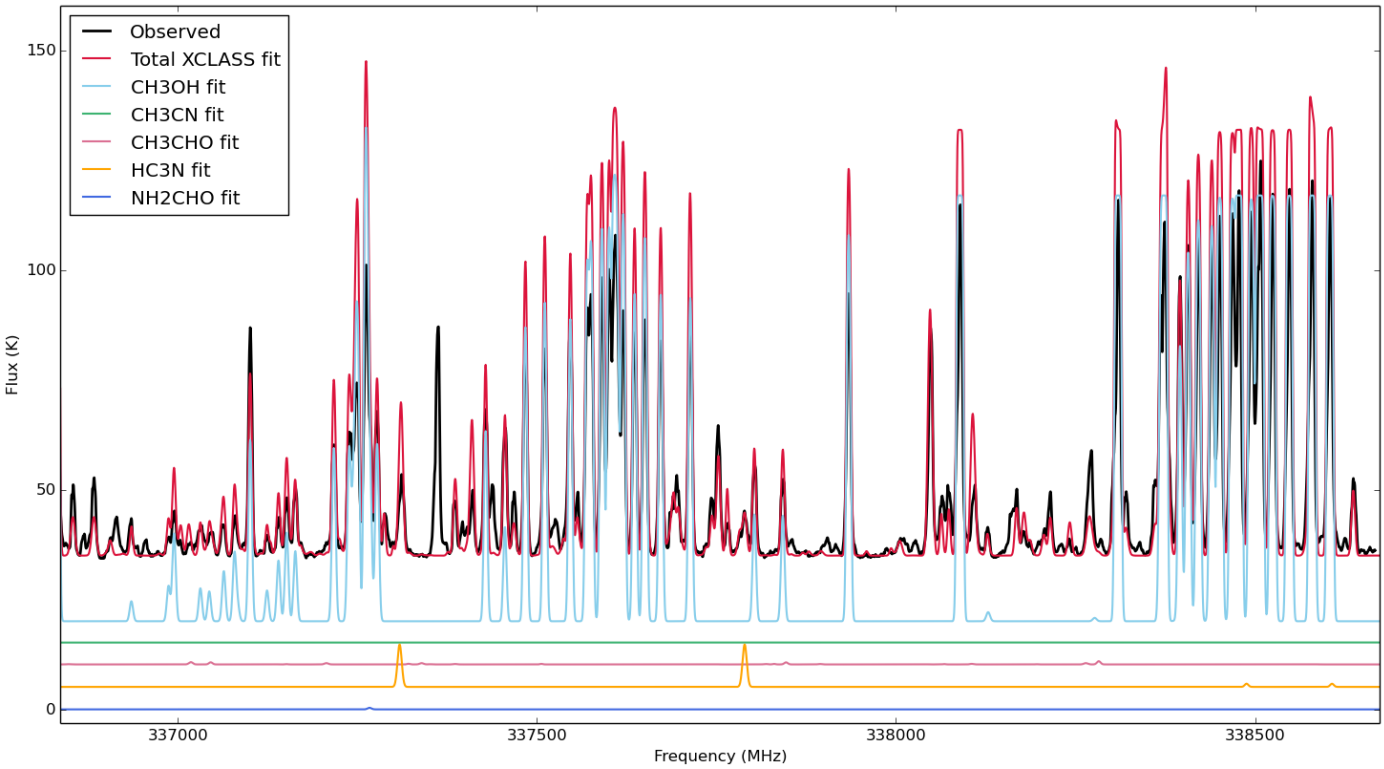

Fig. E.2. G35.20 peak A spectral window 0 (336.8–338.7 GHz), XCLASS total fit, plus selected species.

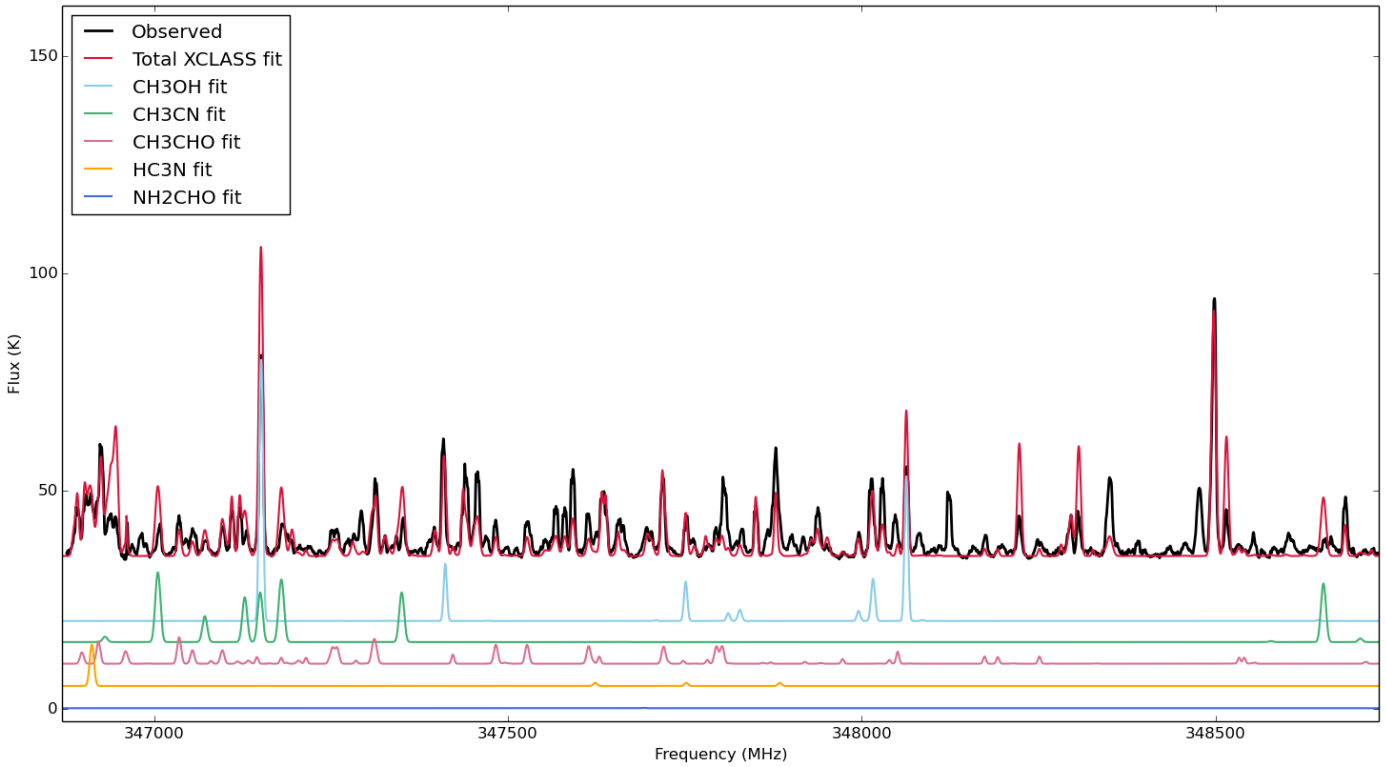

Fig. E.3. G35.20 peak A spectral window 3 (346.9–348.7 GHz), XCLASS total fit, plus selected species.

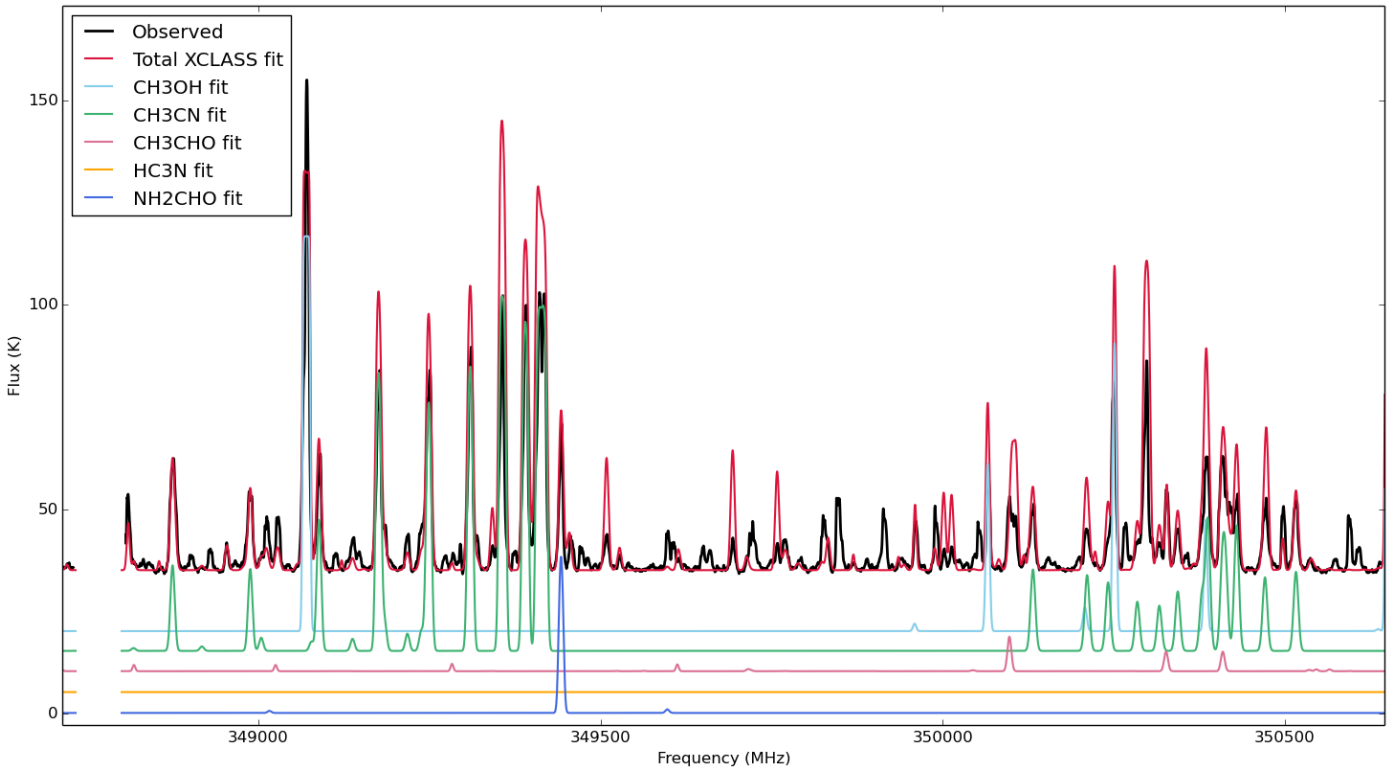

Fig. E.4. G35.20 peak A spectral window 2 (348.8–350.7 GHz), XCLASS total fit, plus selected species.

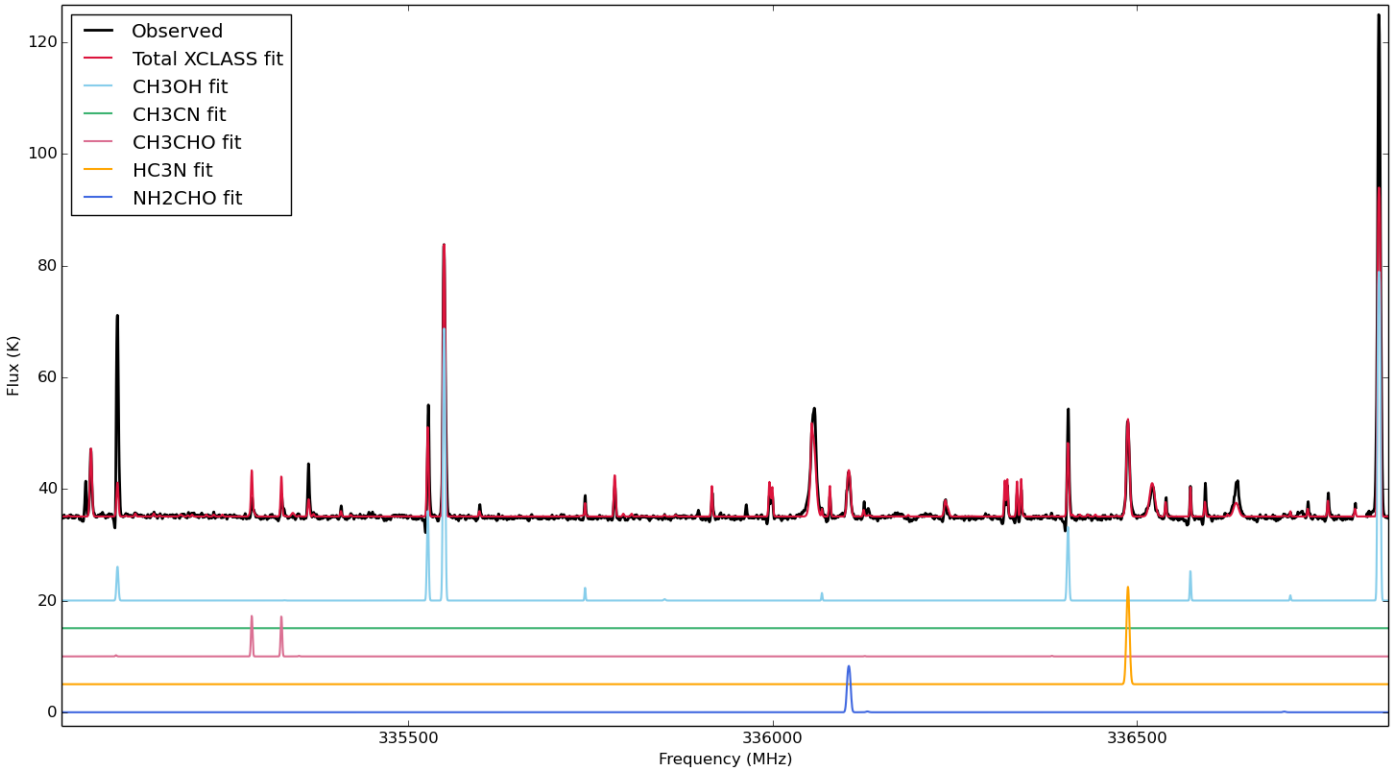

Fig. E.5. G35.20 peak B1 spectral window 1 (334.9–336.8 GHz), XCLASS total fit, plus selected species.

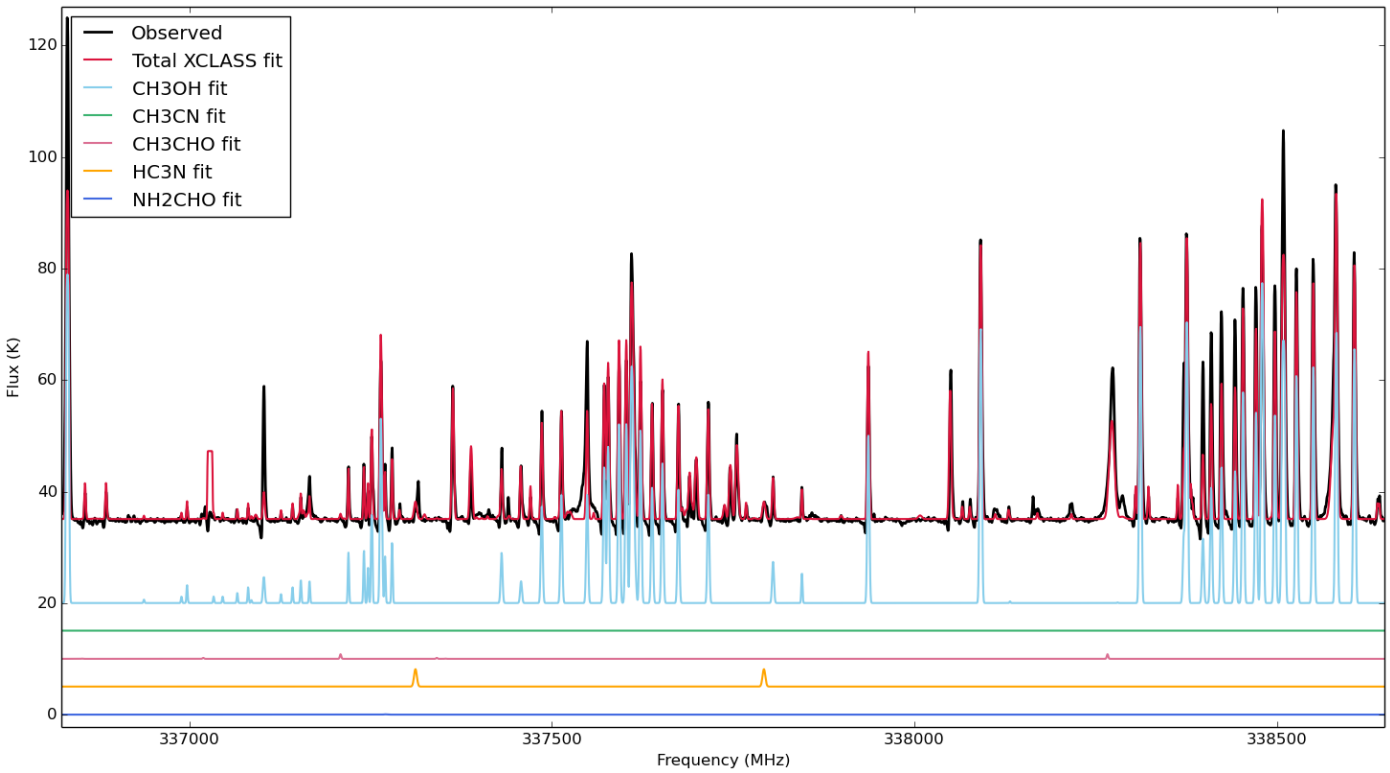

Fig. E.6. G35.20 peak B1 spectral window 0 (336.8–338.7 GHz), XCLASS total fit, plus selected species.

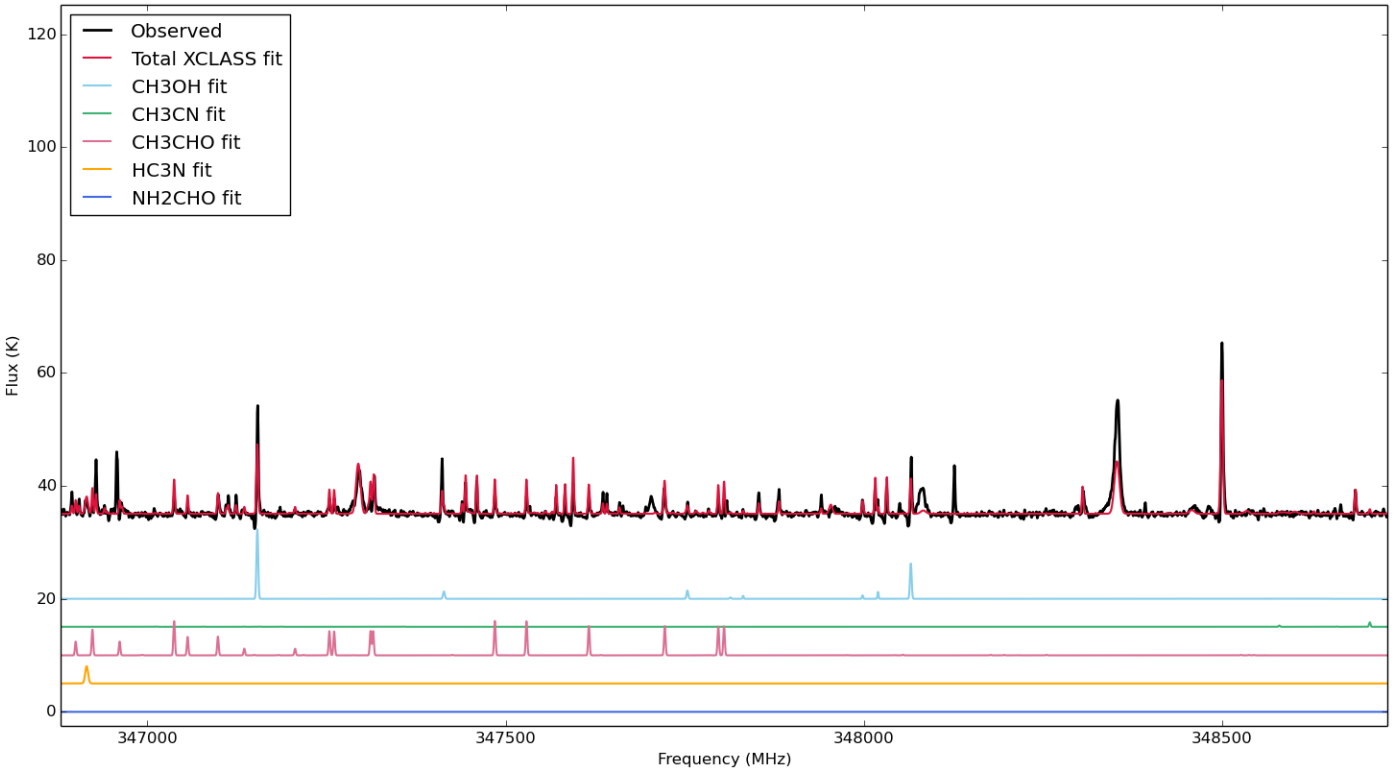

Fig. E.7. G35.20 peak B1 spectral window 3 (346.9–348.7 GHz), XCLASS total fit, plus selected species.

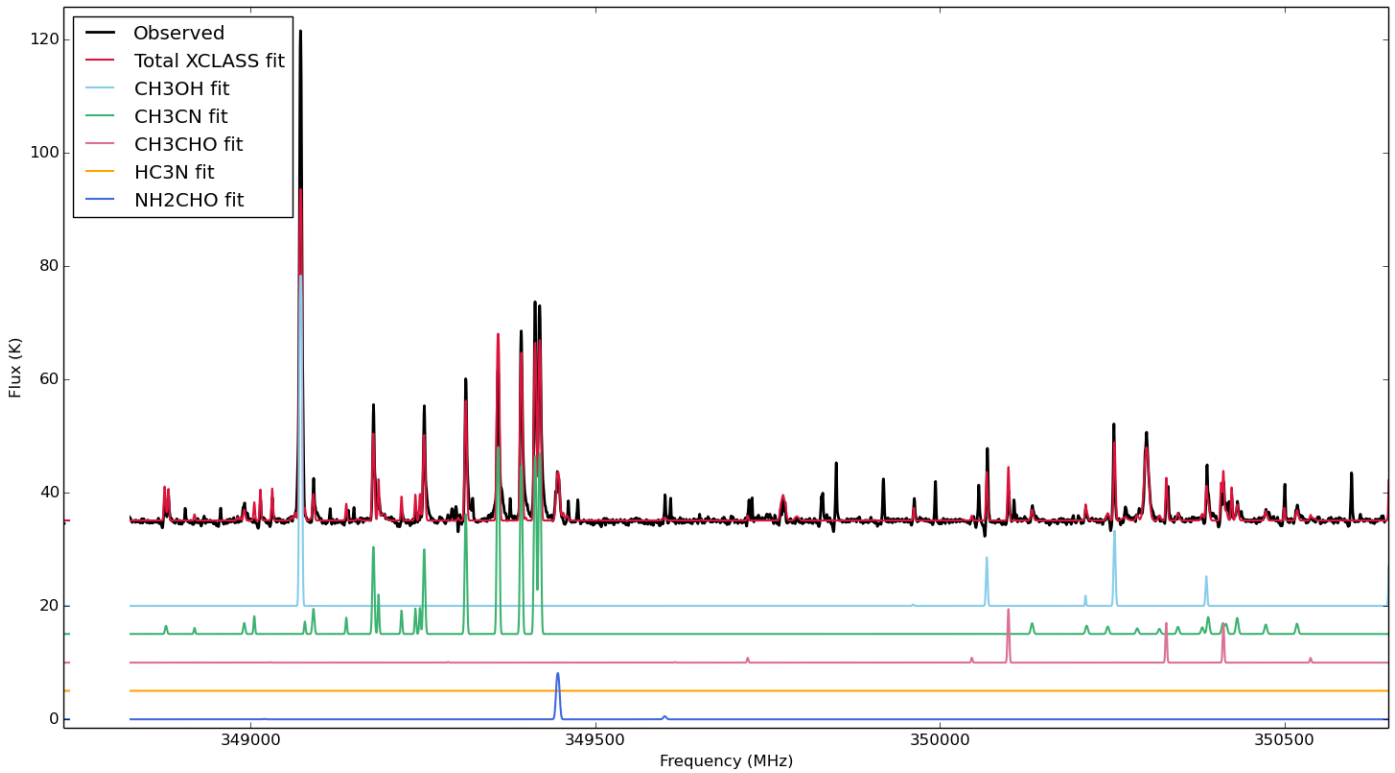

Fig. E.8. G35.20 peak B1 spectral window 2 (348.8–350.7 GHz), XCLASS total fit, plus selected species.

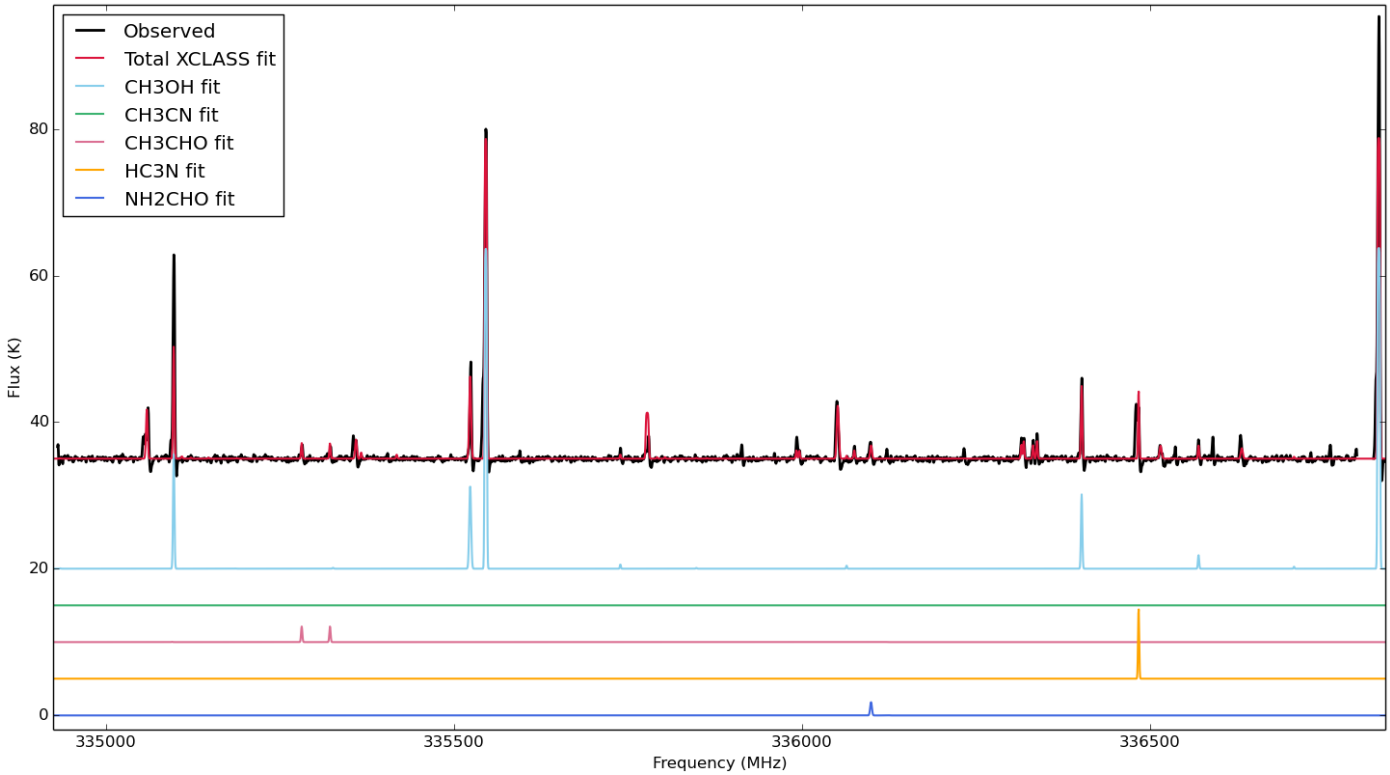

Fig. E.9. G35.20 peak B2 spectral window 1 (334.9–336.8 GHz), XCLASS total fit, plus selected species.

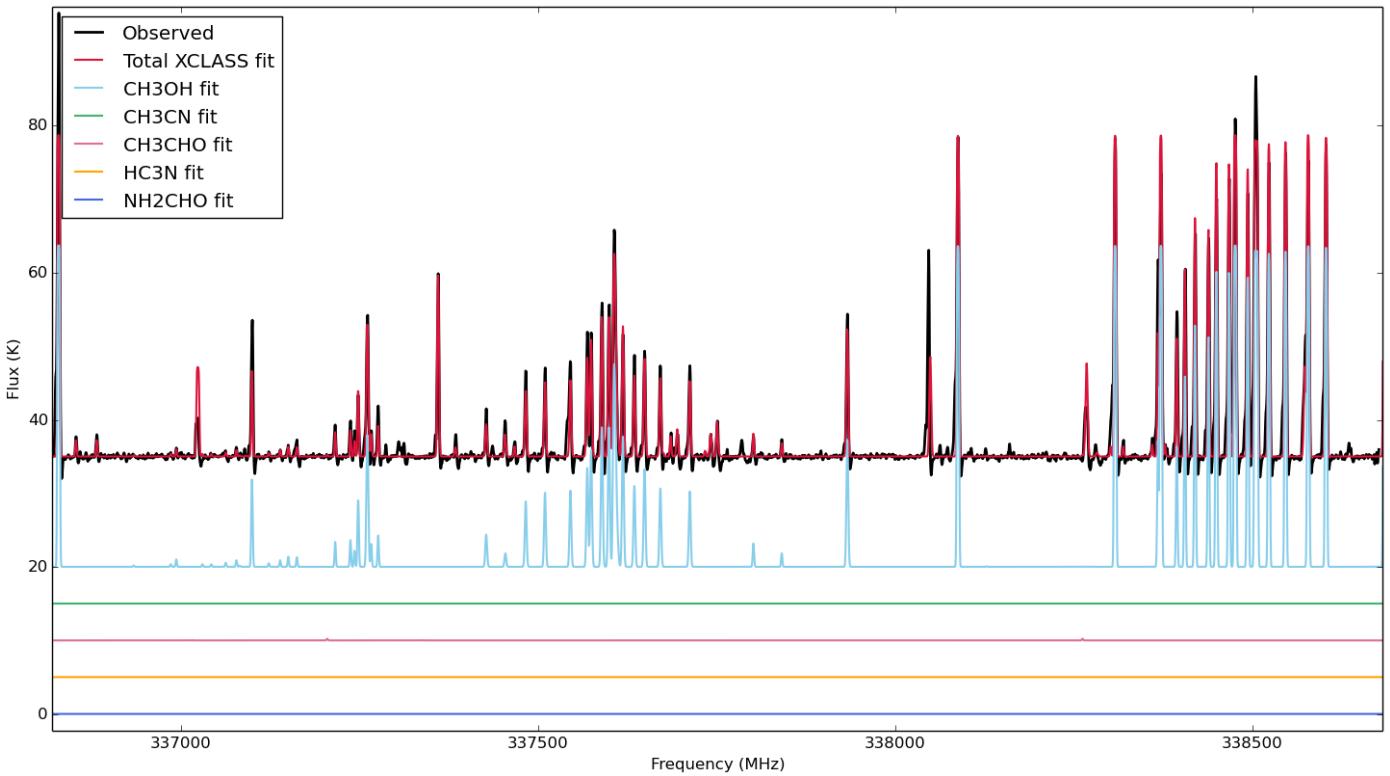

Fig. E.10. G35.20 peak B2 spectral window 0 (336.8–338.7 GHz), XCLASS total fit, plus selected species.

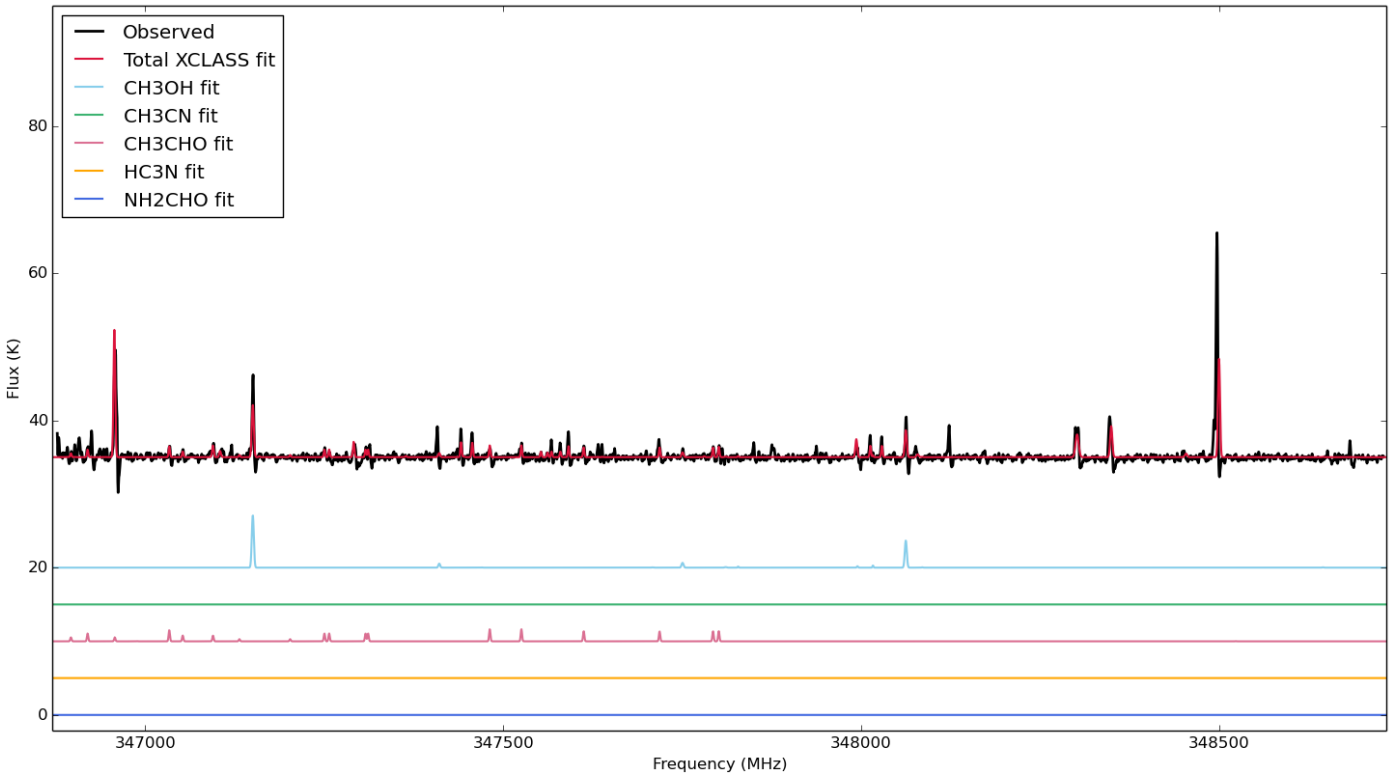

Fig. E.11. G35.20 peak B2 spectral window 3 (346.9–348.7 GHz), XCLASS total fit, plus selected species.

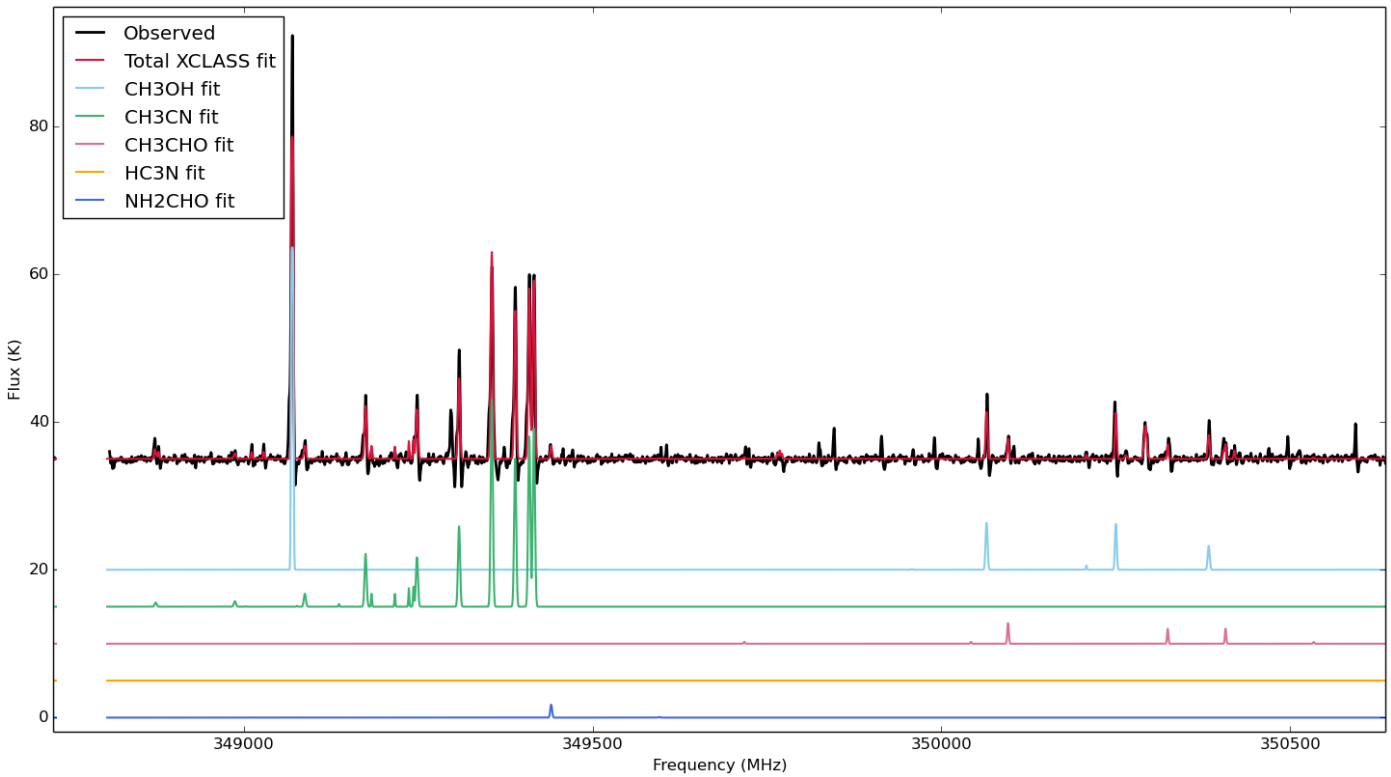

Fig. E.12. G35.20 peak B2 spectral window 2 (348.8–350.7 GHz), XCLASS total fit, plus selected species.

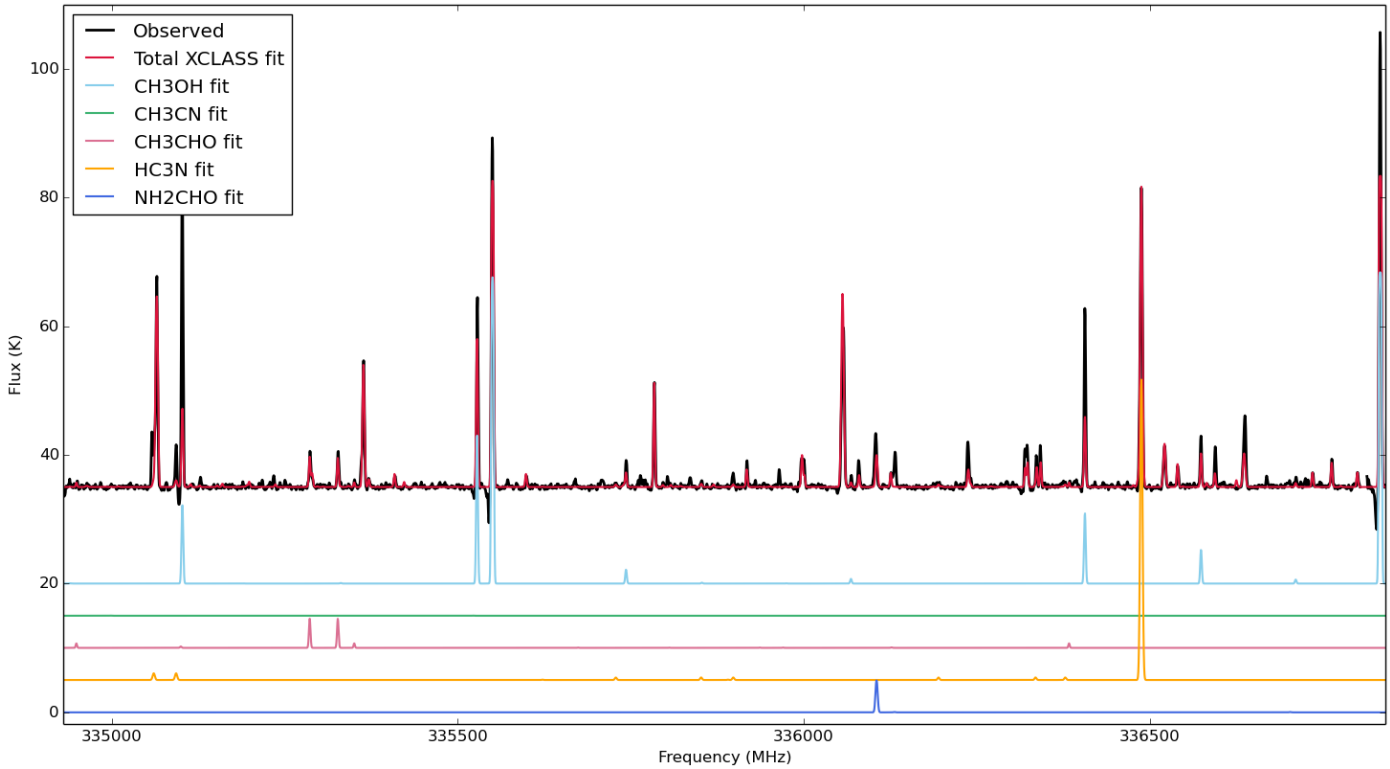

Fig. E.13. G35.20 peak B3 spectral window 1 (334.9–336.8 GHz), XCLASS total fit, plus selected species.

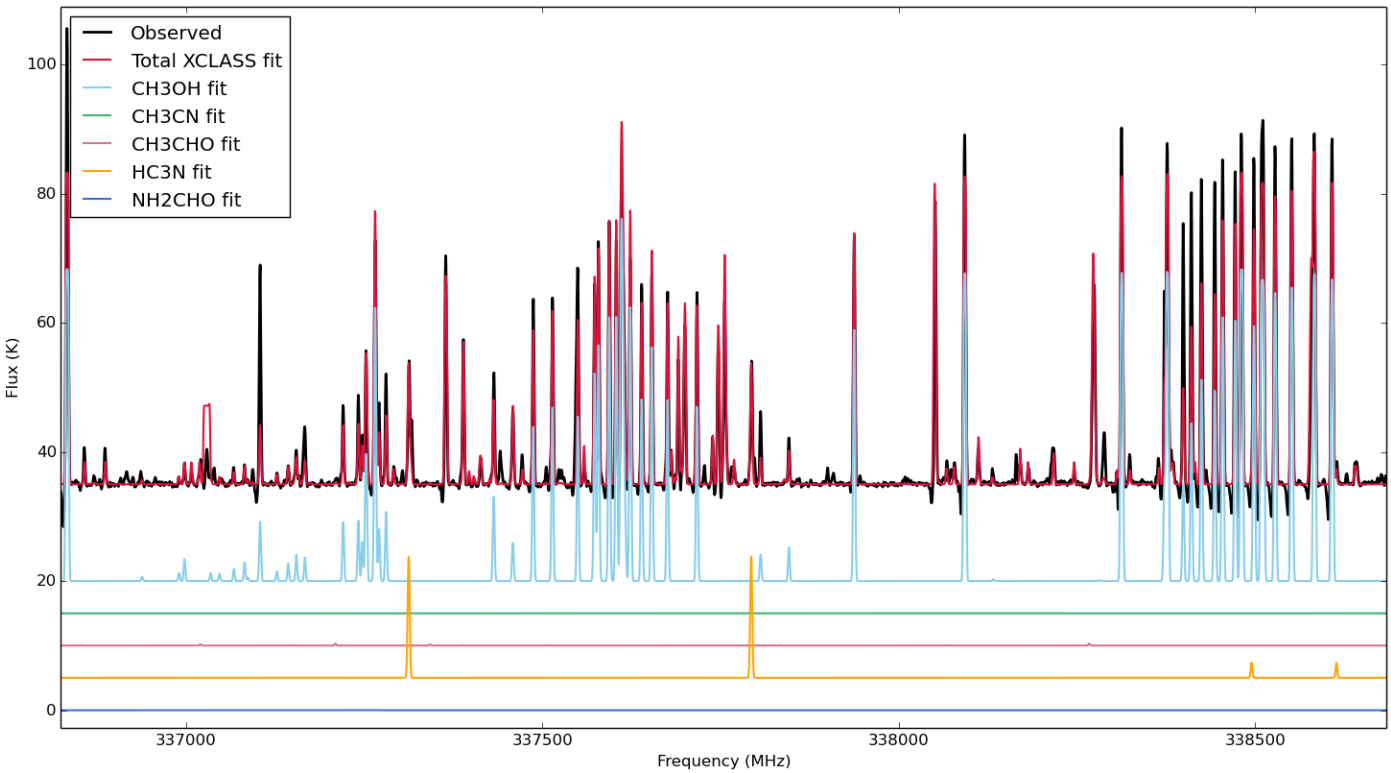

Fig. E.14. G35.20 peak B3 spectral window 0 (336.8–338.7 GHz), XCLASS total fit, plus selected species.

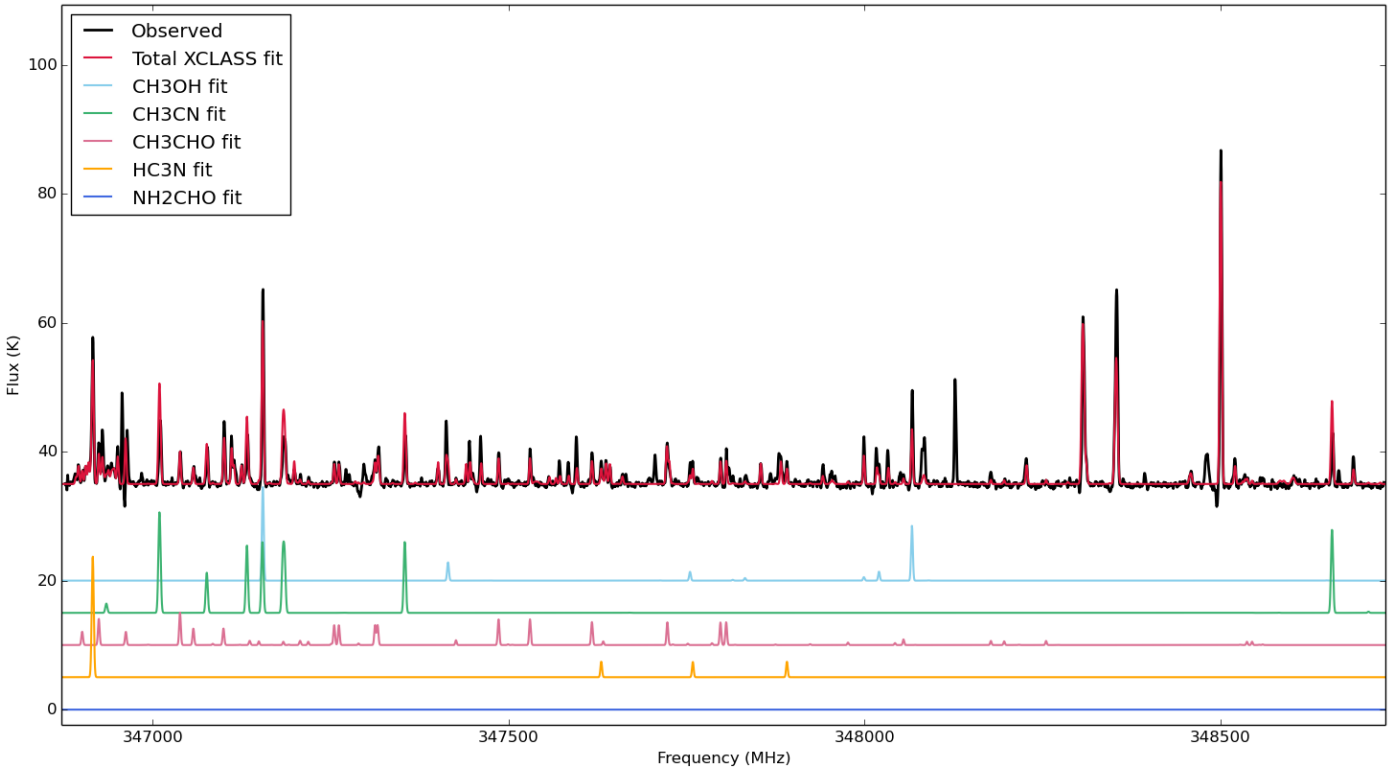

Fig. E.15. G35.20 peak B3 spectral window 3 (346.9–348.7 GHz), XCLASS total fit, plus selected species.

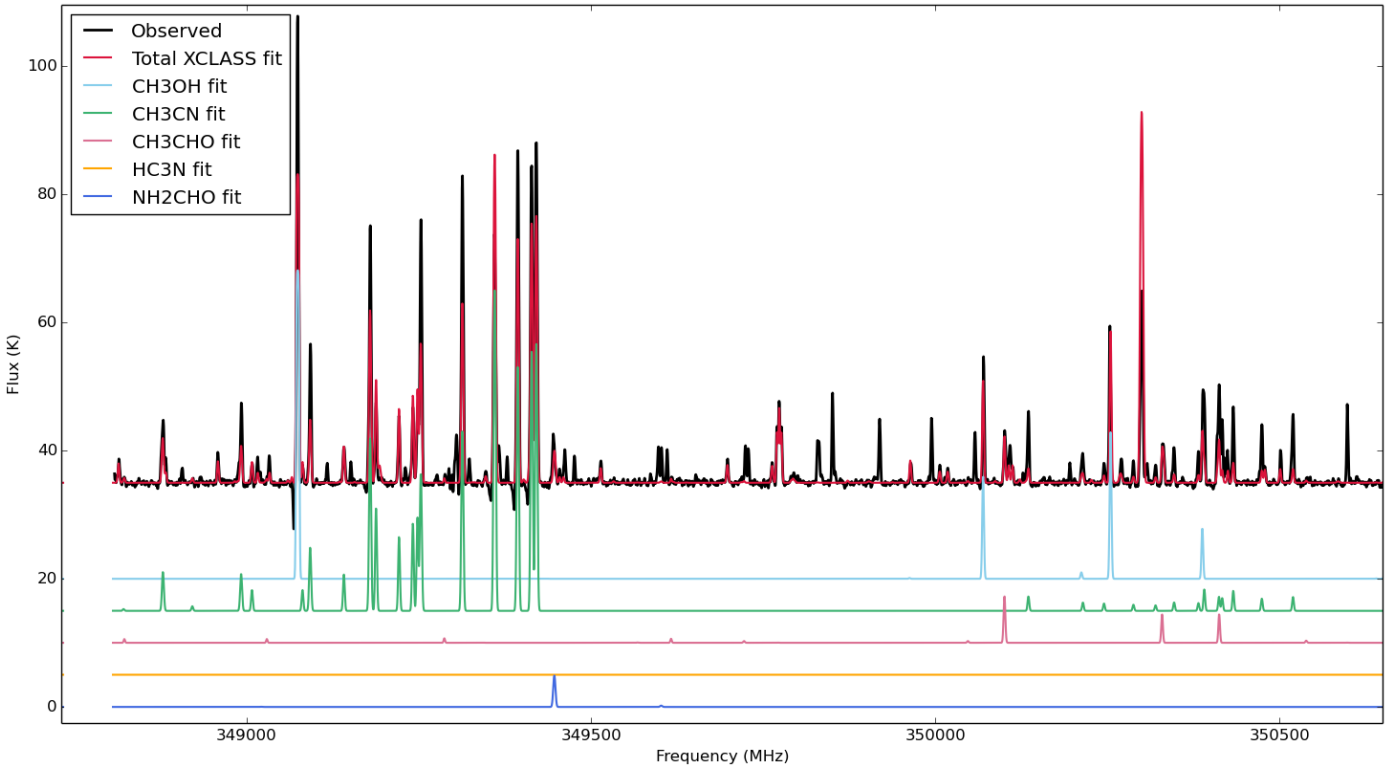

Fig. E.16. G35.20 peak B3 spectral window 2 (348.8–350.7 GHz), XCLASS total fit, plus selected species.

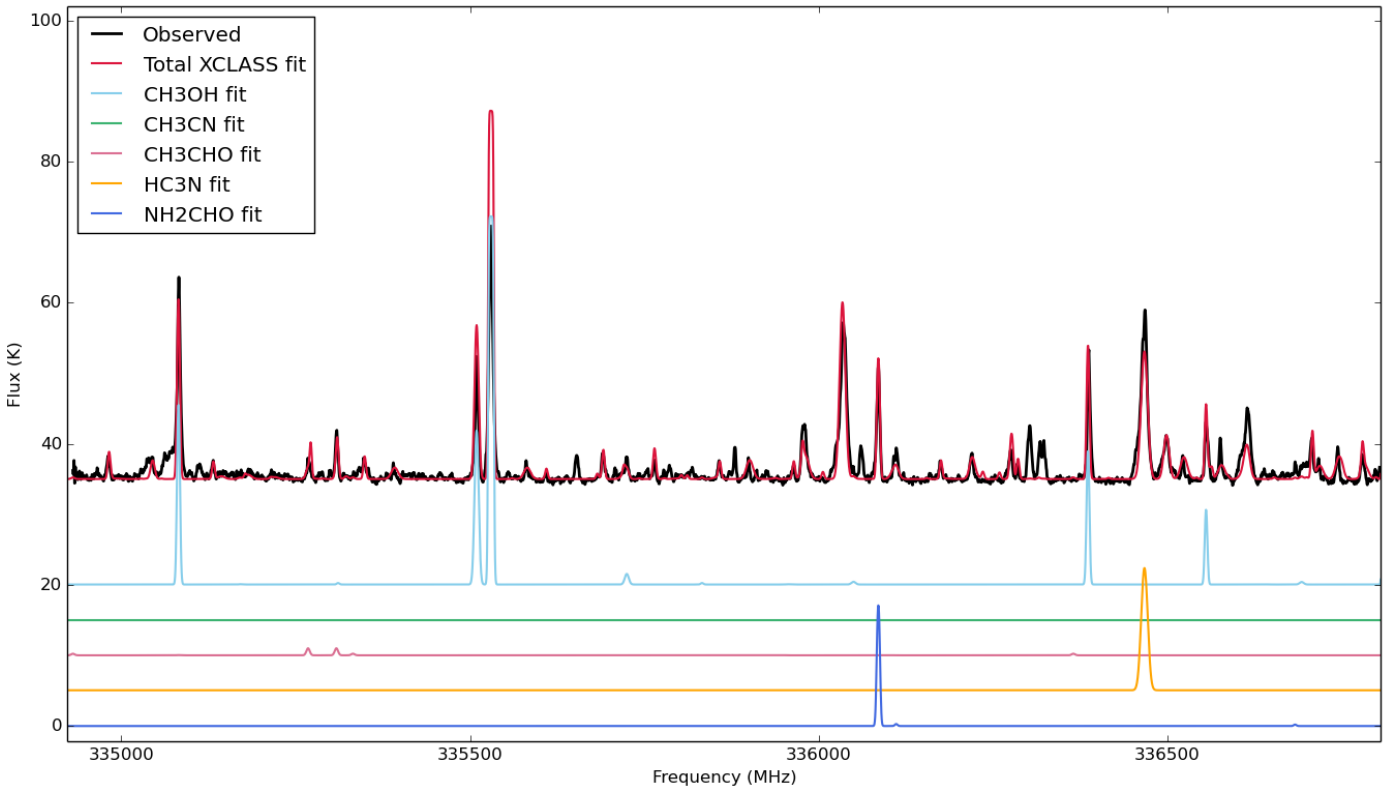

Fig. E.17. G3503 spectral window 1 (334.9–336.8 GHz), XCLASS total fit, plus selected species.

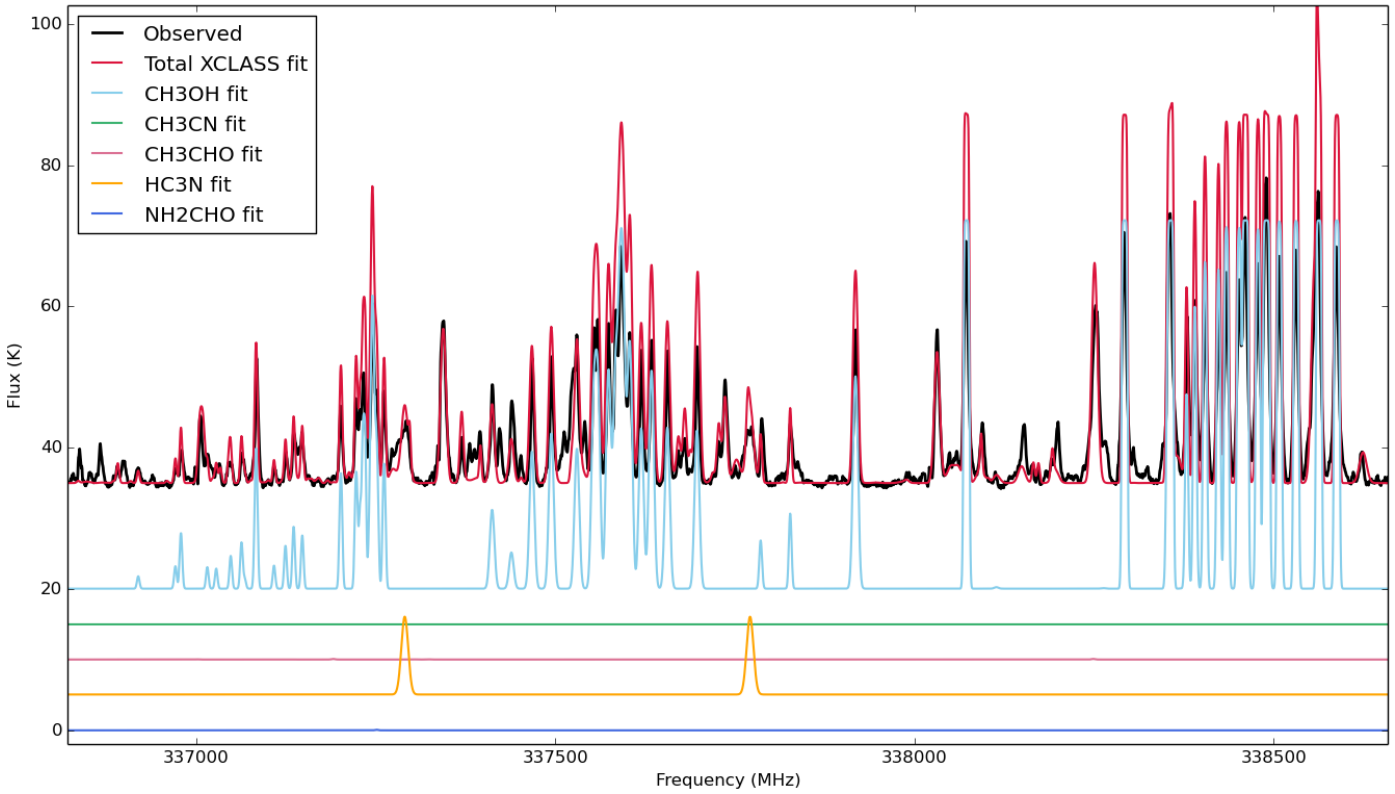

Fig. E.18. G3503 spectral window 0 (336.8–338.7 GHz), XCLASS total fit, plus selected species.

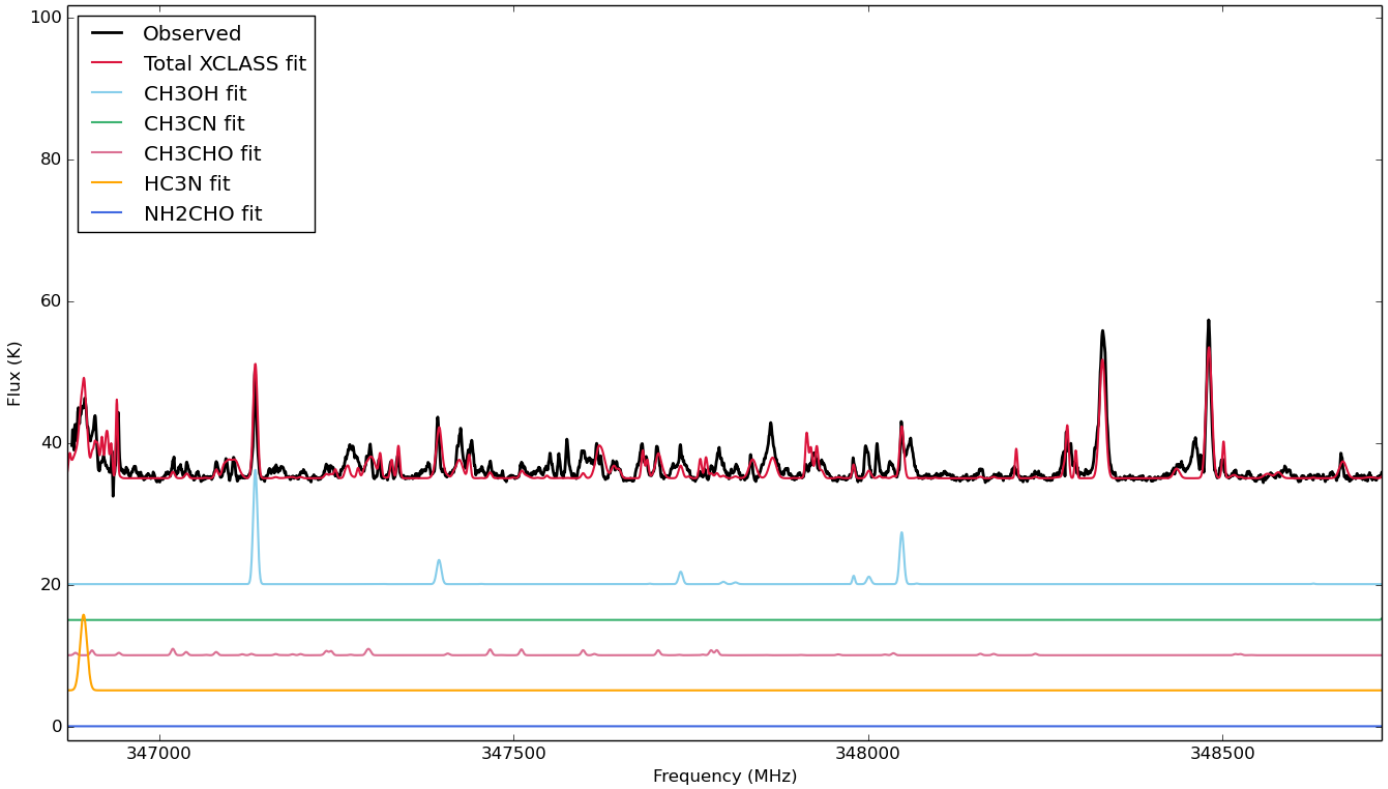

Fig. E.19. G3503 spectral window 0 (336.8–338.7 GHz), XCLASS total fit, plus selected species.

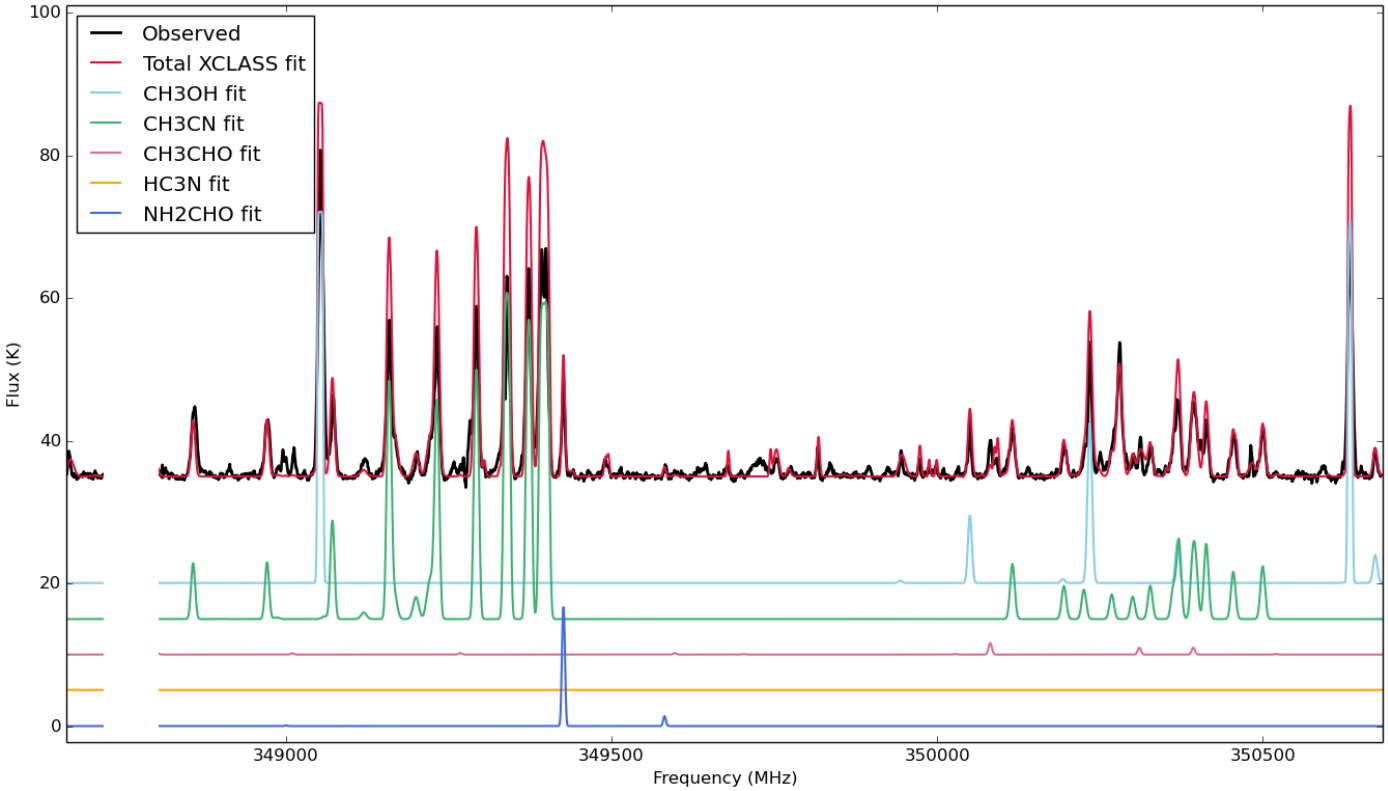

Fig. E.20. G35.03 spectral window 2 (348.8–350.7 GHz), XCLASS total fit, plus selected species.